4. DETAILED MODELLING OF FA AND DDT*

4.1 Introduction

4.1.1 On the Notion of "State of the Art": Research versus Applications

The "state of the art" in numerical turbulent combustion modelling is a notion that strongly depends on individual interpretation. As in many fields of science and engineering, there is a considerable gap between the "state of the art in research" and the "state of the art in applications". A rough estimate of the time delay for a theory to grow from the research to the application level is about 10 years! Even though this report addresses the end user more than the researcher, we will attempt to strike a balance by including relevant information on ongoing research efforts in order to provide an impression where the research community currently sees a need for improvements.

4.1.2 Building Blocks of a Numerical Turbulent Combustion Model

There are two primary constituents to a numerical turbulent combustion model:

1. the abstract mathematical turbulent combustion model, and
2. its numerical implementation.

An abstract mathematical model for turbulent combustion must include submodels for [4.1]

1a. turbulent non-reacting variable density flows,

1b. the influence of turbulence on combustion, and

1c. the influence of combustion on the turbulent flow.

Obviously, all these ingredients must be properly represented numerically, leading to a demand for associated numerical discretizations.

4.1.3 Outline of this Chapter

Each section in this chapter will begin by stating the key problems addressed and will introduce some basic concepts needed to follow the subsequent explanations.

The numerical modelling of turbulent combustion depends heavily on the underlying flow model. Thus Section 4.2 first describes current approaches to the modelling of non-reacting turbulent flows. The major emphasis will be on models based on the Reynolds-averaged Navier-Stokes equations. Both simplified gradient transport closures as well as more advanced Reynolds stress models will be discussed. An important practical issue for large-scale applications in nuclear reactor containments, oil platforms, and

* Professor Dr.-Ing. Rupert Klein
is the lead author for Chapter 4.

other systems with similar geometric complexity is the modelling of subgrid-scale obstacles such as pipes, metal grids, armatures etc.. Related subgrid-scale "porosity models" have been designed in the context of oil platform safety analysis. They will be covered in a separate Subsection. The concluding Subsection summarizes the key ideas of large eddy simulation (LES).

Section 4.3 describes 3 categories of turbulent combustion models. There are heuristic closures, which aim at covering the major transition from kinetics-determined to turbulent-mixing-determined reaction progress. The more sophisticated "flamelet" models include detailed information about the underlying physical mechanisms in the turbulence-determined regime of combustion. The third category is most appropriate in the well-stirred reactor regime, in which turbulent mixing is extremely intense and chemical kinetics controls the reaction progress. Most appropriate for this regime are methods based on the probability density function (PDF) approach. The concluding Subsection summarizes LES ideas in the context of turbulent combustion. Each of the modelling approaches will be discussed with reference to the list of necessary submodels (1a – 1c) given in Section 4.1.2.

Even for the simple hydrogen-oxygen reaction system, there are on the order of 15 chemical species and 40 elementary chemical kinetic reactions. Realistic hydrocarbon chemistry or the reaction kinetics of polluted hydrogen-air-steam systems require the solution of even larger reaction kinetic systems. Besides the sheer size of the resulting equation system, realistic chemistry represents a substantial challenge to numerical modellers because of its wide range of inherent time scales and because of the fact that many of the rapid degrees of freedom are stiff relaxation processes. Section 4.4 first discusses the problems related to fast time scales and stiff reactions in more detail. Summaries of more or less heuristic models for the net effects of chemical reactions as well as more sophisticated reduced chemical models follow (see also the related Subsection on computational chemistry reduction in Section 4.5)

Section 4.5 first gives an account of the particular numerical challenges posed to a numerical flow solver in the context of FA and DDT. In the light of these issues, we will then discuss the current most popular finite-difference and finite-volume numerical methods. The relevant Subsection ends with a summary of open issues and pointers to current research in this area, including applications of finite-element techniques.

The numerical representation of turbulent premixed combustion events requires a priori decisions regarding the resolution of the combustion front. The alternatives are (i) to include detailed models of all relevant physical processes within the turbulent combustion region or (ii) to consider the reaction front as a surface of discontinuity separating burnt from unburnt gases. The former ansatz requires higher numerical resolution and more sophisticated and detailled modelling; the latter compromises on details but provides better control of what is and what is not modelled because it restricts modelling to a few well-defined submodules. The turbulent combustion models introduced in Section 4.3 are reconsidered and evaluated regarding the numerical requirements necessary for their implementation. The Section ends with an explanation of recent developments aiming at a systematic, mathematically sound and purely numerical/algorithmic approach to chemistry reduction. These methods, when applicable, largely free the user of acquiring detailed first-hand experience with the chemical kinetics at hand.

Section 4.6 summarizes some of the key issues raised in this chapter.

4.2 Turbulent Flow Models

4.2.1 The Necessity of Turbulence Closure

High Reynolds number (low friction) flows are characterized by the fact that flow instabilities can occur at a broad range of length scales. The largest scale is limited in size only by the overall system dimensions, whereas the smallest possible length scale of instability is associated with viscous damping. Following Kolmogorov's scaling arguments [4.2, 4.3] the ratio of the largest "integral scale of turbulence" to the smallest "Kolmogorov length" is of the order $O(\mathrm{Re}^{3/4})$. Suppose that, as a rough estimate, one needed about 10 grid points to accurately resolve a smooth flow structure with a given numerical method. Then, a three-dimensional numerical simulation that resolves all the details of a fully developed turbulent flow will require on the order of $10 \times \mathrm{Re}^{9/4}$ grid points. Current computer capacities allow computational grids with about 10^7 grid cells, so that Reynolds numbers of $\mathrm{Re} \approx 1000$ are close to the limit of what can be dealt with today.

Given the characteristic viscosities, densities and flow velocities in practical gas-phase combustion systems, a Reynolds number $\mathrm{Re} \sim 1000$ is associated with domain sizes on the order of a few centimetres or less! Correlating, on the other hand, the aforementioned Reynolds number dependence of the required numerical degrees of freedom with the fact that realistic Reynolds numbers in large-scale systems are of the order of $\mathrm{Re} > 10^7$, we conclude that fully resolved numerical turbulence simulations will stay out of reach for quite some time to come. As a result, the net effects of the fine scales of turbulence on the large resolved ones need to be modelled.

Practically all numerical turbulent flow models rely on Reynolds' idea [4.4] of separating the statistical means of the flow variables from their fluctuations ((LES) will be addressed shortly). One is interested in computing the former, while the effects of the latter should be modelled. This separation is formally done by suitable averaging procedures, which can be spatial, temporal, or formal ensemble averages. Reynolds originally considered constant density incompressible flows. His "Reynolds averaging" procedure implies splitting the velocity field into mean and fluctuations according to

$$\boldsymbol{v} = \overline{\boldsymbol{v}} + \boldsymbol{v}' \,, \tag{4.2.1}$$

where the averaging procedure $\overline{\{\,\cdot\,\}}$ implies that

$$\overline{\boldsymbol{v}'} \equiv 0 \,. \tag{4.2.2}$$

For compressible variable density flows, averaging the velocity field turns out to be inconvenient, [4.5]. More appropriate is the density-weighted "Favre-average":

$$\boldsymbol{v} = \tilde{\boldsymbol{v}} + \boldsymbol{v}'' \,, \tag{4.2.3}$$

where

$$\overline{\rho}\tilde{\boldsymbol{v}} = \overline{\rho \boldsymbol{v}} \tag{4.2.4}$$

by definition, and ρ is the fluid density. A simple characterization of Favre-averaging states that one averages *densities* of physical quantities rather than the specific quantities, i.e., rather than "quantities per unit mass".

Consider, for example, the conservation laws for mass, momentum, and energy of an inert ideal gas

$$\begin{array}{rcrcrcl} (\rho)_t & + & \nabla\cdot(\rho\boldsymbol{v}) & & & = & 0 \\ (\rho\boldsymbol{v})_t & + & \nabla\cdot(\rho\boldsymbol{v}\circ\boldsymbol{v}+\nabla p) & + & \nabla\cdot\boldsymbol{\tau} & = & 0 \\ (\rho e)_t & + & \nabla\cdot(\boldsymbol{v}\,[\rho e+p]) & + & \nabla\cdot(\boldsymbol{j}_T+\boldsymbol{\tau}\cdot\boldsymbol{v}) & = & 0\,. \end{array} \tag{4.2.5}$$

Here $\rho, \boldsymbol{v}, p, e$ are the mass density, fluid flow velocity, pressure, and total energy per unit mass, respectively, and $\boldsymbol{\tau}, \boldsymbol{j}_T$ denote the molecular transport of momentum and heat, respectively. These transport terms and the pressure are related to the mass, momentum, energy and species densities ρ, $\rho\boldsymbol{v}$, ρe through the caloric equation of state

$$\rho e = \frac{p}{\gamma-1} + \frac{1}{2}\rho\boldsymbol{v}^2 \tag{4.2.6}$$

and the transport models

$$\begin{array}{rcl} \boldsymbol{\tau} & = & -\mu\left(\nabla\boldsymbol{v}+(\nabla\boldsymbol{v})^T\right)-\eta\,(\nabla\cdot\boldsymbol{v})\,\mathbf{1} \\ \boldsymbol{j}_T & = & -\kappa\,\nabla T\,. \end{array} \tag{4.2.7}$$

The temperature T is related to pressure and density through the thermal equation of state

$$T = \frac{p}{\rho R}\,. \tag{4.2.8}$$

The quantities $\gamma, R, \mu, \eta, \kappa$ are the isentropic exponent, the ideal gas constant, the shear and bulk viscosities and the heat conductivity, respectively. All of them are assumed constant here because we wish to elucidate some principles of turbulence modelling rather than providing a detailed tutorial for direct application. The reader should consult fundamental text books on combustion such as Reference [4.6] for a comprehensive summary of the fundamental governing equations, including more complex equations of state and sophisticated molecular transport schemes.

The key problem of turbulence modelling arises from averaging the non-linear terms in Equation (4.2.5). For instance, the averaged non-linear momentum flux reads

$$\overline{\rho\boldsymbol{v}\circ\boldsymbol{v}} = \overline{\rho}\,\tilde{\boldsymbol{v}}\circ\tilde{\boldsymbol{v}} + \overline{\rho\,\boldsymbol{v}''\circ\boldsymbol{v}''}\,. \tag{4.2.9}$$

The correlation between the velocity fluctuations in the turbulent stress tensor

$$\boldsymbol{\tau}_\tau = \overline{\rho\,\boldsymbol{v}''\circ\boldsymbol{v}''} \tag{4.2.10}$$

cannot generally be expressed analytically as a function of the mean field variables such as $\tilde{\boldsymbol{v}}$. Therefore, the goal pursued when averaging the equations—namely to derive a system of equations for the mean quantities only—has not been achieved. To obtain a closed system (with a sufficient number of equations for all the unknowns), one introduces closure approximations that replace the unknown correlations with explicit functions or functionals of the mean quantities. There is no rigorous theory yet that would provide a rigid guideline for the construction of such a closure. Therefore, a number of more or less heuristic closure approximations have been developed in recent years.

4.2.2 Algebraic, One- and Two-equation Models

The common feature of this class of closures is that practically all of them rely on a gradient diffusion approximation for the turbulent transport terms (such as the second one in Equation (4.2.9)). An analogy between the net transport induced by turbulent velocity fluctuations and the molecular transport that is due to thermal fluctuations of molecules is invoked. For monatomic gases, the gradient expressions for the viscous stress tensor and heat flux from Equation (4.2.7) can be derived rigorously. For the analogous turbulent fluxes one postulates

$$\boldsymbol{\tau}_\tau = -\mu_\tau \left(\nabla\tilde{\boldsymbol{v}} + (\nabla\tilde{\boldsymbol{v}})^T\right) - \eta_\tau \left(\nabla\cdot\tilde{\boldsymbol{v}}\right) \mathbf{1} + \frac{2}{3}\overline{\rho}k\,\mathbf{1} \tag{4.2.11}$$

where

$$\overline{\rho}k = \frac{1}{2}\overline{\rho\boldsymbol{v}''\cdot\boldsymbol{v}''} \tag{4.2.12}$$

is the average kinetic energy of turbulent fluctuations per unit volume, and μ_τ, η_τ are suitable modelled effective turbulent transport coefficients. For consistency with the definition of the turbulent stress tensor from Equation (4.2.10) and of the turbulent kinetic energy from Equation (4.2.12), one must require that $\eta_\tau = -\frac{2}{3}\mu_\tau$. Given the gradient diffusion ansatz, the next issue is the determination of the effective transport coefficients such as μ_τ.

Algebraic turbulence models. These models proceed by invoking Prandtl's mixing length hypothesis. The idea is that compact packets of turbulent fluid traverse a characteristic length ℓ_{mix} relative to the mean flow, thereby carrying fluctuations of energy, momentum etc. to other fluid regions. Obviously, statistical velocity fluctuations will then lead to a net transport of energy and momentum whose intensity is strongly influenced by (i) the mixing length and (ii) the amplitude of the fluctuations carried by the fluid packets. Assuming that a typical mass element should carry fluctuations that correspond to the difference in the mean flow quantities across the mixing length, one characterizes the fluctuations of any quantity ϕ by $\ell_{\text{mix}}|\nabla\tilde{\phi}|$.

With these intuitive considerations, a typical algebraic approximation to the turbulent viscosity reads, [4.5, 4.7],

$$\mu_\tau = \overline{\rho}\,\ell_{\text{mix}}^2|\tilde{\boldsymbol{\omega}}| \tag{4.2.13}$$

where

$$\tilde{\boldsymbol{\omega}} = \nabla\times\tilde{\boldsymbol{v}} \tag{4.2.14}$$

is the mean vorticity vector. (Alternative linear expressions involving the mean velocity gradients may replace $|\boldsymbol{\omega}|$ in other algebraic turbulence models.)

The remaining task is the modelling of the mixing length, for which we will give an example that is valid for constant density incompressible flows: Elaborate algebraic closure models take into account the experimental observation that typical turbulent boundary layers exhibit a two- or more-layer structure. Within the immediate vicinity of bounding walls, turbulent fluctuation displacements increase roughly in proportion with the distance y from the wall. Outside this inner region, the amplitudes saturate or may even decay. The inner region, called the logarithmic sublayer, leads to expressions such as [4.5, 4.7]

$$\ell_{\text{mix}} = k\,y\,\left[1 - e^{-y^+/y_A}\right] \tag{4.2.15}$$

with y_A a function of the mean flow conditions near the wall, but independent of the wall distance y. For the outer region Reference [4.7] proposes

$$\mu_\tau = \alpha C_{cp} F_{\text{wake}} F_{\text{Kleb}}(y; y_{\max}/C_{\text{Kleb}}) \tag{4.2.16}$$

with the Klebanov function

$$F_{\mathrm{Kleb}}(y;\delta) = \left[1 - 5.5\left(\frac{y}{\delta}\right)^6\right]^{-1} \tag{4.2.17}$$

and

$$\begin{aligned} F_{\mathrm{wake}}(y;\delta) &= \min\left[y_{\max}F_{\max}, C_{\mathrm{wk}}y_{\max}U_{\mathrm{dif}}^2/F_{\max}\right] \\ F_{\max} &= \frac{1}{\kappa}\left[\max_y(\ell_{\mathrm{mix}}|\boldsymbol{\omega}|)\right] . \end{aligned} \tag{4.2.18}$$

Moreover, U_{dif} is the maximum mean velocity difference across a boundary layer, a wake or a jet flow, $y_{\max}$ is the distance from a wall or symmetry line at which $\ell_{\mathrm{mix}}|\boldsymbol{\omega}|$ attains its maximum, and $\kappa, \alpha, C_{\mathrm{cp}}, C_{\mathrm{Kleb}}, C_{\mathrm{wk}}$ are modelling constants that must be fitted to experimental data sets.

The key message here is not the detailed structure of this sample closure model. It should rather be noticed that all the features of the shear stress model have been generated in a heuristic, empirical way. They are not derived from first principles, and thus cannot be considered as general turbulent flow closures. The structure of these models reflects very detailed experimental observations and with proper choices of all model constants many experimental findings. However, as noted in Reference [4.5], one such set-up can be expected to operate with sufficient accuracy only for applications whose flows fall within a range of similar flows that were used to establish both the model structure and the values of all free constants.

It is also important that most algebraic models have been designed to represent wall-bounded or free shear flows or both, but that they are not designed and well tested for more general multi-dimensional flow situations. As a consequence, flow computations based on algebraic turbulence models that deal with very general initial and boundary data may yield utterly incorrect results—unless tuned to the specific kind of application.

One- and two-equation models. These models also start from the Reynolds- or Favre-averaged equations, but incorporate more fundamental principles in constructing closure approximations. These models also employ a gradient flux approximation, so that the increased sophistication relative to algebraic closures manifests itself through the modelling of the effective transport coefficients.

One key observation is that the intensity of the velocity fluctuations—or in other words, the turbulent kinetic energy—should critically influence the net turbulent transport. Thus if one were able to obtain—e.g., a characteristic length ℓ_τ or time scale t_τ of turbulence—then dimensional arguments would automatically lead to $\nu_\tau = \mu_\tau/\overline{\rho} \sim \ell_\tau\sqrt{k} \sim kt_\tau$.

This observation is crucial, because an *exact* equation for the turbulent kinetic energy can be derived. Wilcox [4.5] provides a derivation of the turbulent kinetic energy equation in the context of variable density flows

$$\begin{aligned} \bar{\rho}\frac{\partial k}{\partial t} + \bar{\rho}\tilde{\boldsymbol{v}}\cdot\nabla k &= \bar{\rho}\,\boldsymbol{\tau}_\tau : \nabla\tilde{\boldsymbol{v}} - \overline{\rho\,\boldsymbol{\tau}:\nabla\boldsymbol{v}''} + \nabla\cdot\left\{\overline{\rho\,\boldsymbol{\tau}\cdot\boldsymbol{v}''} - \overline{\rho\,\boldsymbol{v}''\frac{\boldsymbol{v}''^2}{2}} - \overline{p'\boldsymbol{v}''}\right\} \\ &\quad -\overline{\boldsymbol{v}''}\cdot\nabla\bar{p} + \overline{p'\nabla\cdot\boldsymbol{v}''} . \end{aligned} \tag{4.2.19}$$

With such an equation at least part of the closure model can be based on exact information, even though a number of terms within that equation representing fluctuation correlations must again be modelled.

One- and two-equation models now differ in how they obtain the second missing dimensional characteristic scale ℓ_τ or t_τ. One-equation models proceed in a similar fashion as the algebraic models discussed earlier [4.5]: The mixing length is assessed through an algebraic formula. Experience shows that this formula generally needs to incorporate explicitly some specific reference to the flow configuration considered. Thus a one-equation model is not closed in the sense that it would consist of a given set of *universal* partial differential equations whose solutions are determined by supplementing initial and boundary conditions. In contrast, the model equations themselves are changed from one set of such input data to another through adjustments of the mixing length and the associated variations of the turbulent transport coefficients.

Two-equation models introduce an additional transport equation for the missing quantity. There are models that directly model a characteristic turbulent mixing length ℓ, the product $k\ell$ or the inverse ω of a characteristic turbulence time scale, (see References [4.3,4.8 to 4.12] and related references in Reference [4.5]). These lead to "k-ℓ", "k-$k\ell$", "k-ω"–models, all of which aim at improvements of generality over the aforementioned algebraic and one-equation models.

The most popular approach, however, is the k-ϵ–model [4.13]. The approach may be motivated by the desire to model one of the unclosed terms in the turbulent kinetic energy equation, namely

$$\bar{\rho}\tilde{\epsilon} = \overline{\rho\,\boldsymbol{\tau} : \nabla \boldsymbol{v}''}\,. \tag{4.2.20}$$

This term describes the molecular level dissipation of turbulent kinetic energy. Besides being one of the unclosed terms from Equation (4.2.19), the turbulent dissipation also plays a key role in Kolmogorov's fundamental paper on scaling laws of turbulence [4.2]. In that paper, Kolomogorov postulates a self-similar energy cascade, defined by (i) energy input on the largest scales of turbulence, (ii) transformation through a cascade of smaller and smaller flow structures through non-linear inertia effects, and (iii) the ultimate dissipation of this energy at the smallest scale, which is called the "Kolmogorov scale". The existence of such a cascade with a rate of energy transfer between scales that is independent of scale itself has considerable consequences which Kolmogorov explored by means of dimensional analysis. The turbulent dissipation—or the turbulent kinetic energy transfer rate—being such a fundamental quantity, it is tempting to include it directly in a turbulence model, thereby introducing a model variable that captures some of the essence of the energy cascade.

Unfortunately, the turbulent kinetic energy dissipation rate from Equation (4.2.20) satisfies a tremendously complex governing equation with unclosed terms that are very hard to measure or assess accurately by other means. As a consequence, modelling has been guided by scaling and dimensional arguments. Modelled equations have been introduced that are *completely heuristic* but composed of all ingredients that formally appear in the exact equation (see Reference [4.5]). These key ingredients are convection by the mean flow, turbulent transport, molecular transport, production, and dissipation.

The k-ϵ / k-ω approaches have first been established for constant density incompressible flows but were extended later to variable density incompressible and (weakly) compressible flows in References [4.14 to 4.16]. These extensions are far from trivial. New equations describing the mass and energy balances must be introduced, and a number of new turbulence effects arise that lead to new unclosed terms [4.5]:

- turbulent heat fluxes,
- dilatation-induced dissipation of kinetic energy ($\nabla\cdot\boldsymbol{v} \neq 0$!),

- pressure-diffusion and pressure-dilatation correlations, and
- pressure work from velocity fluctuations.

A detailed description of how these effects are incorporated into existing turbulence models is beyond the scope of the present report. It may suffice here to say that modelling in the framework of two-equation models remains, based on judicious scaling and dimensional arguments.

4.2.2.1 Summary and qualifications

Two-equation turbulence models should be considered the current "state of the art in applications". These models are found in all major commercial flow simulation codes. The simpler algebraic and one-equation models still have their merits when used in applications that they have been especially tuned to. In these situations they provide results comparable in quality to two-equation models, albeit at the cost of a much narrower range of applicability of a given set-up of all model coefficients and constants.

There are a number of qualifications to be made that are, unfortunately, often disregarded in engineering applications. Algebraic, one- and two-equation models have been developed originally for specific flow situations, such as shear and boundary layers. They are not well suited without special tuning to more complex flows with recirculation zones, flow detachments etc.. This is of particular importance for real-life applications in fire and explosion safety. The relevant flows and flow geometries are hardly ever within the domain of applicability of these relatively simple turbulent flow models. Thus any results generated with these models must be considered with considerable scepticism! This $does\ not$ imply that k-ϵ- or k-ω-based models cannot be applied, but it $does$ imply that one should expect considerable fine tuning of these models to be necessary from one application to another. To overcome these pitfalls, two major research and development directions have emerged over the years.

- *Reynolds stress models* go beyond two-equation models in that they relax the gradient transport approximation for turbulent fluxes such as those of Equation (4.2.11) and instead introduce new dynamic equations for the turbulent fluxes themselves. This adds flexibility in incorporating new physical effects and allows us to construct models that are applicable over a much wider range of physical situations without fine-tuning, at the cost of increased model complexity.
- *Large eddy simulation* models stay with simpler modelling of small-scale effects, but they run at much higher numerical resolution. Therefore, these models generate part of the turbulent energy cascade all by themselves and aim at using the gained information to improve the description of the unresolved scales. With this approach, the underlying models remain simple and are expected to be even simpler than the more sophisticated two-equation models, but much higher demands on computing power arise.

Common to both Reynolds stress and large eddy simulation models is the possibility of a much-improved description of turbulent transport in turbulent premixed flames. This issue will be discussed in more detail in connection with turbulent flame-flow coupling in a later section.

Reynolds stress models and LES for inert flows are discussed next.

4.2.3 Reynolds Stress Models

Instead of assuming a specific form of the relation between mean flow quantities and turbulent transport, Reynolds stress models compute the transport terms themselves from modelled transport equations. Thus in three space dimensions six equations for quantities $\overline{\rho u_i'' u_j''}$ are added to the mass, momentum and energy balances. (Because of the symmetry of the Reynolds stress tensor, it is not necessary to calculate all the nine stress components independently.) Generally, this approach adds flexibility to incorporate new physical effects and allows us to construct models with a much wider range of applicability without fine tuning.

The stress transport equations are derived, more or less straightforwardly, by manipulating the original equations. Thus one first subtracts the averaged momentum equation from the original one in order to obtain an equation for the averaged momentum $\overline{\rho \boldsymbol{v}''}$. Tensorial multiplication by $\boldsymbol{v}''$ and subsequent averaging leads to equations of the form

$$\overline{\boldsymbol{v}'' \circ \frac{\partial \rho \boldsymbol{v}''}{\partial t}} + ... = ... \tag{4.2.21}$$

In a similar fashion, one derives from the non-conservative from of the momentum equation the counterpart

$$\overline{\rho \boldsymbol{v}'' \circ \frac{\partial \boldsymbol{v}''}{\partial t}} + ... = ... \tag{4.2.22}$$

Addition of these 2 equations yields the desired transport equation for the Reynolds stresses. Wilcox [4.5] provides the following compact formulation of these equations for the case of constant density, incompressible flows, which we cite here for illustration of the modelling issues involved:

$$\frac{\partial \boldsymbol{\tau}_\tau}{\partial t} + \bar{\boldsymbol{v}} \cdot \nabla \boldsymbol{\tau}_\tau = -\boldsymbol{\tau}_\tau \cdot \nabla \bar{\boldsymbol{v}} - (\boldsymbol{\tau}_\tau \cdot \nabla \bar{\boldsymbol{v}})^t + \boldsymbol{\epsilon} - \boldsymbol{\Pi} + \nabla \cdot (\nu \nabla \boldsymbol{\tau}_\tau + \boldsymbol{C}) \tag{4.2.23}$$

where

$$\boldsymbol{\Pi} = \overline{\frac{p'}{\rho} (\nabla \boldsymbol{v}' + (\nabla \boldsymbol{v}')^t)} \tag{4.2.24}$$

$$\boldsymbol{\epsilon} = 2\overline{\nu (\nabla \boldsymbol{v}')^t \cdot \nabla \boldsymbol{v}'} \tag{4.2.25}$$

$$\rho \nabla \cdot \boldsymbol{C} = \rho \overline{\boldsymbol{v}' \circ \boldsymbol{v}' (\nabla \cdot \boldsymbol{v}')} + \nabla (\overline{p' \boldsymbol{v}'}) + \left(\nabla (\overline{p' \boldsymbol{v}'}) \right)^t . \tag{4.2.26}$$

The key advantages of including a stress transport model are that certain effects that are lost in the more simplified algebraic, one- and two-equation models are now included and provide for the desired enhanced capabilities and more general applicability. These include

- effects of flow history;
- convection, production and body force effects which—under appropriate closure—allow the inclusion of streamline curvature, system rotation, and stratification effects at least qualitatively [4.5]; and
- unequal normal stresses, allowing proper adjustment under sudden non-isotropic changes of strain rates.

On the other hand, this ansatz changes not only the number of equations to be solved, but also modifies the mathematical character of the equation system: Molecular transport in the original Navier-Stokes equations figures as a second derivative damping term changing the equation type from hyperbolic (elliptic/hyperbolic) for the inviscid case to parabolic (elliptic/parabolic) for viscous unsteady compressible (incompressible) flows. In the Reynolds stress equations, the turbulent transport terms are now unknown variables themselves, and thus the character of the original balance equations remains unchanged, whereas the equation type is now determined by the Reynolds stress equations. Their type, in turn, depends on the closure approximations introduced for all triple correlations. The change of the equation type obviously has consequences for the choice of appropriate numerical techniques, and a general recipe is hard to provide because of this dependence on modelling assumptions.

Notice also, that closure requires determination of $\boldsymbol{\Pi}, \boldsymbol{\epsilon}, \boldsymbol{C}$. The most popular Reynolds stress models (see e.g., [4.17]) introduce explicit closures for the pressure strain and triple correlations covered by $\boldsymbol{\Pi}, \boldsymbol{C}$, but keep an additional dynamic equation for the dissipation tensor $\boldsymbol{\epsilon}$. Thus one introduces, e.g.,

$$\boldsymbol{\epsilon} = \epsilon \left(\frac{2}{3}\mathbf{1} + 2 f_s \boldsymbol{B} \right) \tag{4.2.27}$$

where $\boldsymbol{B}$ is the Reynolds stress anisotropy tensor

$$\boldsymbol{B} = \frac{1}{2\,k} \left(\boldsymbol{\tau}_\tau - \frac{2}{3}\,k\,\mathbf{1} \right) , \tag{4.2.28}$$

k is the turbulent kinetic energy

$$k = \frac{1}{2}\,\mathrm{tr}(\boldsymbol{\tau}_\tau) \tag{4.2.29}$$

and f_s is a Reynolds number dependent weight function

$$f_s = \left(1 + \frac{1}{10} Re_t \right)^{-1} . \tag{4.2.30}$$

Then, in order to obtain the full dissipation tensor, $\boldsymbol{\epsilon}$, one needs to model the time evolution of its trace ϵ from Equation (4.2.27). This is done by including either a dissipation evolution equation as in a k-ϵ model (see [4.17,4.18] and many other references in Reference [4.5]) or by modelling the evolution of a characteristic turbulence time scale $t_t \sim \omega^{-1}$ through an ω-equation [4.19, 4.20].

4.2.3.1 Summary and qualifications

Reynolds stress transport models do succeed in overcoming many of the shortcomings of the simpler models discussed in the last subsection. There are a number of well-documented Reynolds stress models in the literature and their performance on various flow configurations has been extensively tested by comparison with experimental data. Flows with streamline curvature, boundary layers with strong pressure gradients, rotating flows, and boundary layer flows with separation have been modelled with much higher accuracy than has been possible with algebraic, one- or two-equation models [4.5].

These improvements are obtained at the cost of considerably increased model complexity involving equation systems whose structure differs substantially from that of the Navier-Stokes equations. This last fact should be considered as one of the major obstacles to a more widespread application of Reynolds stress transport models in everyday engineering investigations: Navier-Stokes solvers are more or less readily available and are straightforwardly extendable to algebraic, one- and two-equation turbulence modelling. Incorporation of Reynolds stress models requires dramatically more intense efforts.

In the context of combustion simulations, we will see later on that Reynolds stress transport models provide a very natural framework for sophisticated flame-flow coupling schemes. The importance of this aspect should not be underestimated and will be discussed in detail in Section 4.3.4.2.

We should not leave unmentioned the recent development of an intermediate complexity turbulence closure by Oberlack [4.21 to 4.23]. Oberlack observes that one of the major shortcomings of algebraic, one- and two-equation models is their inherent assumption of local isotropy of turbulent transport. He reconsiders Rotta's [4.24] original derivations of multi-point statistics of turbulent flows and essentially derives an anisotropic version of a k-ℓ model. The key advantage of this approach is that the model structure remains comparable to that of a k-ϵ or k-ω model, while the above-mentioned shortcomings regarding isotropy assumptions are removed! The model is still awaiting wider application but should be kept in mind as a promising compromise between algebraic, one- and two-equation models on the one hand and full-fledged Reynolds stress models on the other.

4.2.4 Large Eddy Simulation (LES)

4.2.4.1 The key ideas of LES

An important aspect of all the Reynolds averaged flow models from Sections 4.2.2, 4.2.3 is that they model *all* turbulent fluctuation scales while only the gross flow features are computed explicitly. As a consequence, $none$ of the small-scale turbulent fluctuations are computed in a dynamical fashion, and the turbulence statistics are completely unaccessible. No information on the inherently unsteady nature of turbulence is provided by these models. This observation is particularly disturbing if one aims at an improved understanding of these unsteady fluctuations or, as in combustion, is interested in the interactions between small-scale turbulent fluctuations and the aero-thermochemistry. (See also Section 4.3.1.)

There is an additional aspect of Reynolds-averaged models that is relevant to the subsequent discussions of LES: In practically all real-life applications the largest turbulent fluctuations (on the integral scale of turbulence) are inhomogeneous and non-isotropic. Thus much of the advanced theory of turbulence, which is based to a large extent on just these assumptions of homogeneity and isotropy, is—strictly speaking—not applicable. This obviously complicates the task of modelling considerably.

Both these problems are addressed by LES as follows: One begins by noting that—according to the widely accepted Kolmogorov theory—turbulence is characterized by an energy cascade from large to ever-smaller scales. Energy is fed into a turbulent system at the largest scales comparable to the characteristic system dimensions. It is re-distributed through non-linear instabilities to a hierarchy of smaller and smaller flow structures. Ultimately, it is dissipated at the Kolmogorov dissipation scale. As more and more non-linear energy transfers take place, one intuitively assumes that the emerging small scales are less and less influenced by the detailed larger scale flow patterns that they originate from. One expects the smaller scales to nearly satisfy the restrictive assumptions of homogeneity and isotropy, thereby allowing simplified modelling procedures.

Large eddy simulation thus operates with numerical resolutions that allow one to represent a sufficient range of scales so that (i) most of the kinetic energy of the turbulent fluctuations is captured and that (ii) the smallest resolved scales are considerably smaller than the integral scale of turbulence. Obviously, one still cannot completely resolve all the flow features down to the Kolmogorov dissipation scale, and some kind of "subgrid modelling" is still required.

Common to all LES models is the concept of "filtering". The space, time, or ensemble averaging of standard Reynolds-averaged models is replaced by spatial filtering procedures that only in the simplest case are actual spatial averages with a fixed averaging domain size. More generally, an LES filter is of the form

$$\overline{\boldsymbol{v}}(\boldsymbol{x},t) = \iiint G(\boldsymbol{x}-\boldsymbol{\xi};\Delta)\boldsymbol{v}(\boldsymbol{\xi},t)\,d^3\boldsymbol{\xi} \tag{4.2.31}$$

with a filter function $G(\boldsymbol{r};\Delta)$ satisfying the conditions

$$G \geq 0\,, \qquad G(\boldsymbol{r};\Delta) \to 0 \qquad \text{as} \qquad \frac{|\boldsymbol{r}|}{\Delta} \to \infty \tag{4.2.32}$$

and the normalization

$$\iiint G(\boldsymbol{r};\Delta)\,d^3\boldsymbol{r} = 1\,. \tag{4.2.33}$$

The filtered flow quantities such as $\overline{\boldsymbol{v}}$ in Equation (4.2.31) are the primary unknowns in an LES model. One of the first choices in constructing a LES model is to choose such a filter. Simple algebraic space averaging, corresponding to a box filter, filtering in Fourier space, Gaussian filter weights in physical space, and a host of alternatives have been proposed [4.5, 4.25]. The common point is that any filter introduces a characteristic length Δ, which defines the smallest resolved scale and thus separates computed from modelled flow structures.

Given a filter definition one can proceed to derive new governing equations for the filtered quantities by applying the filter to the original unfiltered equations. For example, for incompressible constant density flow, the divergence constraint and momentum equation read

$$\nabla\cdot\overline{\boldsymbol{v}} = 0 \tag{4.2.34}$$

and

$$\frac{\partial\overline{\boldsymbol{v}}}{\partial t} + \nabla\cdot(\overline{\boldsymbol{v}\circ\boldsymbol{v}}) + \frac{1}{\rho}\nabla\overline{p} - \nu\nabla^2\overline{\boldsymbol{v}} = 0\,. \tag{4.2.35}$$

The challenge in LES modelling becomes clear when the filtered non-linear convection term is decomposed as

$$\overline{\boldsymbol{v}\circ\boldsymbol{v}} = \overline{\boldsymbol{v}}\circ\overline{\boldsymbol{v}} + \boldsymbol{L} + \boldsymbol{C} + \boldsymbol{R} \tag{4.2.36}$$

where

$$\begin{aligned} \boldsymbol{L} &= \overline{\overline{\boldsymbol{v}}\circ\overline{\boldsymbol{v}}} - \overline{\boldsymbol{v}}\circ\overline{\boldsymbol{v}} \\ \boldsymbol{C} &= \overline{\overline{\boldsymbol{v}}\circ\boldsymbol{v}'} + \overline{\boldsymbol{v}'\circ\overline{\boldsymbol{v}}} \\ \boldsymbol{R} &= \overline{\boldsymbol{v}'\circ\boldsymbol{v}'} \end{aligned} \tag{4.2.37}$$

are subgrid-scale non-linear flux contributions that require modelling. These terms are dubbed the "Leonard stress", the "cross-term stress", and the "subgrid-scale (SGS) Reynolds stress", respectively.

Notice that, depending on the choice of filter, one may have

$$\overline{\overline{\boldsymbol{v}}} \neq \overline{\boldsymbol{v}}\,, \tag{4.2.38}$$

which is in contrast to standard Reynolds averaging and implies that the cross-term stresses are generally non-zero. This non-standard behaviour of LES filtering can also have a non-negligible influence on subgrid-scale modelling.

Two major modelling approaches have emerged over the past decade: Explicit subgrid-scale models, the origin of which go back to Smagorinsky's fundamental work, [4.26], and the more recent dynamic LES models following a seminal paper by Germano et al. [4.27], (see also the reviews in References [4.28 to 4.31]).

4.2.4.2 Explicit subgrid-scale models

An important presumption of this kind of model is a *directed* energy cascade, in which energy as well as information are transferred from large to small scales. Under these conditions it would be irrelevant at which scale precisely the cascade is truncated. It would be sufficient to capture and dissipate the transferred flux of energy at some scale that is small enough to guarantee that there is negligible dynamic "backscatter" from this smallest resolved scale back up to the larger dynamic flow structures.

Models using an explicit small-scale viscosity build on this concept and essentially assign the smallest resolved numerical grid scale to be the dissipation scale Δ. In the simplest case, an effective mixing length eddy viscosity is introduced [4.26] that has the smallest mesh size as the effective mixing length. Since the fundamental problem of representing the net effect of small scales that are *not* resolvable on the given numerical mesh remains the same as in Reynolds-averaged models, one can go to any sophistication in modelling the subgrid-scale effects. Thus while the above-mentioned Smagorinsky methodology corresponds to an algebraic turbulence model, a one-equation subgrid-scale model has been proposed by Lilly [4.32], a second-order closure by Deardorff [4.33], and novel non-linear stress-strain relations by Bardina et al. [4.34]. The reader should consult the above-mentioned reviews and the original papers referenced therein for more detail.

4.2.4.3 Dynamic subgrid-scale models

Germano et al. [4.27] went one step further in exploring the cascade idea for subgrid-scale modelling. They observed that according to standard concepts, the cascade is directed from the large to the small scales and that at the small-scale end of the spectrum the dynamics is close to self-similar. Under these conditions, an LES that resolves a considerable part of the cascade already features a suitable representation of small-scale dynamics. All that is needed to close the subgrid-scale problem is to extrapolate the computed grid-based results in a suitable fashion to the unresolved scales.

Under this premise, one should expect that the subgrid-scales act on the smallest resolved scales in a fashion that is completely analogous—except for suitable rescaling—to the action from the smallest resolved scales to the next larger ones. This latter action is accessible within the data produced in the LES computation, so that the remaining task is to find the appropriate extrapolation and re-scaling rules.

Invoking a mixing length hypothesis for subgrid-scale turbulent fluxes, the subgrid-scale stress tensor is written as

$$\boldsymbol{\tau}_{\mathrm{SGS}} = 2\,\mu_{\mathrm{SGS}}\overline{\boldsymbol{S}} - \frac{2}{3}\mu_{\mathrm{SGS}}(\nabla\cdot\overline{\boldsymbol{v}})\;\mathbf{1} \tag{4.2.39}$$

where

$$\overline{\boldsymbol{S}} = \frac{1}{2}\left(\nabla\overline{\boldsymbol{v}} + (\nabla\overline{\boldsymbol{v}})^t\right) \tag{4.2.40}$$

and where the subgrid-scale viscosity is defined as

$$\mu_{\mathrm{SGS}} = C_s\,\rho\,\Delta^2\,|\overline{\boldsymbol{S}}|\;. \tag{4.2.41}$$

This very simple approach leaves one with a single open modelling coefficient C_s that remains to be determined. The crucial new idea in dynamic modelling now is to not assign this coefficient in advance but to adjust it in a suitable fashion *dynamically* from the computed data.

It is assumed that the smallest resolved scale acts on the next larger scales in the same fashion as the unresolved scales should influence the smallest resolved scales. If that is so, the unknown coefficient C_s should be computable from resolved data only. Thus Germano et al. [4.27] introduce a second filter in addition to the original subgrid-scale filter, whose filter scale $\hat{\Delta}$ is larger than Δ. Next the $\hat{\Delta}$ filter is applied to the Δ filtered equations and it is required that the new field $\hat{\overline{\boldsymbol{v}}}$ satisfies an equation analogous to that for the $\overline{\boldsymbol{v}}$-field. Considering the combined convective and subgrid-scale viscosity terms (for constant density incompressible flows as an example) one obtains

$$\widehat{\overline{\boldsymbol{v}} \circ \overline{\boldsymbol{v}}} - 2\,C_s\Big(\Delta^2\,\widehat{|\overline{\boldsymbol{S}}|\overline{\boldsymbol{S}}}\Big) = \hat{\overline{\boldsymbol{v}}} \circ \hat{\overline{\boldsymbol{v}}} - 2\,C_s\,\hat{\Delta}^2\,|\hat{\overline{\boldsymbol{S}}}|\hat{\overline{\boldsymbol{S}}} \tag{4.2.42}$$

or, equivalently,

$$2\,C_s\,\Delta^2\,\boldsymbol{M} = \boldsymbol{L} \tag{4.2.43}$$

with the obvious definitions

$$\begin{aligned} \boldsymbol{L} &= \widehat{\overline{\boldsymbol{v}} \circ \overline{\boldsymbol{v}}} - \hat{\overline{\boldsymbol{v}}} \circ \hat{\overline{\boldsymbol{v}}} \\ \boldsymbol{M} &= \widehat{|\overline{\boldsymbol{S}}|\overline{\boldsymbol{S}}} - \frac{\hat{\Delta}^2}{\Delta^2}\,|\hat{\overline{\boldsymbol{S}}}|\hat{\overline{\boldsymbol{S}}}\,. \end{aligned} \tag{4.2.44}$$

A single equation for C_s is now extracted by contracting that equation with $\boldsymbol{M}$ and averaging the result over at least the larger filter scale $\hat{\Delta}$. Let this average be denoted by angular brackets, then

$$C_s\,\Delta^2 = \frac{\langle \boldsymbol{L} : \boldsymbol{M} \rangle}{2\,\langle \boldsymbol{M} : \boldsymbol{M} \rangle}\,. \tag{4.2.45}$$

Some conceptual problems with spatially isotropic and temporally instantaneous averages for $\langle\cdot\rangle$ have been removed by Meneveau et al. [4.35] by introducing averages along particle paths. This approach introduces an improved flow history dependence and properly accounts for strong anisotropy that may develop, e.g., in separation flows, flows over obstacles etc.. For an implementation, see Reference [4.36].

Dynamic subgrid-scale modelling has the crucial advantage that the model viscosity properly responds to local flow structures. As can be seen from the above derivation, subgrid-scale viscosity is introduced only when the Tensor $\boldsymbol{L}$ detects considerable differences between the net convective non-linear flux on the Δ-scale and the non-linear flux from the $\hat{\Delta}$-filtered velocities. If there is no small-scale activity underneath the $\hat{\Delta}$-scale, then subgrid dissipation is not invoked.

In an interesting fashion, dynamic subgrid viscosities of the Germano type respond not only to the computed flow data but also, in an intricate fashion, to the numerical method used. When a more dissipative numerical scheme is employed, the numerical dissipation automatically suppresses some of the small scale dynamics. As a consequence, the the tensor $\boldsymbol{L}$ will sense less activity than it would under a non-dissipative numerical scheme. In this fashion, the dependence of the sum-total of numerical and subgrid-model dissipation will be diminished. (Obviously, this kind of model will not and should not introduce negative viscosities under normal conditions, so that overly dissipative numerics *will* have a negative effect in smooth flow regions! The dynamic subgrid model thus does not relieve one from the demand to use high-accuracy numerical methods in general.)

4.2.4.4 Summary and qualifications

Large eddy simulation is an alternative to Reynolds-averaged turbulence modelling. It requires much higher numerical resolution and therefore is not yet applicable to very large-scale systems. To provide a scale, we cite Haworth [4.37] who predicts that LES will be routinely applicable for internal combustion engine simulations (lengths scales of order 10 cm) within the coming years. On the other hand, successful LES provides insight into the dynamics of turbulence that Reynolds-averaged flow simulations cannot offer. Since the upper range of length scales is resolved numerically, much of the non-linear chaotic dynamics of turbulence is represented and can be compared with experimental measurements. Moreover, integral-scale flow statistics can be evaluated and probabilities of selected events can be extracted. This could be of primary importance for combustion modelling as will be elucidated in a later section on LES in combustion.

The original hope that the principal tasks of modelling would be simplified has been fulfilled in the sense that, for example, high-resolution LES allows proper resolution of near-wall flows without specialized wall interaction models. The dynamic extension of the very simple Smagorinsky one-coefficient model has already brought considerable progress and success. It should be kept in mind, however, that the dynamic adjustment idea of Germano et al. can be transferred also to intrinsically more complex models (with many more free coefficients) as has been pointed out by Jimenez [4.38].

Despite this "success story" of LES , Reynolds-averaged modelling will not be replaced completely in the near future for the following reasons:

- For large-scale systems, reliable LES with sufficient resolution will be computationally too demanding for years to come.
- The detailed flow dynamics information provided by LES is simply not of interest in many applications where global statistical mean values are all that is needed.
- Large eddy simulation models are far from being fully established and proven for the tremendous range of engineering fluid mechanical applications. In particular, proper LES approaches for flows that involve additional physics, such as multiple fluid phases, strong gravitational stratification or the aero-thermochemistry of combustion are still in their infancy. For some of these systems it is, for example, not at all clear that there is a well-defined cascade, so that the LES methodology itself may become questionable.

4.2.5 Subgrid-scale Porosity Models

Many practical applications involve very complex geometries with a wide variety of obstacles such as tubes and grids. Since such obstacles may be much smaller than the enclosure, it is often prohibitively expensive to resolve each obstacle.

This problem can be addressed by implementing a sub-grid model for obstacles that are smaller than the computational grid. Subgrid models have been developed to address the flow resistance, heat transfer, turbulence generation, and the enhanced combustion resulting from the subgrid obstacles. The flow resistance is introduced as a source term in the momentum Equation $(4.2.5)_2$ after it has been averaged

and closed though a suitable turbulence model. The momentum source term can be written as

$$S_v = -\frac{\alpha}{d} C_d \frac{1}{2} \rho |\boldsymbol{v}| \boldsymbol{v} \tag{4.2.46}$$

where d is the characteristic dimension of the obstacle; C_d is the drag coefficient; and the constant, α, is a friction factor that depends on the shape of the obstacle, the number of obstacles per unit volume and the spatial arrangement of the obstacles. The above approach has been used extensively in the modelling of explosions on off-shore platforms [4.39]. The drag coefficient may be assumed to be constant for a particular obstacle shape or may vary with the Reynolds number and the Mach number of the gas flow over the obstacle. Similarly, the subgrid heat transfer can be modelled by including a heat loss term [4.40, 4.41] in the energy equation. For a dense obstacle array, the density ρ in Equation $(4.2.5)_2$ should be multiplied by a porosity factor, ϕ, which corresponds to the volume fraction occupied by the gas.

Subgrid obstacles can produce turbulence that, as discussed in the following section, can greatly increase the rate of combustion. The turbulence produced by subgrid obstacles can be modelled by adding an appropriate source term in the equation for the turbulent kinetic energy, k, discussed in Section 4.2.2. One approach is to assume that the turbulent kinetic energy produced by the obstacles is a constant fraction, C_k, of the energy loss associated with momentum loss caused by drag [4.39]. Another approach is to use a one-parameter turbulence model for a particular geometry. Sha et al. [4.40] have used this approach to model multi-phase heat transfer in tube bundles. Finally, the turbulent length scale, ℓ, required by many combustion models, is usually expressed as a fraction of a characteristic length scale, such as the size of the obstacle or the spacing between obstacles. Benchmark tests, performed for a steady flow though a finite length (5 m) of obstacles [4.39], indicate that subgrid obstacle models can provide an accurate solution inside the obstacle array. However, a grid size approaching that of the obstacles can be required to resolve the strong gradient in the turbulent flow properties immediately downstream of the obstacles.

4.3 Turbulent Combustion Models

4.3.1 Regimes of Turbulent Premixed Combustion

A coarse estimation of how a turbulent flow field and premixed combustion may interact can be generated by comparing their respective characteristic length and time scales. As a basis for the subsequent discussions, we list the major relevant scales and provide brief explanations of their physical meaning:

Scales and characteristics of fully developed turbulence:

k	Turbulent kinetic energy	Kinetic energy per unit mass of turbulent velocity fluctuations.
ϵ	Energy dissipation rate	According to Kolmogorov's theory, [4.2,4.3], the dissipation rate is characteristic for both the actual rate of molecular energy dissipation at the Kolmogorov scale and the energy transfer rate through the cascade between ℓ and ℓ_K.
ℓ	Integral scale	Largest identifiable scale of turbulent fluctuations.

$u' \sim \sqrt{2k}$	Fluctuation velocity	Characteristic magnitude of turbulent velocity fluctuations; observed at the integral scale.
$\tau \sim \dfrac{\ell}{u'}$	Integral time scale	Also called "eddy turnover time".
$\mathrm{Re}_t \sim \dfrac{u'\ell}{\nu}$	Turbulent Reynolds number	Notice this Reynolds number is based on turbulent fluctuation length and velocity scales, but *not* with the scales of the overall flow field. Reynolds numbers based on system dimensions and mean flow velocities may be orders of magnitude greater than Re_t
$\ell_{\mathrm{Kol}} \sim \left(\dfrac{\nu^3}{\epsilon}\right)^{\frac{1}{4}} \sim \ell\,\mathrm{Re}_t^{-\frac{3}{4}}$	Kolmogorov scale	Smallest identifiable scale of turbulent fluctuations. At the Kolmogorov scale, the fluctuation energy that has cascaded down from the integral scale is dissipated.
$\tau_{\mathrm{Kol}} \sim \left(\dfrac{\nu}{\epsilon}\right)^{\frac{1}{2}} \sim \tau\,\mathrm{Re}_t^{-\frac{1}{2}}$	Kolmogorov time scale	Characteristic time of motion of the smallest turbulent eddies; also inverse of a characteristic strain rate at the Kolmogorov scale.
$u_{\mathrm{Kol}} \sim \dfrac{\ell_{\mathrm{Kol}}}{\tau_{\mathrm{Kol}}} \sim u'\mathrm{Re}_t^{-\frac{1}{4}}$	Kolmogorov velocity scale	Velocity fluctuation at the Kolmogorov scale.

Scales and characteristics of aero-thermochemistry:

s_L	laminar flame speed	Characteristic propagation velocity of a laminar flame *relative to the unburnt gas*.
ℓ_F	laminar flame thickness	Characteristic thickness of a laminar flame *including* the preheat and reaction zones.
ℓ_R	laminar reaction zone thickness	Characteristic thickness of the reaction zone within a laminar flame.
$t_F \sim \frac{\ell_F}{s_L}$	Flame passage time scale	Time a laminar flame needs to pass over its own structure.

t_Q	Quenching time scale	Inverse of a typical strain rate sufficient to quench the reaction zone of a laminar flame. t_Q may also be considered as a characteristic chemical reaction time scale.

Relevant characteristic non-dimensional numbers:

$\mathrm{Re}_t \sim \dfrac{u'\ell}{\nu}$	Turbulent Reynolds number	See above
$\mathrm{Da} \sim \dfrac{\tau}{t_F}$	Damköhler number	Indicates whether chemistry is fast $(\mathrm{Da} \gg 1)$ or slow $(\mathrm{Da} \ll 1)$ relative to the integral scale turbulence dynamics.
$\mathrm{Ka} \sim \dfrac{t_F}{\tau_{\mathrm{Kol}}}$	Karlovitz number	Indicates at which point $(\mathrm{Ka} \approx 1)$ the smallest turbulent eddies penetrate into the laminar flamelet preheat zones.
$\mathrm{K} \sim \dfrac{t_F}{\tau_{\mathrm{Kol}}}$	Karlovitz Stretch Factor	Indicates at which point $(\mathrm{K} \approx 1)$ the turbulence correlation time becomes comparable with the laminar flamelet passage time ℓ_F/s_L.
$\mathrm{Kq} \sim \dfrac{t_Q}{\tau_{\mathrm{Kol}}}$	Quench-Karlovitz number	Indicates at which point $(\mathrm{Kq} \approx 1)$ the smallest turbulent eddies quench the quasi-laminar thin reaction zones.

As we follow Peters [4.42, 4.43] closely, we consider the Borghi-Diagram displayed in Figure 4.3.1-1. There are two extreme regimes. The "the well-stirred reactor regime" is characterized by limitingly slow chemistry, whereas in the "eddy breakup regime" there is infinitely fast chemistry and infinitely slow molecular transport. Notice that the conceptually possible regime of infinitely fast chemistry at finite molecular transport efficiency is not of interest for applications because this regime would correspond with infinitely fast laminar flame propagation as shown in Reference [4.44].

Well-stirred reactor regime. Here the chemistry is so slow compared to the turbulent motions that all chemical species are always locally well mixed and chemical reactions proceed essentially at a kinetics-dominated rate. Modelling in this regime will proceed by separating the processes of mixing and reaction: Turbulent mixing and convection generate statistical distributions of the aero-thermochemical scalar variables (species mass fractions, enthalpy, temperature) and chemistry progresses according to the appropriate chemical kinetic scheme in a quasi-homogeneous fashion. Because of the typical strong non-linearity of realistic chemical reaction mechanisms, modelling must generally take into account that the mean kinetic reaction rates are *not* equal to the reaction rate functions evaluated with the mean scalars. Only under extreme conditions will scalar fluctuations be sufficiently damped to allow straightforward evaluation of chemical rates with the mean values of the relevant scalars. To capture the influence of scalar fluctuations on the mean rates under more general circumstances, the most appropriate

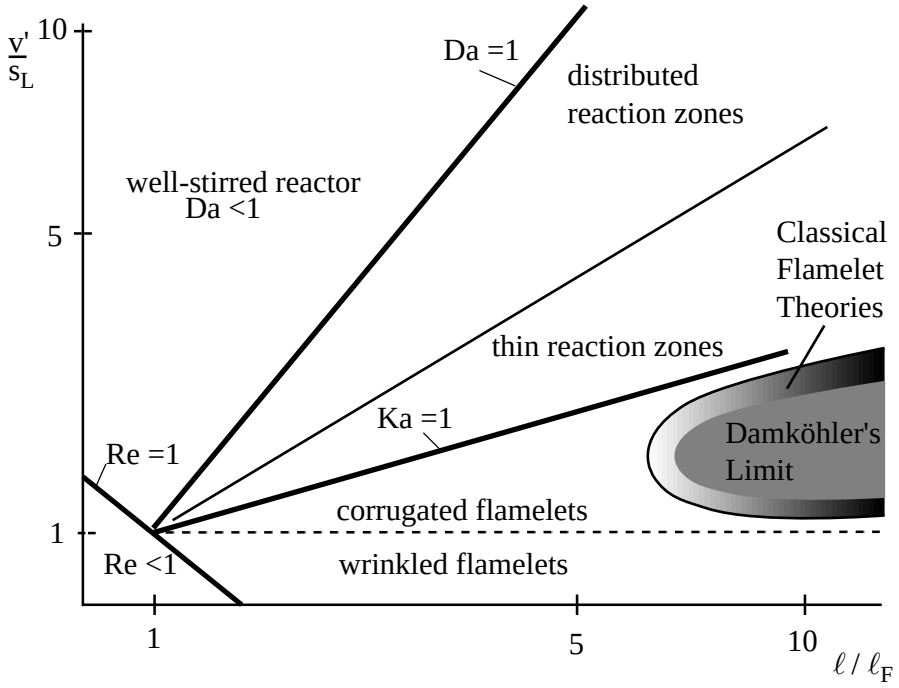

Figure 4.3.1-1: The Borghi diagram for regimes of turbulent premixed combustion

approaches include a joint probability density function (PDF) for the reactive scalars. Mean reaction rates are then evaluated by averaging the chemical rates with respect to this probability distribution. These PDF-methods are discussed in Section 4.3.7.

Eddy breakup regime. This is the opposite limit of infinitely fast chemistry and infinitely slow molecular transport. The label "eddy breakup" implies that as soon as a turbulent eddy mixes reactive gases that have suitable thermodynamic states these are burnt instantaneously. This picture of "mixed is burnt" is most appropriate for non-premixed combustion where in fact the fuel and oxidizer species can react only when brought together by molecular-level mixing. Turbulence greatly enhances this mixing process by multiple folding of the fuel-oxidizer separation layer and increasing the scalar gradients responsible for driving the molecular level diffusive fluxes. For premixed combustion, the "mixed is burnt" picture is less intuitive as fuel and oxidizer species are by definition already premixed. However, the cold reactants are unable to burn under most realistic conditions since the highly non-linear chemistry is frozen at ambient temperatures. Thus for the reaction front to progress, it is necessary that the unburnt gases be prepared for reaction on the molecular level by getting into close contact with the hot and radical-loaded burnt gases. Here, turbulent mixing comes in by multiple folding of the separation layer between unburnt and burnt gases, which is nothing but a locally one-dimensional laminar flame. Under these conditions, the turbulent flame folding determines the net reactant consumption, and the mean chemical rates are proportional to the inverse of the turbulent integral time scale τ. Modelling in the eddy breakup regime is discussed in Section 4.3.3.

Most realistic combustion systems do not satisfy the drastically simplifying assumptions underlying the two limit regimes described above. A hierarchy of increasingly complex models has been developed in recent years to cope with the fact that turbulence and chemistry generally interact on a wide range of length and time scales, depending on the specific application.

Laminar flamelet regime. This regime is similar to the eddy breakup limit in that reaction takes place within narrow, quasi-laminar flame zones. The key difference is that turbulence is not sufficiently intense to override the inherent laminar flame dynamics. On the one hand, the geometrical distortion of the flame surfaces (which may be multiple connected) is governed by both turbulent transport and laminar flame propagation dynamics. The latter includes the relative motion between flame and unburnt gases and laminar flame instabilities [4.1, 4.45]. On the other hand, the flame progression speed is perturbed by flame stretch, flame curvature, and unsteady thermodynamic conditions in the vicinity of the flame. The most important task of modelling in the flamelet regime is a proper description of the flame surface area increase, while higher-order corrections are induced by perturbations of the laminar flame structure [4.46, 4.47]. One may distinguish the "wrinkled flamelet" and "corrugated flamelet" regimes, depending on whether the inherent laminar flame dynamics or turbulent convection dominates the evolution of the flame surface.

Thin reaction zone regime. With increasing turbulence intensity, the smallest turbulent eddies decrease in size until their extension becomes comparable to the laminar flame thickness. Peters [4.43] introduces the "thin reaction zone regime" in which the laminar flame structure is disrupted by turbulent mixing, while the generally much thinner quasi-laminar reaction zones still survive. Thus the pre-conditioning process that brings the unburnt gas to thermodynamic-chemical conditions at which reaction commences is modified by turbulence, while the ultimate progress of reactions still proceeds in a locally quasi-laminar fashion. In this regime, the net rate of fuel consumption is influenced at a comparable level by both the effective reaction surface area and the turbulence-dominated pre-conditioning process. Consistent models appropriate for this regime are being introduced into numerical modelling only as this report is being compiled.

Distributed reaction zone regime. At even higher turbulence intensities, the turbulence-induced strain on the reaction zones becomes sufficient to quench them at least locally. Thus because of the intermittency of turbulence, thin reaction zone combustion and well-stirred reactor regions begin to co-exist. Currently, there are no models that would appropriately interpolate across this threshold. The most promising ansatz in this direction appears to be extended PDF methods that would properly account for the intimate coupling between reaction and molecular transport in the flamelet and thin reaction zone regimes, while keeping the option of modelling the turbulence-dominated well-stirred reactor regime.

4.3.2 Modelling Strategies: Distributed Reaction versus Reaction Fronts

Two principally different approaches to modelling the progress of turbulent premixed combustion must be distinguished. The most popular approach describes turbulent combustion by an equation system that is as close in structure to the original reactive Navier Stokes equations as possible. In this set-up the key modelled quantities are the mean volumetric reaction rates (for a characteristic reaction progress variable) and the net turbulent transport within the effective turbulent "flame brush". The interaction between mean reaction and turbulent transport then yields the overall reactant consumption rate [4.48 to 4.52].

The alternative approach considers a turbulent premixed flame as an effective reacting discontinuity. Here, the detailed internal processes within the flame brush are not resolved, but the overall reaction progress is described as being a net turbulent flame speed s_T, in analogy with the laminar burning velocity s_L, [4.53, 4.54].

Although the former approach has the advantage of incorporating detailed models of all the sub-processes within the flame brush, its disadvantage is that it actually *must* incorporate these detailed models in order

to properly function at all. The only modelled quantities for the second approach are the turbulent burning velocity s_T and suitable jump conditions for the turbulence quantities across the flame, which cannot be derived straightforwardly from the conservation principles. Its disadvantage is that there are highly unsteady combustion regimes where the internal turbulent flame structure is far from quasi-steady and the notion of a turbulent burning velocity becomes questionable in the first place.

The importance of a proper interaction between turbulent transport and net chemical reaction progress in a resolved flame brush cannot be overestimated. As pointed out, e.g., by Chorin [4.55] and by Teng et al. [4.56], the net propagation speed of deflagration wave (i.e., of a "flame") with respect to the unburnt gases depends on the detailed internal flame structure. This is in contrast to shock or detonation waves, whose propagation speed is determined solely by initial and boundary data of the flow problem (see also Section 4.5.4 below). As a consequence, the first modelling strategy described above must always incorporate proper submodels for both the mean reaction rates and the turbulent transport processes. Neglect of one of these ingredients will provoke utterly wrong results!

4.3.3 Eddy breakup and extensions

Eddy breakup models are typically formulated according the the first modelling strategy described in Section 4.3.2. It should be noted, however, that the eddy breakup limit corresponds, under the propagating flame front modelling paradigm, to Damköhler's [4.57] classical turbulent flame speed prediction,

$$s_T \sim u' \; . \tag{4.3.1}$$

High-speed combustion simulations for the large-scale RUT facility using this modelling approach have been reported in References [4.53, 4.58].

4.3.3.1 Mean reaction rate modelling

As discussed above, in this regime turbulent mixing dominates the net reactant consumption. Thus the characteristic consumption rate is proportional to the inverse of the turbulence integral time scale τ. In addition, it is known that reactions are frozen in the cold unburnt and that they cease when all the reactants are consumed. Introducing a suitably defined reaction progress variable $\tilde{c}$, with $\tilde{c} = 0$ in the unburnt gas and $c = 1$ in the burnt, the mean reaction progress is modelled as

$$\frac{\partial \bar{\rho}\tilde{c}}{\partial t} + \nabla\cdot(\bar{\rho}\tilde{c}\tilde{\boldsymbol{v}}) = \nabla\cdot(\mu_\tau \nabla\tilde{c}) + \bar{\rho}\tilde{\omega} \tag{4.3.2}$$

where

$$\tilde{\omega} = \frac{1}{\tau_{\mathrm{EBU}}}\,\tilde{c}(1-\tilde{c}) \; . \tag{4.3.3}$$

In actual numerical implementations, the determination of the turbulent characteristic time scale depends on the underlying flow turbulence model. For the most-often-used one- and two equation models—which provide a characteristic turbulent kinetic energy k and either a turbulent mixing length ℓ, a turbulent energy dissipation ϵ, or a turbulent dissipation rate ω_τ—the turbulence time scale is modelled as

$$\frac{1}{\tau_{\mathrm{EBU}}} = \frac{1}{\tau} =\sim \left(\frac{k}{\ell^2}\right)^{\frac{1}{2}} \sim \frac{\epsilon}{k} \sim \omega_\tau \; . \tag{4.3.4}$$

Obviously, this modelling strategy completely neglects chemical kinetic influences. As a consequence, these models systematically overpredict the chemical energy conversion when either chemical reactions

have not yet been ignited at all or when the well-stirred reactor regime with kinetics-dominated reaction is approached. A heuristic correction [4.51, 4.52] that, with appropriate tuning, considerably improves eddy breakup predictions simply replaces the turbulence dictated $1/\tau_{\mathrm{EBU}} = 1/\tau$ from Equation (4.3.4) with

$$\frac{1}{\tau_{\mathrm{EBU}}} = \min\left(\frac{1}{\tau}, \frac{1}{t_{\mathrm{ch}}}\right) , \tag{4.3.5}$$

where $1/t_{\mathrm{ch}}$ is a suitable estimate of the relevant slowest chemical time scale that is controlling the reaction progress. This can be either an ignition delay time for unreacted gases undergoing an auto-ignition process, or it may be a laminar flamelet quenching time scale when the transition between the eddy breakup and well-stirred reactor regimes is to be modelled in a heuristic fashion.

4.3.3.2 Turbulent transport within the flame brush

Eddy breakup models and their extensions as formulated originally in References [4.48, 4.51, 4.52, 4.59, 4.60] typically focus on the mean reaction rate model as described above. The fact, discussed in Section 4.3.2, that there must be a suitably balanced approach taking into account also the turbulent transport processes is normally neglected. The available standard turbulent transport models applied in the burnt and unburnt gases are simply transferred to the flame brush region as well.

Notice, however, that the Bray, Moss, Libby (BML) model [4.49, 4.50], which specifically addresses the issue of turbulent transport in the flamelet regime, is applicable in the eddy breakup limit as well. Thus a very sophisticated turbulent transport scheme, suited for combination with an eddy breakup approach is available in the literature. For more details on the BML model, see Section 4.3.4.2.

4.3.3.3 Summary and qualifications

Eddy breakup modelling provides a crude first approach to turbulent combustion simulations when the primary interest is in (i) worst-case estimates for high-intensity turbulence and (ii) details of the flame acceleration history from ignition to high-speed combustion are irrelevant. Heuristic extensions of EBU models to include characteristic time scales of chemistry lack a systematic derivation from first principles and should be considered as ad hoc "fixes". With suitable fine tuning of the detailed chemical time scale models, one might obtain reasonable agreement with experimental data and obtain limited predictive capabilities within the range of conditions that was used in fine tuning the models.

Much more sophisticated modelling is required to obtain true predictive capabilities both for flame acceleration and the kinetics-dominated high-turbulence intensity regime responsible for potential transition to detonation.

4.3.4 Flamelet Models

The key goals behind flamelet modelling are to incorporate effects of (i) fast but finite reaction rates, (ii) the inherent quasi-laminar flame dynamics, and (iii) the intimate coupling between chemical reactions and molecular transport that arises when rapid chemistry enforces very thin flame structures. Recent work by Peters [4.43] has revealed that in the true flamelet regime, where quasi-laminar flame structures including preheat and reaction zones actually persist, the effects of finite rate chemistry appear as perturbations only. The dominant effect to be accounted for is the inherent flamelet dynamics, including various forms of flame instability, [4.1], and the competition between self-induced flame motion and turbulent convection.

4.3.4.1 *Mean reaction rate modelling*

We distinguish again between the two principal modelling strategies from Section 4.3.2.

Flame fronts and turbulent burning velocities. Much of the flamelet modelling literature ([4.45, 4.61] and references in [4.1]) focus on deriving effective turbulent burning velocities s_T, which could readily be incorporated in numerical flame front tracking schemes [4.53, 4.54]. Given a mean laminar flamelet burning velocity $\overline{s_L}$, averaged along the flamelet surface(s), the key problem is to assess the net flame area increase that is due to the influence of turbulent convection. The net turbulent burning velocity is then expressed as

$$s_T = \frac{A}{\overline{\overline{A_{\text{eff}}}}}\,\overline{s_L}\,, \tag{4.3.6}$$

where A_{eff} denotes the net flame area of an averaged turbulent flame surface that is centred within the flame brush region, while A is the total laminar flamelet surface area for the same section of the turbulent flame brush.

The laminar and turbulent flame surface dynamics are conveniently described by a level set procedure. The flame surface is defined as the zero level set of a scalar function $G(\boldsymbol{x}, t)$ satisfying the G-equation

$$\frac{\partial G}{\partial t} + (\boldsymbol{v} + s\boldsymbol{n}) \cdot \nabla G = 0 \quad \text{on} \quad G(\boldsymbol{x}, t) = 0 \tag{4.3.7}$$

and some constraint away from the flame front, such as, [4.62],

$$|\nabla G| = 1 \quad \text{for} \quad G(\boldsymbol{x}, t) \neq 0\,. \tag{4.3.8}$$

Various different approaches towards assessing the area ratio in Equation (4.3.6) have been proposed. Fractal surface ideas have been introduced, e.g., in Reference [4.63]. Assuming the flame surface to be a fractal with dimension D one obtains expressions of the type

$$\frac{A}{\overline{\overline{A_{\text{eff}}}}} = \left(\frac{\ell}{\ell_{\min}}\right)^{D-1} \tag{4.3.9}$$

where D is the fractal dimension of the flamelet surface and $\ell_{\min}$ is the shortest characteristic length of flamelet corrugations. At the time there had been intense discussions as to whether this minimum length scale would correspond to the Kolmogorov length of the unburnt gas turbulent flow or whether this length was determined by a balance of turbulent flame advection and flame propagation relative to the unburnt. The latter approach naturally introduces the Gibson length ℓ_{G}. It is the characteristic length that is defined as the very fluctuation length scale within the turbulent energy spectrum at which the turbulent fluctuation velocity matches the laminar burning velocity [4.42]. A brief dimensional analysis based on the Kolmogorov scalings leads to

$$\frac{\ell}{\ell_{\text{G}}} = \left(\frac{u'}{s_L}\right)^3\,. \tag{4.3.10}$$

Re-normalization group procedures applied to the level set formulation from Equation (4.3.7) for the laminar flame surface motion are suggested in Reference [4.61], leading essentially to the Damköhler limit in Equation (4.3.1). Another corroboration of this result is provided by Peters [4.45], who suggests closure of the level set equation along the lines of more standard turbulence closure procedures.

As mentioned, most of these models end up reproducing Damköhler's law from Equation (4.3.1) in the limit of large turbulence intensity $u'/s_L \gg 1$ and providing some kind of interpolation down to small turbulence intensities $u'/s_L \ll 1$, in which case $s_T \sim s_L$. The net burning velocity law in these cases would read

$$\frac{s_T}{s_L} = 1 + \left(\frac{u'}{s_L}\right)^n \tag{4.3.11}$$

with some power n close to unity.

These earlier attempts have concentrated, in fact, on the limit of large turbulence intensity hoping to derive the experimentally observed sublinear growth of s_T with u' (the bending effect) solely from the flame surface dynamics under turbulence. It has only recently been clarified that this bending effect arises—most likely—not from flame surface dynamics but from a transition into the thin reaction zone regime (see Section 4.3.5).

The more important range of turbulence intensities, where $u'/s_L = O(1)$ has been largely neglected as pointed out by Bray [4.1]. Consequently, it is in this regime where new modelling ideas incorporating the inherent stability features of laminar flames are needed. Unfortunately, this regime is of primary importance for flame acceleration in the early stages after initiation of a laminar flame kernel.

Resolved flame brushes and mean reaction rates. The alternative modelling strategy has been pursued for the flamelet regime since the first introduction of the Bray-Moss-Libby model (BML), [4.49, 4.50]. Even though, these authors focus most of their attention on the proper modelling of turbulent transport in the flame brush, their principal approach follows the resolved flame brush strategy and thus they do propose closure approximations for the mean reaction rates. One major result in this context is a more systematic derivation of the eddy breakup formulae from Equations (4.3.3), (4.3.4) in the limit of high turbulence intensity. For moderate turbulence intensities, their mean reaction rate modelling is similar to more recent approaches based on "flame surface area densities", as described next.

An approach that is based on effective continuum equations for turbulent combustion in the flamelet regime (in the sense of homogenization) must provide net distributed source terms per unit volume in the finite-volume framework or per unit mass in a primitive variable formulation. A relation between these effective distributed source terms and the singular surface based sources on the flamelet microscale must be provided. This is done by introducing the "surface area density" Σ, i.e., the flamelet surface area per unit volume. The burnt gas production rate per unit volume $\tilde{\omega}$ from Equation (4.3.2) would then read

$$\tilde{\omega} = \overline{s_L}\,\Sigma\,, \tag{4.3.12}$$

and the key task of modelling is to obtain the surface area density $\Sigma(\boldsymbol{x}, t)$.

The flamelet surface evolves because of (i) convection by the unburnt gas velocity $\boldsymbol{v}_u$ immediately in front of the flamelet and the self-induced motion of the surface in its normal direction at speed s_L. Given $\boldsymbol{v}_u$ and s_L, an exact flame surface area evolution equation can be derived [4.64, 4.65]. Two alternative formulations have been proposed that are mathematically equivalent, but lend themselves to different modelling strategies:

As an example, we provide here the propagative formulation, [4.46],

$$\frac{\partial \Sigma}{\partial t} + \nabla\cdot\left(\langle \boldsymbol{v}_u + s_L \boldsymbol{n}\rangle_s\,\Sigma\right) = \langle \nabla\cdot\boldsymbol{v}_u - (\boldsymbol{n}\circ\boldsymbol{n}) : \nabla\boldsymbol{v}_u\rangle_s\,\Sigma + \langle s_L\kappa\rangle_s\,\Sigma \tag{4.3.13}$$

where $\boldsymbol{n}$ is the local flamelet surface normal, $\kappa = \nabla \cdot \boldsymbol{n}$ is the mean flamelet curvature, and $\langle \cdot \rangle_s$ denotes conditional averaging along the flamelet surface. The respective terms in this equation describe (i) the temporal accumulation of flame surface area, (ii) mean transport by the combined action of unburnt gas flow, and self-induced motion, (iii) surface stretching by the unburnt gas flow and (iv) surface stretching because of the self-induced motion of the curved flamelet surface.

The alternative "reaction-diffusion formulation" contains terms that directly correspond to those in Equation (4.3.13), but these are cast into a form that more resembles a standard reaction-diffusion equation as implied by its name. It is a matter of modelling strategies and numerical techniques, as to which of the formulations is actually used.

Obviously, most of the terms in these flame surface area density equations are not known exactly in a turbulent flow, so that the resulting equation needs closure [4.66 to 4.70]. Vervisch and Veynante, [4.46] provide an excellent summary of various modelling approaches as well as their numerical and experimental validation in References [4.71] and [4.72], respectively. Various aspects of observations from direct numerical simulations and experiments are well reproduced by the modelled flame surface area equations.

Unfortunately, the key ingredients of inherent flamelet stability, which become important under moderate turbulence intensities are not yet considered in these models [4.1].

4.3.4.2 Turbulent transport within the flame brush

It is remarkable that there is only one serious strain of work, originally authored by Bray et al. [4.49] and Bray et al. [4.50], that aims at a systematic assessment of combustion-induced modifications of turbulent transport. This is particularly disturbing in light of the outstanding importance of the effective transport for the net combustion rates, (see Sections 4.3.2 and 4.5.4).

Bray et al. [4.49, 4.50], and Bray and Peters [4.47] start off by observing that in the flamelet regime the probability of actually landing within a flamelet is extremely low, even within the turbulent flame brush. (See also References [4.1, 4.73].) The reason is that—by definition of the regime—preheating and combustion are concentrated within asymptotically thin layers that occupy only a small amount of space. Based on this observation, they conclude that the probability density of a characteristic reaction progress variable c, say, must be of the form

$$P(c; \boldsymbol{x}, t) = \alpha(\boldsymbol{x}, t)\, \delta(c) + \beta(\boldsymbol{x}, t)\, \delta(1 - c) + \gamma(\boldsymbol{x}, t)\, f(c; \boldsymbol{x}, t) \tag{4.3.14}$$

where $\delta(\cdot)$ is the Dirac-delta distribution, $f(c; \boldsymbol{x}, t)$ is an order $O(1)$ function, whose detailed form is not specified, and where the coefficients α, β, γ satisfy the *crucial* estimates

$$\alpha, \beta = O(1) \qquad \text{but} \qquad \gamma \ll 1\,. \tag{4.3.15}$$

The progress variable varies from $c = 0$ in the unburnt gas to $c = 1$ in the burnt, so that $\alpha(\boldsymbol{x}, t), \beta(\boldsymbol{x}, t)$ correspond to the probabilities of finding unburnt and burnt gas conditions, respectively.

After introduction of conditional averages $\overline{\cdot}^u, \overline{\cdot}^b$ with respect to unburnt and burnt conditions and heavily using the fact that $\gamma \ll 1$, the authors arrive at asymptotic formulae for the turbulent transport terms such as $\widetilde{\boldsymbol{v}'' c''}$ in the Favre-averaged turbulent transport equation for the reaction progress variable or $\widetilde{\boldsymbol{v}'' \circ \boldsymbol{v}''}$ in the momentum equations

$$\widetilde{\boldsymbol{v}'' c''} = \tilde{c}\,(1 - \tilde{c})\,(\overline{\boldsymbol{v}}^b - \overline{\boldsymbol{v}}^u) \tag{4.3.16}$$

and

$$\widetilde{\boldsymbol{v}'' \circ \boldsymbol{v}''} = (1-\tilde{c})\,\overline{\boldsymbol{v}' \circ \boldsymbol{v}'}^{u} + \tilde{c}\,\overline{\boldsymbol{v}' \circ \boldsymbol{v}'}^{b} + \tilde{c}\,(1-\tilde{c})\,(\overline{\boldsymbol{v}}^{b} - \overline{\boldsymbol{v}}^{u}) \circ (\overline{\boldsymbol{v}}^{b} - \overline{\boldsymbol{v}}^{u})\;. \tag{4.3.17}$$

It should be noted that in a natural way, this theory suggests the introduction of Reynolds stress models, as the primary quantities appearing here are the Reynolds stresses themselves. One does *not* obtain any formulae justifying a gradient transport approximation.

In fact, an interesting observation concerns the counter gradient transport. (cf. [4.72]). In a regime of not too intense turbulence, one may expect that the conditional mean velocities $\overline{\boldsymbol{v}}^{u}$ and $\overline{\boldsymbol{v}}^{b}$ will differ by the thermal expansion induced within the turbulent flame brush, i.e.,

$$\overline{\boldsymbol{n}} \cdot (\overline{\boldsymbol{v}}^{b} - \overline{\boldsymbol{v}}^{u}) \approx -s_T\,(\frac{\rho_u}{\rho_b} - 1) < 0\;, \tag{4.3.18}$$

where $\overline{\boldsymbol{n}}$ is the mean flame front normal pointing towards the unburnt gases. From the sign of this expression, we conclude that the net turbulent scalar transport of c will be directed towards the *burnt* gases. On the other hand, $c = 1$ in the burnt and $c = 0$ in the unburnt gases, so that a standard gradient transport approximation would yield

$$\overline{\boldsymbol{n}} \cdot (-D_t \nabla \tilde{c}) > 0 \tag{4.3.19}$$

so that the standard approximation would predict transport towards the *unburnt* gases. This somewhat surprising result is neglected in practically all turbulent combustion models that are not derivatives of the Bray, Moss, and Libby approach!

Veynante et al. [4.74] have closely analyzed direct numerical simulations by Rutland and Trouvé [4.75] and Trouvé et al. [4.76], which are set up in different regimes of turbulence intensity and surprisingly imply contradictory conclusions about the presence or not of countergradient transport. Veynante et al. conclude (see also [4.46]) that *both* numerical simulation results are nevertheless compatible with the BML formalism explained above: It turns out that the underlying presumption leading to the sign in Equation (4.3.18), namely that the *conditional* mean velocities within the flame brush satisfy an overall estimate based on the total thermal gas expansion, becomes less and less accurate as the turbulence intensity increases. For high turbulence intensities, turbulent mixing dominates the expansion-induced separation of burnt and unburnt gases and the net scalar transport changes sign.

Thus one may conclude that less-sophisticated modelling approaches based on standard gradient transport approximations throughout the combustion region will yield reasonable results for high-speed flames. But, as observed previously, the regime of low-to-moderate intensity turbulence, which is most crucial for the initial stages of flame acceleration, is not properly represented by such simplified schemes.

4.3.4.3 Statistical evaluation through presumed PDFs

The flamelet ansatz introduces strong statistical correlations between various flow variables and transport fluxes. The knowledge that molecular diffusion always occurs in conjunction with chemical reaction simplifies statistical evaluations considerably. Given a characteristic coordinate c that resolves the flamelet structures (such as a normalized reaction progress variable), chemical reaction source terms, diffusive fluxes, species concentrations etc. can all be expressed explicitly in terms of c and a few additional parameters $\boldsymbol{\chi}$ characterizing the flamelet structure (such as an outer strain or the flamelet surface curvature). Statistical averages of any such quantity $Q(c)$, say, can then be obtained if a probability density for c and the flamelet parameters is available:

$$\overline{Q}(\boldsymbol{x}, t) = \int\!\!\int Q(c)\, P(c; \boldsymbol{\chi}; \boldsymbol{x}, t)\, dc\, d\boldsymbol{\chi}\;. \tag{4.3.20}$$

Now we will see in Section 4.3.7 below that a full-fledged model describing the time evolution of such a PDF is extremely complex and that its introduction at the level of flamelet models would destroy their appealing simplicity.

The standard compromise here is to introduce presumed PDFs. One a priori assumes that the PDF will have shapes close to a certain class of representative functions that have few free parameters. Thus given those parameters, the PDF is known. Next, one derives governing equations for those free parameters, solves these (or their closed counterparts) numerically, and uses the obtained fields of parameters to locally define the presumed PDF.

The typical "β-PDF", [4.46, 4.77], has two free parameters, which can be related uniquely to mean and standard deviation of the distribution. Under these conditions it is sufficient to obtain appropriate estimates of the mean and of the fluctuations in order to determine the probability distribution. In the "presumed PDF approaches" one introduces, in fact, in addition to a transport equation for the turbulent mean of c an additional model equation for the standard deviation. These equations can formally be derived rigorously, but the resulting terms generally need closure. In summary, a presumed PDF model requires one additional equation for the turbulent scalar fluctuations, while avoiding the complexities of a full PDF transport equation.

Presumed PDF models are very popular in the context of flamelet, thin reaction zone, and the various conditional moment closure approaches.

4.3.4.4 Summary and qualifications

Flamelet models provide a systematic methodology, based on first principles, to address turbulent combustion modelling in a regime that covers the eddy breakup limit. Combustion is still concentrated in narrow fronts, but the length, time, and velocity scales of thin flame dynamics begin to non-trivially interact with the flow turbulence. Following recent arguments by Peters [4.43], the interaction of the self-induced flame geometry evolution—including flame instabilities—with turbulent convection is the most important aspect in the flamelet regime.

Promising and successful models for the mean volumetric chemical reaction progress, for effective turbulent flame speeds as well as for the modifications of turbulent transport by combustion have been proposed and widely tested. A host of flamelet models cater to various different numerical simulation strategies, such as reaction-turbulent diffusion type of modelling or flame front tracking approaches (see Section 4.5).

Unfortunately, most of the modelling efforts have been focused on the regime of high-intensity turbulence where turbulent motions dominate over the intrinsic flamelet dynamics. As previously stated, this is not the regime where flamelet models are most suitable [4.43]. As a consequence, the regime of low-to-moderate intensity turbulence, which is most important for the early stages of flame acceleration, is still in its modelling infancy.

The intimate interplay between reaction progress and turbulent transport that is crucial for the establishment of overall combustion rates has widely been neglected, except in the seminal work by Bray, Moss, Libby and their co-workers. It is of outmost importance that further developments of the flamelet theory for the low-to-moderate turbulenc intensity regime will include proper turbulent transport models from the start.

4.3.5 Thin Reaction Zones

As turbulence levels increase, one moves up vertically in the Borghi diagram from Figure 4.3.1-1 and approaches the line $\mathrm{Ka} = 1$. At this point the smallest fluid mechanical eddies (on the Kolmogorov scale) are comparable in size to the laminar flame preheat zone thickness, and these eddies will begin to non-trivially distort the laminar flamelet structures. Recent observations from direct numerical simulations by Poinsot et al. [4.78] indicate that this does not immediately imply a breakdown of all determinstic structures and the transition to the regime of truly distributed reactions. Rather, they continue to observe very strong correlations between reactions and molecular transport for Karlovitz numbers much higher than $\mathrm{Ka} = 1$.

Peters [4.43] independently argues that one must distinguish a complete laminar flame from its reaction zone. A laminar flame alway includes a reaction zone, but thin reaction zones may well exist without a flamelet's quasi-oned-imensional, quasi-steady preheat zones. In fact, since the reaction zones of laminar flames are typically thinner by an order of magnitude than the preheat-reaction zone complex of a laminar flamelet, one may expect thin reaction zones to exist up to much higher Karlovitz numbers than are necessary to disrupt the preheat zones.

Peters [4.43] proposes a new theory for turbulent premixed combustion that includes this new ansatz of "thin reaction zones" and unifies it with the classical flamelet ansatz. Implementations of this theory are current work in progress, so that no details will be given here. It may suffice to mention the probably most important result of this theory, namely a consistent explanation of the "bending effect" in turbulent premixed combustion: It is found experimentally that effective turbulent burning velocities do not follow Damköhler's limit of $s_T \sim u'$ for large turbulence intensities. One rather finds a sublinear growth and even a decay of the effective flame speed for very intense turbulence. The "classical" flamelet ansatz, which accounts for combustion in only quasi-laminar, quasi-one-dimensional flamelets, does not predict this bending. Rather, as pointed out earlier, the limit of classical flamelet theories for large turbulence intensities *should* be the Damköhler law, which in turn is equivalent to the eddy breakup limit.

The new theory in Reference [4.43] includes the effect of intense stirring within the preheat zone in front of the "thin reaction zones". Multi-dimensional turbulent fluctuations are accounted for when modelling the fluxes of species and heat into and out of the reaction zones. A formulation, based on the the G-equation or level set approach is developed that successfully unifies earlier flamelet theories and the new theory for the thin reaction zone regime. Limit considerations for quasi-stationary turbulent flames also lead to a new and unified effective turbulent burning velocity law.

4.3.6 Conditional Moment Closures

The ansatz of "conditional moment closure" was first introduced by Bilger [4.79]. Noticing that the typical fast chemistry of combustion reactions induces strong statistical correlations between reaction, diffusion, and convection, he proposed to systematically build combustion closure models by introducing statistical moments that are conditioned on selected characteristic reaction variables. Thus, for example, a vector of mean reaction rates is expressed as

$$\overline{\dot{\omega}} = \int_0^1 P(c)\, dc \tag{4.3.21}$$

where

$$\langle \boldsymbol{\omega} | c \rangle = \int_\xi \boldsymbol{\omega}(\xi, c) P(\xi|c)\, d\xi \tag{4.3.22}$$

is the conditional average of the reaction rate vector for a given value of the reaction progress variable. The variable ξ represents other quantities that the local reaction rate may depend on, such as temperature, other species concentrations etc..

The advantage of this approach is the following: If strong correlations between reaction rates and a structure variable such as c exist, and if these correlations capture the strongest fluctuations of the variable to be averaged, then modelling is greatly simplified: Conditional averages as in Equation (4.3.22), e.g., be approximated by simple evaluation at the mean state (conditioned on c) and all the statistics is covered by the probability density $P(c)$ in Equation (4.3.21).

This ansatz automatically captures the classical flamelet theories for premixed as well as non-premixed combustion and this author is convinced that it also describes the essence of the new theory of "thin reaction zones" formally. However, one should be aware that the formulae in Equations (4.3.21), (4.3.22) are mere formal representations that, all by themselves, do not yet represent a turbulent combustion closure. In order to actually evaluate these formulae, one must introduce concrete specifications regarding $P(c)$ and regarding the evaluation of Equation (4.3.22).

Thus specific closure models for the detailled distributions of, say, $\boldsymbol{\omega}$ with respect to the key progress variable c are to be invoked. It is at this point, where the formal framework of conditional moments must be backed by physical insight. Obvious candidates for the physical closure are flamelet models for premixed and non-premixed combustion, or one my borrow from the new thin reaction zone theory in Reference [4.43]. A wealth of publications is available that covers various modelling approaches as well as comparisons with experimental observations (see e.g., [4.80 to 4.82, 4.82] or [4.1]).

4.3.7 Statistical Modelling Based on a PDF Evolution Equation

Flamelet, thin reaction zone and conditional moment closure models all try to explore the fact that under many realistic conditions chemistry is fast and imposes strong correlations between those variables that describe the chemical reactions. This presumption, however, becomes inapplicable when Damköhler numbers decrease to order $O(1)$ or smaller. In this case, chemistry will generally still be stiff and fast enough to leave local traces in the form of strong fluctuations, but it is no longer strong enough to dominate the evolving flow structures. In this situation, a more general approach is needed that does not rely on a priori knowledge about statistical correlations.

4.3.7.1 The general PDF ansatz

Pope [4.83] has laid the foundation for a turbulent combustion modelling strategy that differs significantly from the other approaches described earlier. From the start, he assumes an inherently statistical nature of turbulent combustion and introduces a joint PDF—in the most general case involving all reactive and thermodynamic scalars as well as the flow velocities. The idea then is to model the temporal evolution of this probability density, say $P(\boldsymbol{Y}, p, T, \boldsymbol{v}; \boldsymbol{x}, t)$, and to obtain the measurable statistical means and correlations by integrating suitable moments of the PDF.

An involved derivation leads to the following exact PDF evolution equation [4.83]

$$\frac{\partial P}{\partial t} + \boldsymbol{v} \cdot \nabla_{\boldsymbol{x}} P + \boldsymbol{\omega}(T, p, \boldsymbol{Y}) \cdot \nabla_{\boldsymbol{Y}} P = \mathrm{MolecularTransport} \tag{4.3.23}$$

The first term denotes accumulation of probabilities, the second denotes transport in physical space by

the (fluctuating) velocities, the third describes deformation of the PDF because of chemical reactions, and the term on the left-hand side is responsible for the effect of molecular scale mixing (heat conduction, diffusion, etc) on the PDF.

Notably, the chemical reaction term is *closed*; that is, since all the arguments of $\boldsymbol{\omega}$ in Equation (4.3.23) are *in*dependent variables for the PDF, the "convection velocity" in the space of the reactive scalars is an explicit function that depends on the arguments of, but not on the PDF itself. This observation is absolutely crucical and is the reason for the considerable attractiveness of PDF models. While in other turbulent combustion closures one goes to great lengths in constructing expressions for the mean chemical reaction rates, one gets the analogue in PDF equations for free!

Even more striking, but less used in practice, is the fact that the convective term $\boldsymbol{v} \cdot \nabla_{\boldsymbol{x}} P(\boldsymbol{Y}, p, T, \boldsymbol{v}; \boldsymbol{x}, t)$ is also *closed*! The velocity, too, is an independent variable for the PDF, and hence the vector $\boldsymbol{v}$ in this expression is a known quantity. Hence the only term to be modelled is the microscopic molecular transport term on the right-hand side of Equation (4.3.23). To be clear, the convective transport term includes turbulent convection. Thus a full-fledged PDF-model that includes the velocity components as independent variables does not require a turbulence closure in the standard sense. Only those effects taking place at the very smallest scales on the level of molecular transport do require modelling.

As astounding and attactive as this property of joint PDF models might be at a first glance, it is not explored in many applied modelling systems. The reasons are that this kind of formulation does not fit into any of the more standard flow simulation frameworks, where the standard momentum balances are discretized and solved computationally. In addition, PDF implementations are computationally extremely demanding, simply because of the high dimensionality of the problem posed: The space of independent variables for the PDF comprises three space coordinates, time, three velocity coordinates, and as many additional independent scalars as there are independent chemical concentrations. Solving a partial differential equation in more than six-dimensional spaces by standard techniques is utterly unfeasible given the expected computational capacities for the coming decade. A compromise that saves at least the advantage on closed reaction terms will be summarized shortly.

The only contribution in Equation (4.3.23) that does require closure is the term on the right-hand side, which is induced by molecular transport. As molecular transport fluxes are driven by gradients of the relevant species, an exact and consistent PDF model description would require multi-point statistics [4.83]. This is generally avoided because it would increase the computational costs even further. Thus a number of mixing models have been developed in recent years that attempt to approximate the mixing term by known terms that only involve the one-point PDF, (see [4.83]).

4.3.7.2 Reduction of complexity by turbulence closure

Most flow simulation and combustion codes that are readily available (commercially or as research codes) rely on discrete integration of the balance equations of mass, momentum, and energy in addition to a set of species transport and reaction equations. Generally, modelling systems are developed "bottom up" by first implementing a flow solver and then adding the effects of chemistry with increasing complexity. To save considerable computational capacities and to avoid the effort of new code implementations of major dimension, a compromise is often introduced to simplify the PDF Equation (4.3.23)—albeit at the cost of greater uncertainty or imprecision. The idea is to consider the joint PDF for the reactive scalars and thermodynamic variables $P(\boldsymbol{Y}, p, T; \boldsymbol{x}, t)$ only. In this case, the convective term in Equation (4.3.23) can no longer be expressed explicitly in terms of the arguments of the PDF, but must be modelled. In

the most popular approach, which couples the PDF evolution to a standard flow turbulence model, one replaces the velocity $\boldsymbol{v}$ by its turbulent mean $\overline{\boldsymbol{v}}$ and fluctuations $\boldsymbol{v}''$, so that the PDF convection term becomes

$$\boldsymbol{v} \cdot \nabla_{\boldsymbol{x}} P = \overline{\boldsymbol{v}} \cdot \nabla_{\boldsymbol{x}} P + \overline{\boldsymbol{v}'' \cdot \nabla P} \, . \tag{4.3.24}$$

Given a mean velocity field $\overline{\boldsymbol{v}}$, computed by a standard turbulent flow model, the first term is closed. The second term denotes the statistical mean overall velocities of transport deviating from the mean motion. This turbulent transport term requires closure and again a number of closure models have been proposed (see e.g., [4.83,4.84]). This present simplification of the PDF modelling approach does not affect the key advantage of a closed reaction progress term as described above. Yet it allows a much easier embedding of the reaction modelling strategy in existing computational fluid dynamics (CFD) codes.

4.3.7.3 Regime of applicability and extended models

In assessing the regime of applicability of PDF models, one realizes that the key advantage of a closed reaction term is at the same time a limiting factor in applications: The tight statistical correlation between chemical activity and molecular transport, as observed above for flamelets and in the thin reaction zone regime, is by construction neglected in the PDF ansatz. The closures of the molecular mixing and turbulent transport terms are uncorrelated with the reaction progress in most PDF models, whereas in these quasi-deterministic regimes of combustion they are absolutely crucial and, in fact, are the fundamental basis of turbulent combustion modelling. As a consequence, without further modification, the regimes of applicability of PDF and flamelet or thin reaction zone models are disjoint.

Since most practical engineering applications belong to the flamelet regime, various efforts have been undertaken to extend the regime of applicability of PDF models. Anand and Pope [4.85] split the molecular transport term into 2 contributions. One corresponds to uncorrelated mixing of fluid away from chemically active zones, whereas the other incorporates the quasi-deterministic nature of reaction fronts in the flamelet and thin reaction zone regimes. Alternatives have been proposed, but a convincing unified framework for bridging the gap between flamelet and PDF models is still pending.

4.3.7.4 Monte Carlo simulation

As mentioned above, the dimensionality of the argument space of a PDF for combustion applications is large. In particular, it increases with the number of chemical species to be traced and, in realistic systems, can easily reach eight or more dimensions. Traditional discrete solution methods for partial differential equations lead to an exponential growth of computational requirements with the number of argument space dimensions, and hence quickly to unfeasible conditions.

A solution to this problem comes from Monte Carlo simulation. The PDF is implicitly represented by a cloud of quasi-Lagrangian particles in state space. A large set of state vectors is initialized, and the probability to find a state within a given subcell of the state space is set equal to the number of discrete particles within that cell divided by the total number of particles available. The time evolution of the PDF according to the evolution Equation (4.3.23) is mimicked by letting the particle states evolve in time in a suitable fashion. Pope [4.83] discusses how suitable actions on the particle states lead to an associated evolution of the discrete distribution that correspond in the limit of large particle numbers to the differential operators in the PDF equation.

It turns out that the computational effort of a Monte Carlo method grows *linearly* with the number of dimensions of the state space, so that PDF-based simulations become feasible for systems that are larger

than systems with the most simplified one- or two-step chemical models.

The closure models from References [4.83, 4.84] for molecular mixing and turbulent transport are also formulated as actions on particle states rather than state space (integro-) differential operators.

4.3.8 Large Eddy Simulation

Large eddy simulation for combustion problems is becoming increasingly popular for the same reasons explained in the context of LES for non-reacting flows. Considerable complications arise, however, because combustion processes considerably affect the turbulent flow structures. The general idea of dynamically computing all fluctuations on the largest turbulent scales, while modelling only those phenomena whose scale falls below the grid resolution is kept. However, major uncertainties remain as to what is the appropriate mathematical description of a turbulent flame on the smallest resolved scale. Vervisch and Veynante [4.46] list at least three different approaches that are currently pursued by various research groups:

1. *Artificially thickened flame fronts* [4.86]. Here, a modification of effective transport coefficients and reaction rate coefficients is introduced that artificially thickens the laminar flame structure so that it can be resolved on the given computational mesh, but in such a manner that a given effective flame speed is maintained. Combustion is then treated on the resolved scales as if it were laminar. The effective flame speed is the key quantity to be "subgrid modelled", because it is responsible for the increase of net combustion rates over the laminar case. A consistent dynamic subgrid-scale model is not yet available.

2. *G-equation or level set approaches* [4.87, 4.88]. Here the flame is treated at the resolved scale as a reactive discontinuity, and again the key quantity to be modelled is the effective turbulent burning velocity for that scale. This approach appears most consistent with dynamic subgrid-scale models, because there is a direct link between the quantity to be modelled and what is actually computed on the grid: The effective turbulent burning velocity is essentially proportional to the turbulent flame area increase that is due to subgrid-scale wrinkling and corrugation. The flame front wrinkling on the scales larger than the resolved ones is actually simulated by the level set approach and can be extracted by Germano-type filtering techniques. Hence a dynamic subgrid-scale model appears as a natural candidate. Despite these conceptually appealing properties, a successful closed formulation is still work in progress. Notice also that this approach requires a numerical flame front tracking method, which is considerably more complex than the standard reactive Navier-Stokes solver (see Section 4.5.5 below).

3. *Resolved flame structure in combination with flame surface area density modelling* [4.89]. Conceptually, this approach combines the advantages of the easier-to-implement resolved flame structure numerics with the flamelet idea of connecting turbulent flame speeds with effective flame surface areas. Explicit subgrid-scale closures can be tranferred from Reynolds-averaged turbulent combustion models. A conceptual difficulty arises for dynamic subgrid-scale modelling of the Germano type, because the key quantity to be extracted by filtering—namely the flame surface wrinkling—is not readily available on the smallest resolved scales. As the flame structure is represented by, say, five grid points one would have to go up to length scales of tens of grid points in each space direction to actually "see" the flame front wrinkling. That basically destroys the appeal of dynamic subgrid-scale modelling.

Large eddy simulation for combustion applications is gaining momentum in research at an increasing rate, but it cannot be considered "state of the art" by any means at this stage.

4.3.9 Reynolds' Averaging, LES, and PDFs in the Context of DDT

We include some principal considerations regarding the interpretation of results produced by the various modelling approaches described in this section. The key question that is addressed here is the following:

- What can and what cannot be concluded from any given simulation based on a Reynolds-averaged, LES or PDF simulation?

Two extremes elucidate the point: In the first example, we consider a non-reactive incompressible, constant density steady flow over a flat plate. In this case, a Reynolds-averaged computation will yield a steady-state (turbulent mean) velocity profile without visible fluctuations in the computed data. Even though all fluctuations are averaged out by definition, the mean velocity distribution may well be expected to be close to the velocities that one would measure in an experiment. In a typical situation, turbulent fluctuations may be expected to amount to about 10% of the local mean velocities. Thus the computation yields good insight into what would go on in an actual experiment.

A large eddy simulation would, even for steady-state mean flows, never approach a steady state. Persistent instabilities would provide for sustained fluctuations. Because of the chaotic nature of turbulence, one may not expect, however, to compute fluctuations that can—by time of occurance and location—be measured in an experiment. All one may expect from LES is to obtain an impression of the magitude of the fluctuations and hints at the local fluidmechanical mechanisms that are responsible for sustaining the fluctuations. Nevertheless, a single LES would exhibit many features that could directly be measured in an associated experiment, including mean values (upon time averaging), fluctuation levels, and their correlations.

The situation can change dramatically for a simulation of DDT in a mixture that is close to the DDT threshold. Depending on stochastic details of the initial and boundary conditions, the exact location and time of detonation birth will be highly irreproducible. Under suitable circumstances, DDT might even be suppressed. Thus within the ensemble of possible flows for a given set-up, there are subclasses that drastically differ from one another, with a range from "no combustion at all" to "detonation".

Assume for a moment that existing turbulence closures for Reynolds-averaged models would be appropriate in this case at all. Then, the resulting fields from a Reynolds-averaged model computation must be interpreted with great care, nevertheless. How close would the computed fields be to *any* single experimental observation? The answer is not at all! These averaged computations would loose their guiding role in "assessing what could happen" completely, and they take on a role of "exhibiting what a large number of nearly equal experimental runs would do to the mean"! It is clear that an experimental verification and validation of such a model would have to include a large number of measurements, and it remains unclear whether the computed results would be of any value to the design engineer.

For LES, the situation is more subtle. Depending on the nature of the "trigger" that is responsible for establishing the various different paths of evolution, an LES may or may not be interpretable as "close to direct experimental observation". If it is subgrid processes that trigger changes of the evolution path, then the same qualifications given for Reynolds-averaged modelling above hold also for LES. If, however, the

relevant processes occur on the resolved scales, then LES would be able to map out the different possible solution classes and yield representative results for each of them.

Provided again that subgrid models are suitable for the task, PDF models are most generally applicable, and there is little uncertainty regarding the interpretation of results. If the ensemble of possible solutions is made up of largely differing subclasses, then a computed PDF should therefore exhibit peaks or clusters. Interestingly, one cannot, from the standard one-point PDF, reconstruct the solution classes, though. Assume, for example, that the PDF shows bimodal distributions of the reaction progress variable in two different corners of a room in which combustion has taken place. Then, one cannot decide which combinations of

- no burn at all
- corner 1 burnt, corner 2 unburnt
- corner 1 unburnt, corner 2 burnt
- full burnout

are really achieved and are defining the possible sub-classes of solutions. The reason is that a one-point PDF does not allow one to assess spatial correlations!

4.4 Chemical Kinetics in Turbulent Combustion

For most practical purposes, the progress of chemical reactions is much less complex than one might expect on the basis of the overwhelming complexity of detailed chemical kinetic systems. A wide range of approximate modelling techniques has been developed in recent years. Their common goal is to filter from detailed kinetics only the minimal information needed to describe a given phenomenon of interest while discarding any complexity that is of minor importance. Depending on the phenomenon considered, the resulting simplified chemical model will generally be of varying complexity.

If, for example, only the auto-ignition delay of a reactive mixture is of interest, but not the subsequent details of the chemical energy conversion processes, then one can generally capture the essence with a single-step reaction model. A counter-example comes, for example, from automotive engine design. In addition to the dynamics of laminar flamelets, including their quenching limits, one is interested in pollutant formation levels during turbulent combustion. Accurate descriptions of all the relevant subprocesses require quite sophisticated kinetic models, even though considerable simplifications relative to detailed elementary kinetics are still possible, (see [4.90, 4.91]).

Pollutant formation processes should be of minor importance for the present topic of FA and DDT. However, the kinetics of auto-ignition, flamelet propagation, flamelet quenching etc. are of primary interest and require careful consideration.

4.4.1 Simplified Closures for Time Scale Transitions

In the context of the "regimes of premixed turbulent combustion" we have seen in Section 4.3.1 that transitions from chemistry-dominated to turbulence-dominated combustion must be expected. Chemical

kinetics becomes rate-limiting when turbulent mixing is so intense that reactions proceed locally in a quasi-homogeneous environment. In that case, reaction progress can well be modelled by straightforward chemical kinetics evaluated at the turbulent mean state. As turbulence intensities decrease, chemistry will become more intermittent and the mean reaction rates will diverge considerably from "chemical kinetics at the mean state". Yet, turbulent mixing will still be sufficiently intense to inhibit the formation of coherent structures with correlated chemical kinetic and transport sub-structures. This is the standard regime for applications of PDF methods. Chemical kinetics may be described in this regime by "reaction of individual Monte Carlo particles". No tight coupling to molecular transport is to be expected.

As turbulence intensities decrease further, one will observe the establishment of strong correlations of reaction and molecular transport, indicating the transition into the "thin reaction zone" and "flamelet" regimes.

In a coarse, leading order model for fast turbulent combustion, one may want to include only the two extreme cases of (i) infinitely fast chemistry plus high intensity turbulence and (ii) infinitely high turbulence intensity. As discussed earlier, these extremes correspond to the eddy breakup and to the well-stirred reactor regime, respectively. A typical flame acceleration process would start in the eddy breakup regime and, as the self-induced turbulence intensity increases, would transition to the well-stirred reactor type of combustion.

Kochurko et al. [4.51] and Breitung et al. [4.52] use a simple modification of the eddy breakup strategy in order to capture the essence of that transition. The mean reaction rate for an energy carrying progress variable is written as

$$\overline{\omega} = \frac{1}{\tau}\,\tilde{c}\,(1-\tilde{c})\;, \tag{4.4.1}$$

with a dynamic adjustment of the reaction time scale τ. For a given gas mixture with species mass fractions $\boldsymbol{Y}$, the auto-ignition delay time $t_{IGN}(\boldsymbol{Y})$ can be computed from detailed chemical kinetics and stored in either a table or in the form of an interpolation formula. A standard compressible k-ϵ model provides the integral time scale of turbulence as $\tau_t = k/\epsilon$. Now the reaction rate time scale τ from Equation (4.4.1) is simply determined as

$$\frac{1}{\tau} = \min\left(\frac{1}{t_{IGN}}, \frac{1}{\tau_t}\right)\;. \tag{4.4.2}$$

Obviously, any additional information on the important sub-processes that are available from theory or through heuristic arguments can be incorporated in such a simplified approach. One may, for example, consider the characteristic quenching time scale of laminar flamelets as the critical chemical time with which to compare the turbulent integral scale.

Practical implementations [4.51, 4.52] show that this approach does allow one to capture the qualitative behaviour of combustion in the limit of high turbulence intensity. Yet, a satisfactory formulation that would cover a wide range of mixture compositions, initial conditions etc. without fine tuning seems unachievable.

4.4.2 Semi-heuristic Reduced Chemical Kinetics

A more systematic approach is "standard reduced chemical kinetics" based on steady-state and partial equilibrium assumptions. The key ideas can be formulated by considering the system of ordinary differential equations for n_{spec} chemical species represented by their mass fractions $\boldsymbol{Y} = \{Y_i\}_{i=1}^{n_{\mathrm{spec}}}$. The

system

$$\frac{dY_i}{dt} = \sum_{r=1}^{n_{\rm reac}} (a_i^{r,+}\,\omega_r^+(\boldsymbol{Y}) - a_i^{r,-}\,\omega_r^-(\boldsymbol{Y}) \qquad\qquad (i = 1, n_{\rm spec}) \tag{4.4.3}$$

represents a detailed chemical kinetic scheme with $n_{\rm reac}$ reactions.

A **partial equilibrium** assumption states that for one of the elementary reactions the forward and backward rates are in an approximate balance. Thus

$$\frac{\mid \omega_r^+(\boldsymbol{Y}) - \omega_r^-(\boldsymbol{Y}) \mid}{\max\left(\mid \omega_r^+(\boldsymbol{Y}) \mid, \mid \omega_r^-(\boldsymbol{Y}) \mid\right)} \ll 1\,. \tag{4.4.4}$$

In this case, one obtains at leading order an approximate *algebraic* relation between the vector components of $\boldsymbol{Y}$ of the form

$$\omega_r^+(\boldsymbol{Y}) - \omega_r^-(\boldsymbol{Y}) = 0\,. \tag{4.4.5}$$

In favour of this algebraic constraint, one of the species mass fractions can be eliminated from the system of unknowns, and the associated evolution equation can be discarded.

In a similar fashion, the presence of chemical radicals gives rise to *steady-state approximations*. Assume that the consumption reactions for some species k are extremely fast in comparison with their production, i.e., that the species is extremely reactive. In that case, the concentration of that species in the mixture will always remain very small of order $\epsilon \ll 1$, say. In that case, one may conclude that $Y_k = \epsilon y_k$ and

$$\frac{dY_k}{dt} = \epsilon \frac{dy_k}{dt} = O(\epsilon) \ll 1 \tag{4.4.6}$$

provided the kinetic scheme does not allow for high frequency oscillations with characteristic time scale of order $O(\epsilon)$. Under that condition, Equation (4.4.6) gives rise to the algebraic constraint

$$\sum_{r=1}^{n_{\rm reac}} (a_k^{r,+}\,\omega_r^+(\boldsymbol{Y}) - a_k^{r,-}\,\omega_r^-(\boldsymbol{Y}) = 0\,. \tag{4.4.7}$$

Since the combinations of the rate expressions $a_k^{r,+}\,\omega_r^+(\boldsymbol{Y})$ typically contain the mass fraction Y_k, this equation may be used to express this variable as an algebraic function of the other mass fractions. The ordinary differential equation (ODE) governing its temporal evolution can then be discarded.

The combination of partial equilibrium and steady-state assumptions allows one to considerably reduce the complexity of detailled kinetic mechanisms. The result can be cast in the form of a new net reaction mechanism that is in the standard form $\mathrm{reactants} \leftrightarrow \mathrm{products}$, yet with much more complex effective rate expressions. In fact, the reaction rate expressions for these net reaction steps correspond exactly to the original detailled kinetic scheme. The only difference is that the mass fractions of all species whose dynamic evolution equations have been eliminated by steady-state and partial equilibrium assumptions are now expressed as algebraic functions of the remaining species.

The advantage of this approach over purely computational procedures, as described in Section 4.5.7 below, is that the net result is still in the form of an effective reaction mechanism familiar in chemistry. The resulting explicit formulae, allow further use of the reduced scheme in analytical studies of, say ignition delay times or laminar flame structures for the given reactive mixture [4.92, 4.93]. Another potential application is in Monte Carlo simulations of turbulent combustion based on the PDF methodology (see

Section 4.3.7 below), where the computational requirements for integrating the chemical history of many Monte Carlo realizations can be reduced.

Notice, however, that the reduction of the number of governing kinetic equations does not automatically lead to many orders of magnitude in computational savings. The algebraic constraints from steady-state and partial equilibrium assumptions induce additional complications in the numerical integration that are far from trivial [4.94, 4.95].

4.5 Numerical Reactive Flow Solvers

4.5.1 Governing Equations, Non-dimensionalization and General Discussion

To consistently discuss the numerical problems and their solutions that are specific to premixed combustion, some basic theoretical facts need to be summarized. As a basis, we will need a relevant mathematical description of reactive flows. The full governing equations of gas-phase combustion with as little approximation as is currently possible can be found in comprehensive textbooks on combustion theory, such as Reference [4.6]. Here we shall consider a simplified system only, so that the essential lines of thought can be worked out in a straightforward manner.

The simplified system to be discussed here consists, first of all, of the conservation equations for mass, momentum, and energy

$$\begin{array}{rcrcrcl} (\rho)_t & + & \nabla\cdot(\rho\boldsymbol{v}) & & & = & 0 \\ (\rho\boldsymbol{v})_t & + & \nabla\cdot(\rho\boldsymbol{v}\circ\boldsymbol{v}+\nabla p) & + & \nabla\cdot\boldsymbol{\tau} & = & 0 \\ (\rho e)_t & + & \nabla\cdot(\boldsymbol{v}\,[\rho e+p]) & + & \nabla\cdot\left(\boldsymbol{j}_T+\boldsymbol{\tau}\cdot\boldsymbol{v}+\sum_{i=1}^{n_{\mathrm{spec}}}(\Delta H)_i\,\boldsymbol{j}_i\right) & = & 0. \end{array} \tag{4.5.1}$$

Here $\rho, \boldsymbol{v}, p, e$ are the mass density, fluid flow velocity, pressure, and total energy per unit mass, respectively, and $\boldsymbol{\tau}, \boldsymbol{j}_T, \boldsymbol{j}_i$ denote the molecular transport of momentum, heat, and of the mass of the ith species, respectively. These transport terms and the pressure are related to the mass, momentum, energy, and species densities $\rho, \rho\boldsymbol{v}, \rho e, \rho Y_i$ through the caloric equation of state

$$\rho e = \frac{p}{\gamma-1} + \frac{1}{2}\rho\boldsymbol{v}^2 + \sum_{i=1}^{n_{\mathrm{spec}}}(\Delta H)_i\,\rho Y_i \tag{4.5.2}$$

and the transport models

$$\begin{array}{rcl} \boldsymbol{\tau} & = & -\mu\left(\nabla\boldsymbol{v}+(\nabla\boldsymbol{v})^T\right)-\eta\,(\nabla\cdot\boldsymbol{v})\,\mathbf{1} \\ \boldsymbol{j}_T & = & -\kappa\,\nabla T \\ \boldsymbol{j}_i & = & -\rho D_i\,\nabla Y_i. \end{array} \tag{4.5.3}$$

The temperature T is related to pressure and density via the thermal equation of state

$$T = \frac{p}{\rho R}\,. \tag{4.5.4}$$

The quantities $\gamma, R, \mu, \eta, \kappa, D_i, (\Delta H)_i$ are the isentropic exponent, the ideal gas constant, the shear and bulk viscosities, the heat conductivity, the species diffusivities and the species' formation enthalpies, respectively. All of them are assumed constant throughout this text.

The chemical species mass fractions Y_i satisfy the inhomogeneous balance laws

$$(\rho Y_i)_t + \nabla\cdot(\rho Y_i \boldsymbol{v}) + \nabla\cdot\boldsymbol{j}_i = \rho\omega_i \qquad (i = 1 \ldots n_{\text{spec}}) \tag{4.5.5}$$

where $\omega_i = \omega_i(p, \rho, Y_i)$ is the net production rate of species i per unit mass of the gas mixture.

When n_{spec} actually denotes the total number of chemical species in the system, then the sum of all equations in Equation (4.5.5) leads back to the mass conservation equation in Equation $(4.5.1)_1$ and yields a constraint for the rate expressions

$$\sum_{i=1}^{n_{\text{spec}}} \rho\omega_i = 0\,. \tag{4.5.6}$$

In this case, the mass conservation equation or one of the species balances is redundant. This over-determination is overcome here by dropping one of the species balance equations while keeping the total mass balance.

4.5.1.1 Non-dimensionalization and scaling

Key features of these governing equations can be discussed conveniently after transformation to a new set of dependent and independent variables that is adapted to the reactive flow problems at hand. Reference quantities are chosen for non-dimensionalization that guarantee that the new non-dimensional variables are generally of order $O(1)$, while order of magnitude scalings appear in suitable non-dimensional characteristic numbers. We chose reference values $(\rho_{\text{ref}}, p_{\text{ref}}, u_{\text{ref}})$ for density, pressure and velocity, $(t_{\text{ref}}, \ell_{\text{ref}})$ for the time and space coordinates, (ω_{ref}) for chemical reaction rates and $(\mu_{\text{ref}}, \kappa_{\text{ref}}, D_{\text{ref}}, R_{\text{ref}}, (\Delta H)_{\text{ref}})$ for the parameters in the constitutive equations. Next, we define the new dependent and independent variables,

$$\rho' = \frac{\rho}{\rho_{\text{ref}}}, \quad p' = \frac{p}{p_{\text{ref}}}, \quad \boldsymbol{v}' = \frac{\boldsymbol{v}}{u_{\text{ref}}}, \quad T' = \frac{T}{p_{\text{ref}}/(\rho_{\text{ref}} R_{\text{ref}})}, \quad e' = \frac{e}{p_{\text{ref}}/\rho_{\text{ref}}} \tag{4.5.7}$$

and

$$\boldsymbol{x}' = \frac{\boldsymbol{x}}{\ell_{\text{ref}}}, \quad t' = \frac{t}{t_{\text{ref}}}\,. \tag{4.5.8}$$

The governing equations are then transformed into their scaled, non-dimensional analogues:

Conservation Laws:

$$\begin{aligned}
&\frac{1}{\text{Sr}}(\rho)_t &&+ \nabla\cdot(\rho\boldsymbol{v}) && && &&= 0\\
&\frac{1}{\text{Sr}}(\rho\boldsymbol{v})_t &&+ \nabla\cdot(\rho\boldsymbol{v}\circ\boldsymbol{v} + \frac{1}{M^2}\nabla p) &&+ \frac{1}{\text{Re}}\nabla\cdot\boldsymbol{\tau} && &&= 0\\
&\frac{1}{\text{Sr}}(\rho e)_t &&+ \nabla\cdot(\boldsymbol{v}[\rho e + p]) &&+ \frac{1}{\text{Re}}\nabla\cdot\left(\frac{1}{\text{Pr}}\boldsymbol{j}_T + M^2\,\boldsymbol{\tau}\cdot\boldsymbol{v} + \frac{Q}{\text{Sc}}\sum_{i=1}^{n_{\text{spec}}}\delta h_i\,\boldsymbol{j}_i\right) &&= 0.
\end{aligned} \tag{4.5.9}$$

Species Balances:

$$\frac{1}{\text{Sr}}(\rho Y_i)_t + \nabla\cdot(\rho Y_i\boldsymbol{v}) = -\frac{1}{\text{ReSc}}\nabla\cdot\boldsymbol{j}_i + \text{Da}\,\rho\omega_i \qquad (i = 1 \ldots n_{\text{spec}}) \tag{4.5.10}$$

Caloric Equation of State:

$$\rho e \;=\; \frac{p}{\gamma-1} + M^2\,\frac{1}{2}\rho \boldsymbol{v}^2 + Q\,\sum_{i=1}^{n_{\rm spec}} \delta h_i\,\rho Y_i \tag{4.5.11}$$

Thermal Equation of State:

$$T = \frac{p}{\rho}\,. \tag{4.5.12}$$

Transport Models:

$$\begin{aligned} \boldsymbol{\tau} &= -\mu'\left(\nabla\boldsymbol{v} + (\nabla\boldsymbol{v})^T\right) - \eta'\,(\nabla\cdot\boldsymbol{v})\,\mathbf{1} \\ \boldsymbol{j}_T &= -\kappa'\nabla T \\ \boldsymbol{j}_i &= -D_i'\,\nabla Y_i. \end{aligned} \tag{4.5.13}$$

Notice that in Equation (4.5.9) and Equation (4.5.11) we have introduced the scaled reaction enthalpies

$$\delta h_i = \frac{(\Delta H)_i}{(\Delta H)_{\rm ref}}\,, \tag{4.5.14}$$

and that $\mu' = \mu/\mu_{\rm ref}, \kappa' = \kappa/\kappa_{\rm ref}$ etc. in Equation (4.5.13) could all be set to unity in case of constant molecular transport coefficients.

The procedure of scaling the equations has led to a set of seven characteristic numbers:

Abbreviation	**Definition**	**Name**
Sr	$t_{\rm ref}u_{\rm ref}/\ell_{\rm ref}$	Strouhal number
M	$u_{\rm ref}/\sqrt{p_{\rm ref}/\rho_{\rm ref}}$	Mach number
Re	$\rho_{\rm ref}u_{\rm ref}\ell_{\rm ref}/\mu_{\rm ref}$	Reynolds number
Pr	$\mu_{\rm ref}/(\kappa_{\rm ref}/R_{\rm ref})$	Prandtl number
Sc	$\mu_{\rm ref}/\rho_{\rm ref}D_{\rm ref}$	Schmidt number
Da	$\omega_{\rm ref}\ell_{\rm ref}/u_{\rm ref}$	Damköhler number
Q	$(\Delta H)_{\rm ref}/(p_{\rm ref}/\rho_{\rm ref})$	Heat Release Parameter

(4.5.15)

There are several important observations regarding the structure of solutions of the full governing equations that emerge immediately from the exercise of non-dimensionalization and scaling:

1. **The low Mach number singularity**
   Obviously, as the Mach number M vanishes, the pressure gradient term in the momentum equation becomes singular.The mathematical nature of this singularity will be discussed in more detail below. Here, we merely emphasize that the low Mach number limit is of considerable importance during the initial stages of flame acceleration processes because it governs most of the inherent instabilities of laminar flames and flamelets at low-to-moderate turbulence intensities.

2. **The deflagration limit**
   A distinguished limit of large Damköhler numbers $\mathrm{Da} \gg 1$ and inefficient molecular transport $\mathrm{Re} \gg 1$ reveals the mathematical structure of laminar deflagrations (see [4.44, 4.56, 4.96] and Section 4.5.4 below). The mathematical structure of that limit carries over to turbulent combustion processes also, with drastic consequences for suitable reactive flow numerical methods.

3. **Stiff and fast chemistry singularities**
   The limit of large Damköhler numbers is not only relevant for the establishment of well-defined reaction fronts (flames). When chemical reactions that do not considerably contribute to the net chemical energy conversion are associated with large Damköhler numbers, they may nevertheless be of outmost importance when they involve chemical radicals. In that case, numerical challenges arise because minute concentrations of extremely reactive species must be computed on the basis of governing equations with extremely large rates. This leads to the typical numerical problem of "cancellation of significant digits" in finite computer arithmetic. Further computational issues associated with this limit will be discussed in Section 4.5.7.

4.5.2 The Low Mach Number Problem

In most real-life applications, such as spark-ignition engine combustion (no knock), industrial and household burners, flame acceleration in explosion processes etc., combustion-driven velocities are small compared with the speed of sound. This fact has profound consequences for both the mathematical behaviour of solutions to the governing equations from Section 4.5.1 and their numerical approximate solutions. Physically, in the limit of arbitrarily slow flow (or infinitely fast sound propagation) the elasticity of the gas with respect to bulk compression becomes negligible and soundwave propagation becomes unnoticeable. Mathematically, as the Mach number M from Equation (4.5.15) tends to zero, the pressure gradient contribution in the momentum equations Equation $(4.5.9)_2$ becomes singular. In order to explore the consequences of this singularity we consider a formal asymptotic analysis, closely following References [4.44, 4.97] and [4.98].

4.5.2.1 Asymptotic analysis

A systematic derivation of the governing equations for zero Mach number combustion has been given by Majda and Sethian [4.44]. The formulation adopted below, which explicitly focuses on the conservation equations for mass, momentum and energy, has been introduced in Reference [4.97] in conjunction with a multiple length-scale, single time-scale analysis.

In recounting their results we restrict our discussion to the case of an ideal gas mixture with a simple one-step reaction $F \rightarrow P$, where the fuel F is turned into the product species P. The chemical energy conversion rate then is $Q\,\rho\omega_F$ where Q quantifies the specific reaction enthalpy of the fuel species and $\rho\omega_F$ its production density. Under these conditions we need to describe the time evolution of only the fuel mass fraction Y_F using a single transport equation of the type described in Equation (4.5.10).

The asymptotic solution ansatz

$$\begin{aligned} p &= p_0(\boldsymbol{x},t) + Mp_1(\boldsymbol{x},t) + M^2 p_2(\boldsymbol{x},t) + o(M^2), \\ \boldsymbol{v} &= \boldsymbol{v}_0(\boldsymbol{x},t) + M\boldsymbol{v}_1(\boldsymbol{x},t) + o(M), \\ \rho &= \rho_0(\boldsymbol{x},t) + M\rho_1(\boldsymbol{x},t) + o(M), \\ Y_F &= Y_{F,0}(\boldsymbol{x},t) + MY_{F,1}(\boldsymbol{x},t) + o(M) \end{aligned} \tag{4.5.16}$$

is introduced into the dimensionless governing Equations (4.5.9) to (4.5.10). Following standard procedures of asymptotic analysis, one obtains a hierarchy of equations for the various expansion functions $p_i, \boldsymbol{v}_i, \rho_i, Y_{F,i}$ by collecting all terms multiplied by equal powers of the Mach number M and separately equating these to zero. The momentum equations to orders M^{-2} und M^{-1} become

$$\nabla p_0(\boldsymbol{x},t) = 0\,, \quad \nabla p_1(\boldsymbol{x},t) = 0\,. \tag{4.5.17}$$

One concludes that p_0 and p_1 depend on time only in this regime of length and time scales, so that

$$p_0 \equiv P_0(t) \qquad \text{and} \qquad p_1 \equiv P_1(t)\,. \tag{4.5.18}$$

The continuity and energy equations at leading order are then

$$\partial\rho_0/\partial t + \nabla\cdot(\rho_0\boldsymbol{v}_0) = 0 \tag{4.5.19}$$

$$\frac{1}{\gamma-1} d\,P_0/dt + \nabla\cdot(H_0\boldsymbol{v}_0) = \Big(\frac{1}{\mathrm{Pe}}\nabla\cdot(\lambda\nabla T_0) + \mathrm{Da}\,Q\,\rho\omega_F\Big)\,. \tag{4.5.20}$$

where

$$H_0(t) = \frac{\gamma}{\gamma-1}\,P_0(t)\,. \tag{4.5.21}$$

To arrive at Equation (4.5.20), one inserts the expansion Equation (4.5.16) into the energy conservation law Equation $(4.5.9)_3$, takes into account that the kinetic energy is by a factor of M^2 smaller than the thermal energy for $M \ll 1$ according to Equation (4.5.11) and uses the gradient condition from Equation (4.5.17) to pull the pressure out of the energy flux divergence expression. The contribution of the viscous forces to the energy budget, represented by the term $\nabla\cdot(\frac{M^2}{\mathrm{Re}}\,\boldsymbol{\tau}\cdot\boldsymbol{v})$, will appear first in the energy equation at order $O(M^2)$.

The momentum equation at order M^0 reads

$$\partial\rho_0\boldsymbol{v}_0/\partial t + \nabla\cdot(\rho_0\boldsymbol{v}_0\circ\boldsymbol{v}_0) + \nabla p_2 = -\frac{1}{\mathrm{Re}}\nabla\cdot\boldsymbol{\tau}_0\,. \tag{4.5.22}$$

Notice the change in structure of these equations: The pressure evolution equation does *not* determine the pressure variable p_2 appearing in the momentum equation! The appropriate interpretation, corresponding directly to the theory of incompressible flows, is that the equation for P_0 from Equation (4.5.20) is a divergence constraint for the leading order energy flux, i.e.,

$$\nabla\cdot(H_0(t)\,\boldsymbol{v}_0) = -\left[\frac{1}{\gamma-1} d\,P_0/dt - \Big(\frac{1}{\mathrm{Pe}}\nabla\cdot(\lambda\nabla T_0) + \mathrm{Da}\,Q\rho\omega_F\Big)\right] \tag{4.5.23}$$

and that the second-order pressure p_2 is responsible for guaranteeing that constraint to be observed. A useful and more familiar interpretation of this equation results from using explicitly that $H_0(t) = \gamma P_0(t)/(\gamma - 1)$ is a function of time only and deriving a

velocity divergence constraint

$$\nabla\cdot\boldsymbol{v}_0 = -\frac{1}{\gamma P_0}\left[d\,P_0/dt - (\gamma-1)\Big(\frac{1}{\mathrm{Pe}}\nabla\cdot(\lambda\nabla T_0) + \mathrm{Da}\,Q\rho\omega_F\Big)\right]. \tag{4.5.24}$$

We observe that the velocity divergence is driven by chemical energy conversion and energy transport effects: Chemical heat release, heat conduction, and global pressure changes conspire to induce a divergence field for the velocity. As a direct consequence, we derive from the mass continuity Equation (4.5.19) an equation that describes the temporal evolution of the density along particle paths

$$\frac{D\rho}{Dt} := \frac{\partial\rho}{\partial t} + \boldsymbol{v}\cdot\nabla\rho = -\rho\nabla\cdot\boldsymbol{v}\,. \tag{4.5.25}$$

To summarize, the energy conversion and transport processes drive the divergence of the energy flux, which is related to the velocity divergence. The latter, in turn, leads to compression or expansion of individual mass elements and thus to density variations of individual particles.

The original interpretation of Equation (4.5.23) as an energy flux divergence constraint proves to be useful in the construction of energy-conserving finite-volume methods, (see [4.98, 4.99]).

Equations (4.5.19) to (4.5.22) form a closed system, provided the temporal evolution of the leading-order pressure P_0 is known and the state dependence of the reaction rate $\rho\omega_F$ is given. For combustion under atmospheric conditions P_0 equals the atmospheric ambient pressure and is constant in time. For combustion in a closed chamber, we explore the fact that P_0 is homogeneous in space, integrate Equation (4.5.24) over the total flow domain, use Gauß' theorem to replace the divergence integrals with boundary integrals and obtain a global pressure evolution equation:

$$d\,P_0/dt = \frac{1}{\Omega}\left[-\oint_{\partial V}\left(\gamma P_0\boldsymbol{v} - \frac{\gamma-1}{\mathrm{Pe}}\,\lambda\nabla T_0\right)\cdot\boldsymbol{n}\,d\sigma + \mathrm{Da}\int_V(\gamma-1)Q\rho\omega_F\,dV\right] \tag{4.5.26}$$

where $\boldsymbol{n}$ is the outward pointing unit normal at the boundary, and $\Omega = \int_V dV$ is the total volume of the domain of integration V. Given appropriate velocity and thermal boundary conditions all changes of the background pressure are thus related to the overall chemical energy conversion within the domain.

The structure of the above equations is similar to that of incompressible, non-reactive flow in that there is convection, diffusion, and an explicit velocity divergence constraint. Thus appropriate extensions of incompressible flow solvers should, in principle, be able to handle zero Mach number reactive flows as well. See References [4.100 to 4.103] for reviews of typical developments based on this approach.

For a discussion of further aspects of low Mach number asymptotics, including the influence of high-frequency and long-wavelength acoustic perturbations, see References [4.97, 4.104].

4.5.2.2 Numerical consequences of the asymptotics

The most dramatic consequence of the asymptotic results is the pressure decomposition. Both the leading-order spatially homogeneous part $P_0(t)$ and the $O(M^2)$-perturbation $p_2(\boldsymbol{x},t)$ enter the leading-order

system of equations in a non-trivial fashion. The leading order pressure P_0 determines the velocity divergence through the limit form of the energy Equation (4.5.24), but does not appear in the momentum equation at all. In contrast, the second-order pressure $p_2(\boldsymbol{x}, t)$ is energetically negligible, but yields the sole pressure gradient effect in the momentum equation.

This splitting of the pressure is dramatic because a numerical method designed to integrate the original unscaled equations Equation (4.5.1) to Equation (4.5.5) must *necessarily* fail when applied to very low Mach number combustion problems, unless special care is taken to introduce an appropriate separation and re-scaling of the pressure mean and its fluctuations.

To be more precise, consider a smooth low Mach number flow on a domain of characteristic size ℓ. The total pressure variation within the flow domain will be $M^2\,\delta p_2$, where $\delta p_2 = O(1)$ as $M \to 0$. Assume that the flow domain is discretized by n grid points across the length of ℓ so that the grid spacing is $\Delta x = \ell/n$. A second-order discrete representation of the derivative $\partial p/\partial x$ on a carthesian grid with constant spacing in the x-direction would read

$$\frac{\partial\, p}{\partial x} = \frac{p_{i+1,j} - p_{i-1,j}}{2\Delta x} + O((\Delta x)^2)\,. \tag{4.5.27}$$

Obviously, forming a discrete gradient requires that pressure differences be taken between neighbouring grid-cells. These pressure differences will be the smaller, the smaller (i) the Mach number M and (ii) the grid spacing, since we consider a smooth flow. We wish to assess how small a Mach number and how fine a numerical resolution we can afford without having to account for the usual loss of significant digits upon differencing large but almost equal numbers:

In the low Mach number limit, the pressure in the vicinity of the centre cell i can be expressed as

$$p(x) = p_i + M^2(x - x_i)\frac{\partial p_2}{\partial x} + O(M^2(\Delta x)^2) \tag{4.5.28}$$

In a typical situation the pressures p_{i-1}, p_{i+1} would thus scale as

$$p_{i-1} = p_i - M^2\,\Delta x\,p_2'\,, \quad p_{i+1} = p_i + M^2\,\Delta x\,p_2'\,, \qquad \Big(p_2' = O(1) \quad \text{as} \quad M, \Delta x \to 0\Big)\,. \tag{4.5.29}$$

Just to give an example, we let $p_i = 1.0$, $p_2' = 1.0$ and insert the exact results from this equation into the discrete differentiation formula from Equation (4.5.27). We evaluate the discrete gradient using a sequence of Mach numbers $M = 10^{-2}...10^{-4}$ and resolutions $\Delta x = 10^{-1}...10^{-3}$ and compare the numerical round-off error with the truncation error estimate $(\Delta x)^2$ for both single- and double-precision arithmetics. The results are given in Table 4.5.2.2- 1.

$$\frac{\mathrm{err}_{\mathrm{single}}}{(\boldsymbol{\Delta x})^{\mathbf{2}}}$$

There are a number of immediate conclusions to be drawn from the results in this table:

1. Single precision computations of pressure gradients will fail already at $M = 10^{-2}$.
2. Double precision evaluations begin to seriously deteriorate for $M < 10^{-3}$.

Table 4.5.2.2- 1: Round-off versus truncation errors for a single evaluation of $\partial p/\partial x$

$\Delta x/\ell$	M	$\left(\frac{p_{i+1}-p_{i-1}}{2M^2\Delta x}\right)_{ex.}$	$\frac{err_{single}}{(\Delta x)^2}$	$\frac{err_{double}}{(\Delta x)^2}$
0.1	10^{-2}	1.111	$2.12 \cdot 10^{-1}$	$1.72 \cdot 10^{-10}$
	10^{-3}	$''$	7.29	$7.98 \cdot 10^{-8}$
	10^{-4}	$''$	$1.0 \cdot 10^{2}$	$3.72 \cdot 10^{-6}$
0.01	10^{-2}	1.111	$7.23 \cdot 10^{2}$	$1.72 \cdot 10^{-8}$
	10^{-3}	$''$	$1.0 \cdot 10^{4}$	$2.80 \cdot 10^{-5}$
	10^{-4}	$''$	$1.0 \cdot 10^{4}$	$1.63 \cdot 10^{-3}$
0.001	10^{-2}	1.111	$7.29 \cdot 10^{4}$	$7.98 \cdot 10^{-4}$
	10^{-3}	$''$	$1.0 \cdot 10^{6}$	$3.72 \cdot 10^{-2}$
	10^{-4}	$''$	$1.0 \cdot 10^{6}$	0.16

3. There is a general loss of precision with increasing resolution of a fixed pressure distribution, which is aggravated by the low Mach number effect. Thus in contrast to intuition, increasing the numerical resolution may worsen the low Mach problem rather than providing improvements!

The first item is particularly alarming in the context of some current day commercial flow simulation codes, because these often have a user-defined option allowing one to run single-precision calculations in order to save computational capacities. Obviously, such an option should be supplemented with an automatic "low Mach number warning" or it should be automatically linked with special pressure scaling procedures that are suited to separate mean pressures from $O(M^2)$ pressure fluctuations.

For further reading on the round-off error problem for low Mach number computations see Sesterhenn et al. [4.105].

4.5.3 Compressible and Low Mach Number Flow Solvers

4.5.3.1 Compressible flow solvers

The numerical technology for simulating fully compressible flows has advanced to quite a mature state over the past two decades. Numerous textbooks and fundamental texts elucidate the basic ideas, [4.106], the advanced analysis, [4.107 to 4.110], and practical applications in combustion [4.111]. The references cited include finite-volume as well as finite-element approaches. Here, we summarize only the key difficulties associated with compressible flow simulation and sketch some numerical approaches to overcome them.

Weak solutions of non-linear hyperbolic equation systems. The key challenge some 25 years ago in the context of compressible flow simulation was to accurately handle non-linear propagating hyperbolic waves and to specifically allow for the formation of discontinous solutions. The obvious example and major motivation came from blast waves and shock-tube experiments, where one regularly observes the shock waves, i.e., discontinous travelling wave solutions to the compressible flow equations. Two critical features of such weak solutions had to be addressed: The first results from the fact that shock waves travel at speeds that are determined by the constraints of mass, momentum, and energy conservation. In particular, shock speeds cannot be extracted from an analysis of the governing differential equations, which have various equivalent formulations, only one of which respects automatically the above-mentioned conservation laws. The second difficulty is associated with the tendency of then-standard numerical discretizations to invoke spurious oscillations next to steep gradients (the Gibbs-phenomenon). Such oscillations are particularly critical in the context of reactive flow simulations because they may interact with highly non-linear chemical kinetic models to produce utterly false numerical predictions.

The first issue, obtaining the correct weak solutions, was essentially resolved by Lax and Wendroff, [4.112]. The authors proved that IF a numerical method converges AND is in conservation form, THEN it converges to weak solutions of the underlying conservation laws. This result determined much of the further developments, in that major research went into the design of numerical methods that automatically conserve mass, momentum, and energy by construction: Cell averages of these conserved quantities are updated solely by balancing fluxes across grid-cell interfaces. As a consequence, mass, momentum, and energy can only be distributed among the numerical grid-cells but cannot "get lost". It should be emphasized, though, that deviations from conservation mainly affect simulations for situations with strong shocks (order $O(1)$ pressure changes across). Weakly compressible flows, in which non-linear wave propagation essentially follows the theory of characteristics, can be simulated quite well with non-conservative, high-accuracy methods. Some of the extensions of incompressible flow solvers to the compressible regime take advantage of this fact, albeit compromising on the ability to compute strong shocks, [4.109, 4.110, 4.113 to 4.115]. (Note that the last two references include descriptions of finite-element techniques applied to compressible flow simulation.)

Regarding the second issue, avoiding spurious oscillations, two major strategies have been developed, both being essentially successful:

- non-linear artificial dissipation and
- non-linear upwind techniques.

The most successful representative of the first group is the the "flux corrected transport" (FCT) family of schemes. The underlying idea is to combine a quite dissipative first-order accurate numerical method that completely damps oscillations with a scheme of higher accuracy that, however, may allow the development of oscillations. A non-linear correction scheme is developed which, depending on local solution features, forces a transition from the high-accuracy scheme to the more dissipative one. These corrections are added only where necessary, so that the overall accuracy is that of the sophisticated scheme in regions of smooth solution, while the damping capabilities of the dissipative scheme are explored next to discontinuities. Fourth- and higher-order accurate versions of these FCT schemes have been proposed and are being used for combustion simulations [4.111, 4.116].

The second group of schemes, using non-linear upwind techniques, was pioneered by Godunov, see e.g., [4.106, 4.117]. A key observation is that the "damping" that occurs near shocks in gas dynamics

is really restricted to the extremely thin shock transition region, which is of a thickness comparable to merely a few mean free paths of the gas considered. Hence standard second- or higher-order dissipation is not taking place and cannot be responsible for the piecewise smooth, non-oscillatory solution behaviour close to physical shocks. In fact, a close analysis, based on the theory of characteristics, shows that oscillations are controlled by the directed transport of information along characteristics (in one space dimension), which are terminated when reaching a shock front and whose information is then dissipated. Godunov suggested a numerical approach that would automatically incorporate this non-linear selection of information transport, thereby avoiding the need for artificial viscosity terms. He proposed to compute the fluxes across grid cell interfaces in a numerical scheme in conservation form by exactly solving local "Riemann problems" (essentially equivalent to the standard shock tube problem, but with generalized initial states), which use the non-linear wave nature of the underlying system to resolve the jumps of state quantities between adjacent grid-cells. This basic structure proposed by Godunov has been taken up and developed further in various directions, the most established ones being higher-order extensions (the essentially non-oscillatory (ENO) version of the approach achieves the same formal accuracies as the corresponding FCT schemes), and simplifications that replace the originally required exact Riemann solution at grid-cell interfaces by approximate ones. The latter are easier to generalize to systems with non-trivial equations of state and are generally more efficient. For further details, the reader may want to consult the cited text books.

Detonation capturing. The mathematical nature of detonation waves, considered as reacting shock waves, is very similar to that of ordinary gas dynamic shocks. Therefore, one expects that the numerical schemes in the conservation form mentioned in the last paragraphs should be able to also "capture" detonation waves. In fact, the basic argument stating that conservative numerical schemes should produce the correct weak solutions if they converge can also be applied to detonations. As a consequence, there is a multitude of applications of FCT schemes or Godunov-type methods to problems of detonation physics, (see the past Combustion Symposia, the Shock Wave Symposia or the ICDERS conferences). There is one caveat, though, which may lead to surprising unphysical effects if naively overlooked [4.118]. In the limit of very rapid chemistry, equivalent to under-resolved representation of the detonation reaction zone, numerical schemes in conservation form can develop numerical solutions that appear to be very reasonable on the surface but are in fact completely false. The origin is an undesired non-linear interaction between the numerical dissipation resulting from averaging over grid-cells from one time step to the next and the highly non-linear combustion chemistry. This interaction can lead to artifical one-grid-cell-per-time step solutions that correspond to a weak detonation, followed by an ordinary inert shock rather than to a single strong detonation wave. This problem has been addressed in various ways, partly heuristic, partly theoretically founded, in Reference [4.111] and References [4.118 to 4.121].

4.5.3.2 Low Mach number flow solvers

Here, we summarize briefly two numerical approaches for low Mach number flows, which are being or becoming increasingly popular in the field of numerical combustion:

1. SIMPLE-type algorithms following ideas of Patankar [4.103] and
2. Projection-type methods, which borrow from Chorin [4.122 to 4.124].

These methods are finite-difference and finite-volume schemes. Finite-element methods will not be addressed in this section owing to lack of space and my personal experience in using these. The reader is referred to References [4.109, 4.125, 4.126], and [4.110] for further reading.

4.5.3.3 SIMPLE-type methods

The "semi-implicit method for pressure-linked equations" (SIMPLE) was originally designed for simulations of constant density incompressible flows [4.103]. It has later been extended to variable density incompressible and to moderately compressible flows, [4.127 to 4.129]. To explain the underlying strategy, we consider the simplest case of constant density ($\rho \equiv 1$) incompressible inviscid flows first: Thus we wish to solve

$$\frac{\partial \boldsymbol{v}}{\partial t} + \boldsymbol{v} \cdot \nabla \boldsymbol{v} + \nabla p_2 =: \frac{\partial \boldsymbol{v}}{\partial t} + \boldsymbol{C}[\boldsymbol{v}] + \nabla p_2 = 0 \tag{4.5.30}$$

with the divergence constraint

$$\nabla \cdot \boldsymbol{v} = 0\,. \tag{4.5.31}$$

The approach relies on an iteration scheme whose final result is the pressure field p_2, needed to update the velocity field from time level t^n to the next level t^{n+1} in such a way that the new field $\boldsymbol{v}^{n+1}$ satisfies the divergence constraint from Equation (4.5.31). Suppose that an estimated pressure field $p_2^{n,0}$ is available, which could be the pressure field from the last time step as indicated by the notation, but does not have to be. Suppose further that an implicit discretization for the velocity evolution equation is adopted

$$\frac{\boldsymbol{v}^{n+1} - \boldsymbol{v}^n}{\Delta t} + \left[\tilde{\boldsymbol{C}}_i[\boldsymbol{v}^{n+1}] + \tilde{\boldsymbol{C}}_e[\boldsymbol{v}^n]\right] + \tilde{\nabla} p_2^{n+\frac{1}{2}} = 0\,, \tag{4.5.32}$$

with $\tilde{\boldsymbol{C}}_e[\cdot], \tilde{\boldsymbol{C}}_i[\cdot]$ as explicit and implicit contributions to the discretization of the non-linear convection operator $\boldsymbol{C}[\boldsymbol{v}] = \boldsymbol{v} \cdot \nabla \boldsymbol{v}$, respectively (see [4.128, 4.129] for examples) and $\tilde{\nabla}$ a discrete approximation of the gradient operator. For convenience, we rewrite Equation (4.5.32) as

$$\tilde{\boldsymbol{A}}_i[\boldsymbol{v}^{n+1}] = \tilde{\boldsymbol{A}}_e[\boldsymbol{v}^n] - \tilde{\nabla} p_2^{n+\frac{1}{2}}\,. \tag{4.5.33}$$

where

$$\begin{aligned} \tilde{\boldsymbol{A}}_i[\cdot] &= \tfrac{1}{\Delta t}\left[\mathbf{1} + \Delta t\, \tilde{\boldsymbol{C}}_i\right][\cdot] \\ \tilde{\boldsymbol{A}}_e[\cdot] &= \tfrac{1}{\Delta t}\left[\mathbf{1} - \Delta t\, \tilde{\boldsymbol{C}}_e\right][\cdot] \end{aligned} \tag{4.5.34}$$

The SIMPLE method adopts a linear implicit formulation, so that $\tilde{\boldsymbol{A}}_i[\cdot]$ is in fact a linear operator, and then solves Equation (4.5.33) iteratively according to the following sequence:

Start:

$$\begin{aligned} \tilde{\nabla} p_2^{n+\frac{1}{2},0} &= \tilde{\nabla} p_2^{n,0} \\ \tilde{\boldsymbol{A}}_i[\boldsymbol{v}^{n+1,0}] &= \tilde{\boldsymbol{A}}_e[\boldsymbol{v}^n] - \tilde{\nabla} p_2^{n+\frac{1}{2},0} \end{aligned} \tag{4.5.35}$$

Iterative Correction:

$$\begin{aligned} p_2^{n+\frac{1}{2},\nu+1} &= p_2^{n+\frac{1}{2},\nu} + \delta p_2^{\nu} \\ \boldsymbol{v}^{n+1,\nu+1} &= \boldsymbol{v}^{n+1,\nu} + \delta \boldsymbol{v}^{\nu} \end{aligned} \tag{4.5.36}$$

Correction Equations:

$$\begin{aligned} \tilde{\boldsymbol{A}}_i[\delta\boldsymbol{v}^\nu] + \tilde{\nabla}\delta p_2^\nu &= 0 \\ \tilde{\nabla}\cdot\left(\boldsymbol{v}^{n+1,\nu} - \tilde{\boldsymbol{A}}_i^{-1}\left[\tilde{\nabla}\delta p_2^\nu\right]\right) &= 0\,. \end{aligned} \tag{4.5.37}$$

The last equation is the appropriate reformulation of the divergence constraint

$$\tilde{\nabla}\cdot\left(\boldsymbol{v}^{n+1,\nu} + \delta\boldsymbol{v}^\nu\right) = 0 \tag{4.5.38}$$

as an elliptic pressure correction equation. If the linearization of $\tilde{\boldsymbol{A}}_i$ yields a diagonal matrix, then the pressure correction equation is of Poisson type.

For combustion applications, one is interested in variable density flows (the hot burnt gas is typically expanded relative to the unburnt by a factor of 2 to 6) and often also in compressibility effects. Thus one has to consider the full compressible flow equations rather than the idealized case of an incompressible constant density fluid as discussed above.

The SIMPLE method has been extended to compressible flows by Karki and Patankar [4.127] (homentropic flow) and to the more general case of variable entropy compressible flows by Rhie [4.128] and Shyy [4.129]. The idea in all of these approaches is to replace the strict divergence constraint from Equation (4.5.31) by the continuity Equation $(4.5.9)_1$ and to introduce a thermodynamic coupling between pressure and density.

A simple argument shows that this is not yet sufficient to obtain an approximation to the full compressible flow equations: As in the incompressible case we have three momentum equations. The continuity equation now replaces the divergence constraint and is, thus, responsible for determining the pressure field. However, besides the pressure we have a new variable, the density, but no equation for it so far. If one opts to strictly couple pressure and density by a given function, $\rho = \rho(p)$, then this severly constrains the possible thermochemical processes. Combustion changes the entropy of the reacting mass elements and with it the pressure-density relation. Therefore, one more equation needs to be supplemented!

A natural choice that has been adopted frequently in combustion is to explicitly compute the time evolution of temperature T or of the internal energy. For an ideal gas one has

$$T = \frac{p}{\rho R} \qquad\qquad \rho = \frac{p}{RT} \tag{4.5.39}$$

and therefore

$$\frac{\partial\rho}{\partial t} = \frac{1}{RT}\frac{\partial p}{\partial t} - \frac{p}{RT^2}\frac{\partial T}{\partial t}\,. \tag{4.5.40}$$

Here the temperature time derivative must be obtained from a temperature evolution equation, to be derived from energy conservation. Notice that the "gas constant" R is generally not really constant in a reacting flow, but that it depends on the instantaneous local gas composition. In that case an additional term involving $\frac{\partial R}{\partial t}$ must be included in Equation (4.5.40). Variations of R must be computed using the results from the species balances Equation (4.5.10).

A possible extension of the SIMPLE approach now solves an approximate explicit equation for temperature and species, so that $\frac{\partial T}{\partial t}$, $\frac{\partial R}{\partial t}$ are known, and then discretizes the continuity equation as a pressure

correction system. The incompressible flow divergence constraint Equation (4.5.38) is first replaced with an equation of the form

$$\frac{\rho^{n+1,\nu}+\delta\rho^{\nu}-\rho^{n}}{\Delta t}+\nabla\cdot\left(\rho^{n+1,\nu}\boldsymbol{v}^{n+1,\nu}+\delta\rho^{\nu}\boldsymbol{v}^{n+1,\nu}+\rho^{n+1,\nu}\delta\boldsymbol{v}^{\nu}+\delta\rho^{\nu-1}\delta\boldsymbol{v}^{\nu-1}\right)=0\,, \quad (4.5.41)$$

where we have used an implicit first-order discretization for simplicity. The goal is to iterate on this equation based on the updating rules

$$\begin{aligned}\rho^{n+1,\nu+1} &= \rho^{n+1,\nu}+\delta\rho^{\nu}\\ \boldsymbol{v}^{n+1,\nu+1} &= \boldsymbol{v}^{n+1,\nu}+\delta\boldsymbol{v}^{\nu}\end{aligned} \quad (4.5.42)$$

and suitable relations between a pressure correction field δp_2^{ν} and the perturbations $\delta\rho^{\nu}, \delta\boldsymbol{v}^{\nu}$

$$\begin{aligned}\delta\rho^{\nu} &= C(\rho,P_0;M)\;\delta p_2^{\nu}\\ \delta\boldsymbol{v}^{\nu} &= -\tilde{\boldsymbol{A}}_i^{-1}\left[\tilde{\nabla}\delta p_2^{\nu}\right].\end{aligned} \quad (4.5.43)$$

Here $C(\rho,P_0;M)$ is an approximate derivative $\partial\rho/\partial p_2$ evaluated in an explicit fashion at either the old time level or at the last iteration level. In practice one uses an isentropic or an isothermal relation for $C(\rho,P_0;M)$. We notice that this choice is not crucial for the whole procedure because ultimately one iterates until the corrections $\delta\rho^{\nu}, \delta\boldsymbol{v}^{\nu}, \delta p_2^{\nu}$ become negligible and the continuity equation is solved to the desired accuracy. The choice of $C(\rho,P_0;M)$ merely influences the path of the iteration in state space, but not—if it converges—the final result. The velocity correction is analogous to the original version from Equation (4.5.37).

Importantly, the coefficient $C(\rho,P_0;M)$ describes the response of the density to perturbations of p_2, not to the full pressure p, so that

$$C(\rho,P_0;M)=\frac{\partial p}{\partial p_2}\left(\frac{\partial\rho}{\partial p}\right)_{\mathrm{S,T}}=M^2c_{\mathrm{S,T}}^{-2}\,, \quad (4.5.44)$$

where $c_{\mathrm{S,T}}$ is the isentropic or isothermal speed of sound. Thus as the Mach number vanishes, the limit of incompressibility is approached automatically in the sense that the response of the density to the pressure p_2 vanishes.

The perturbed continuity iteration Equation (4.5.41) includes a non-linear term $\nabla\cdot(\delta\rho\,\delta\boldsymbol{v})$. This term is lagged behind in the iteration cycle and is evaluated explicitly at $\nu-1$ so as to render the pressure correction equation a linear system. Here is the form of the pressure correction equation when the operator $\tilde{A}_i$ is diagonal with entries $1/\rho$

$$C\,\delta p_2^{\nu}+\Delta t\nabla\cdot\left(C\,\delta p_2^{\nu}\,\boldsymbol{v}^{\nu}-\nabla\delta p_2^{\nu}\right)=RHS\,. \quad (4.5.45)$$

The right-hand side includes all the terms treated explicitly or stemming from the old time or last iteration level.

An important observation is that the above equation involves a true *Laplacian* for δp_2^{ν} as the elliptic part of the operator. This is in contrast to many other schemes for variable density low Mach number flows, which end up with an elliptic pressure operator of the form $\nabla\cdot(\frac{1}{\rho}\nabla(\cdot))$. If the density is strongly

varying, then the numerical inversion of this latter operator is much more expensive than inverting a true Laplacian, for which special extremely fast schemes have been developed. This observation has been explored extensively in the construction of an efficient numerical scheme for reactive flows, sprays etc. by Haldenwang et al. [4.130].

To complete the picture, we should notice, however, that the formulation described above relies on an explicit estimate for density variations induced by entropy advection along particle paths. These effects must be included in the initial guess $\rho^{n+1,0}$. Otherwise, the assumptions built into the coefficient $C(\rho, P_0; M)$ would dominate the density variations. Currently, there seems to be no numerical technique that would manage to (i) rely on a pressure (correction) equation involving a true Laplacian and (ii) conserve total energy at the same time (see also [4.98]).

Related approaches are the pressure implicit second order (PISO) scheme [4.101, 4.131], which is currently used quite successfully for combustion simulations, [4.132, 4.133], and the method proposed by Geratz et al. [4.114] and Roller et al. [4.115].

4.5.3.4 Projection-type methods

The key idea of projection schemes can best be described by considering constant density incompressible inviscid flows. The governing equations are obtained from those derived in Section 4.5.2.1 by assuming zero heat release, $Q \equiv 0$, and constant density, $\rho \equiv 1$, by passing to the limit of infinite Reynolds and Peclet numbers, $(\mathrm{Re}, \mathrm{Pe} \to \infty)$ and then considering the zero Mach number limit, $M \equiv 0$. The continuity equation in that case becomes redundant, the momentum equation reduces to

$$\frac{\partial \boldsymbol{v}}{\partial t} + \boldsymbol{v} \cdot \nabla \boldsymbol{v} + \nabla p_2 = 0 \tag{4.5.46}$$

and the leading-order energy equation yields the homogeneous velocity divergence constraint

$$\nabla \cdot \boldsymbol{v} = 0\,. \tag{4.5.47}$$

Notice that $\nabla \cdot (\boldsymbol{v} \circ \boldsymbol{v}) \equiv \boldsymbol{v} \cdot \nabla \boldsymbol{v}$ when $\nabla \cdot \boldsymbol{v} \equiv 0$!

A projection scheme consists of 2 steps. Step 1 accounts for non-linear convection, $\boldsymbol{v} \cdot \nabla \boldsymbol{v}$, in an explicit fashion by solving the truncated system

$$\frac{\partial \boldsymbol{v}}{\partial t} + \boldsymbol{v} \cdot \nabla \boldsymbol{v} = 0 \tag{4.5.48}$$

over one time step. Given the velocity field $\boldsymbol{v}^n$ at time t^n, the first step provides a mapping

$$\boldsymbol{v}^* = \boldsymbol{v}^n - \Delta t \, (\boldsymbol{v} \cdot \nabla \boldsymbol{v})^n \tag{4.5.49}$$

with a suitable numerical approximation of the convection terms. There is no guarantee that $\boldsymbol{v}^*$ will satisfy the divergence condition from Equation (4.5.47), and so the second step consists of "projecting" this intermediate velocity field back onto the space of divergence-free fields:

$$\boldsymbol{v}^{n+1} = \boldsymbol{v}^* - \nabla \phi\,, \tag{4.5.50}$$

with ϕ adjusted so as to let $\boldsymbol{v}^{n+1}$ comply with the divergence constraint, i.e.,

$$\nabla^2 \phi = \nabla \cdot \boldsymbol{v}^*\,. \tag{4.5.51}$$

That the correction to $\boldsymbol{v}^*$ should be in the form of a gradient field becomes intuitively clear from a comparison of the original momentum Equation (4.5.46) and the truncated one from the first projection step Equation (4.5.48). It was the pressure gradient field that was left out in formulating the first step of the scheme. More elaborate explanations and justifications, based on the Helmholtz-Hodge decomposition of general vector fields, are given in the original references [4.122 to 4.124] and in related subsequent publications [4.134 to 4.138]. The reader may also want to consult Reference [4.126] for detailed discussions of some difficulties and pitfalls associated with this approach.

Major efforts have recently been spent to extend this approach by introducing higher-order approximations, dynamic adaptive grid refinement (see [4.139]) and by allowing variable densities (while still keeping the zero divergence constraint!), [4.134, 4.138]. Further extensions are aimed at the representation of low Mach number reacting flows [4.135, 4.140].

4.5.4 The Mathematics of Deflagrations

Chemical reactions are typically very fast once they are ignited. As a consequence, the available fuel is quickly burned and reactions typically are concentrated in narrow regions. In fact, the characteristic thickness of a laminar premixed flame front is of the order of fractions of a millimetre. A systematic derivation, showing how fast reaction (large Damköhler number $\mathrm{Da} \gg 1$), and inefficient molecular transport (large Reynolds and Peclet numbers $\mathrm{Re}, \mathrm{Pe} \gg 1$) conspire to lead to thin combustion fronts with finite propagation speeds is given in Reference [4.44].

Numerical methods must cope with these constraints of thin fronts and slow flows. One approach to the thin front problem is dynamic grid refinement, by which one concentrates the numerical spatial resolution dynamically within the flame region. An alternative is front tracking. This approach considers a flame front as a reactive discontinuity converting unburnt to burnt gases. In this fashion, one avoids the stringent resolution requirements associated with a detailed representation of the internal flame structure as well as the technical compications associated with dynamic gridding. On the other hand, the required numerical techniques themselves become more complex because in addition the standard flow solver, the time evolution of the flame geometry and its coupling to the flow field must be represented appropriately. Thus one has to balance complexity that is due to data arrangement, data structures etc. from dynamic grid refinement versus the additional complications implied by front tracking and front flow coupling.

Some important implications for both approaches can be extracted from a general analysis of the mathematical nature of such reactive discontinuities. One central question concerns the mechanisms that determine the front propagation velocity. Obviously, these mechanisms must be represented accurately in a numerical scheme, be it of the "front tracking" or of the "dynamically adaptive" type. The next subsection collects a few mathematical derivations that provide some insight into this question and suggest a number of conclustions regarding appropriate numerical methods.

4.5.4.1 Mathematical features of deflagrations and other discontinuities

For simplicity, we restrict much of the subsequent discussion to a single space dimension. The key observations will not depend on this limitation.

Jump conditions. Consider one-dimensional travelling wave solutions in an unbounded domain of the scaled governing equations from Equations (4.5.9) to (4.5.14). Any variable $\phi(\boldsymbol{x}, t)$ would be described

by

$$\phi(\boldsymbol{x},t) = \tilde{\phi}(x - Dt)\,, \tag{4.5.52}$$

where it is assumed that the wave travels in the x-direction at velocity D. Inserting this ansatz in the governing equations we obtain

$$\begin{aligned}
-D\frac{d}{d\xi}(\rho) \quad &+ \quad \frac{d}{d\xi}(\rho u) \qquad\qquad\quad &= \quad 0 \\
-D\frac{d}{d\xi}(\rho u) \quad &+ \quad \frac{d}{d\xi}(\rho u^2 + \frac{1}{M^2}\,p) \quad &= \quad -\frac{d}{d\xi}\left(\frac{1}{\mathrm{Re}}\tau_{x,x}\right) \\
-D\frac{d}{d\xi}(\rho e) \quad &+ \quad \frac{d}{d\xi}(u[\rho e + p]) \qquad &= \quad -\frac{d}{d\xi}\left(\frac{1}{\mathrm{Pe}}j_{T,x} + \frac{M^2}{\mathrm{Re}}\tau_{x,x}u + \frac{Q}{\mathrm{ReSc}}\sum_{i=1}^{n_{\mathrm{spec}}}\delta h_i\, j_{i,x}\right).
\end{aligned} \tag{4.5.53}$$

from the conservation laws and

$$-D\frac{d}{d\xi}(\rho Y_i) + \frac{d}{d\xi}(\rho Y_i u) = -\frac{d}{d\xi}\left(\frac{1}{\mathrm{ReSc}}\,j_{i,x}\right) + \mathrm{Da}\rho\omega_i \qquad (i = 1 \ldots n_{\mathrm{spec}}) \tag{4.5.54}$$

from the species balances. Here $\xi = x - Dt$ and $\tau_{x,x}, j_{T,x}, j_{i,x}$ are the x-components of the x-stress component, the heat conduction energy flux and the ith species diffusion fluxes, respectively.

Next, we integrate in ξ assuming that constant burnt gas and unburnt gas conditions $(\rho, u, p, Y_i)_b$ and $(\rho, u, p, Y_i)_u$ are attained as $\xi \to -\infty$ and $\xi \to \infty$, respectively. Under these assumptions, the diffusive fluxes and the heat conduction terms vanish as $|\xi| \to \infty$ because they are proportional to gradients of the dependent variables. Integration of Equation (4.5.53) yields

$$\begin{aligned}
-D[\![\rho]\!] \quad &+ \quad [\![\rho u]\!] \qquad\qquad &= \quad 0 \\
-D[\![\rho u]\!] \quad &+ \quad [\![\rho u^2 + \tfrac{1}{M^2}\,p]\!] \quad &= \quad 0 \\
-D[\![\rho e]\!] \quad &+ \quad [\![u(\rho e + p)]\!] \quad &= \quad 0.
\end{aligned} \tag{4.5.55}$$

These are the standard Rankine-Hugoniot jump condtions for gas dynamic discontinuities.

Since we assume that at large distances two constant states of burnt and unburnt should be attained, we must require that the chemical reaction rates vanish at both ends:

$$\boldsymbol{\omega}(T_u, p_u, \boldsymbol{Y}_u) = \boldsymbol{\omega}(T_b, p_b, \boldsymbol{Y}_b) = 0 \tag{4.5.56}$$

where

$$\boldsymbol{Y} = \{Y_j\}_{j=1}^{n_{\mathrm{spec}}} \qquad \text{and} \qquad \boldsymbol{\omega} = \{\omega_j\}_{j=1}^{n_{\mathrm{spec}}}\,. \tag{4.5.57}$$

In the unburnt gas this constraint is normally satisfied automatically because the reactions are frozen at low temperatures. Therefore, as in real-life applications, the unburnt gas composition can be chosen more or less arbitrarily. For the burnt gas one obtains a non-trivial constraint because temperatures will generally be high enough to allow chemical reactions to be active. Thus one may read the second equality in Equation (4.5.56) as algebraic constraints for the equilibrium species mass fractions $\boldsymbol{Y}^{\mathrm{eq}}(T_b, p_b, \boldsymbol{Y}_u)$:

$$\boldsymbol{\omega}\left(T_b, p_b, \boldsymbol{Y}^{\mathrm{eq}}(T_b, p_b, \boldsymbol{Y}_u)\right) = 0\,. \tag{4.5.58}$$

The dependence of $\boldsymbol{Y}^{\rm eq}(T_b, p_b, \boldsymbol{Y}_u)$ on $\boldsymbol{Y}_u$ results from the constraint that their detailed *atomic* compositions must be the same. After all, chemistry is nothing but a re-arrangement of atoms between molecules. The appropriate mathematical description is

$$\sum_{j=1}^{n_{\rm spec}} \nu_i^j \, \frac{1}{\mathcal{M}_j} \, (Y_{j,b} - Y_{j,u}) = 0 \qquad (i = 1 \ldots n_{\rm atoms}) \,, \tag{4.5.59}$$

where ν_i^j is the number of atoms of type i in a molecule of species j, and $\mathcal{M}_j$ is the molecular weight of species j.

Characteristic analysis of the inviscid, inert flow equations. We turn next to the question in which way a reactive discontinuity influences its surrounding flow field and in which way it must respond, in turn, to input from outside. Since in most practical applications the Reynolds and Peclet numbers are very large, important insight can be gained by analyzing the inviscid flow equations. Moreover, we are interested here in the behaviour of the flow *surrounding* a reactive front, so that we may restrict our discussion to the case of a reactive discontinuity embedded between the masses of non-reactive burnt and unburnt gases.

Thus we consider the conservation equations

$$\begin{array}{rcrcl} (\rho)_t & + & (\rho u)_x & = & 0 \\ (\rho u)_t & + & (\rho u^2 + \frac{1}{M^2}\, p)_x & = & 0 \\ (\rho e)_t & + & (u[\rho e + p])_x & = & 0. \end{array} \tag{4.5.60}$$

with

$$(\rho e) = \frac{p}{\gamma - 1} + \frac{M^2}{2} \rho u^2 \,. \tag{4.5.61}$$

Applying the chain rule of differentiation repeatedly and forming a number of linear combinations one may transform these equations to the quasi-linear form

$$\begin{array}{rcrcrcl} \rho_t & + & u\,\rho_x & + & \rho\, u_x & = & 0 \\ u_t & + & u\, u_x & + & \frac{1}{M^2}\frac{1}{\rho}\, p_x & = & 0 \\ p_t & + & u\, p_x & + & \gamma p\, u_x & = & 0. \end{array} \tag{4.5.62}$$

(In fact, the chain rule immediately yields Equation $(4.5.62)_1$, subtraction of [$u \times$ Equation $(4.5.60)_1$] from Equation $(4.5.60)_2$ yields Equation $(4.5.62)_2$ and subtraction of [$u \times$ Equation $(4.5.60)_2$] from Equation $(4.5.60)_3$ yields Equation $(4.5.62)_3$.)

Now subtraction of [$(\gamma p/\rho) \times$ Equation $(4.5.62)_1$] from Equation $(4.5.62)_3$ yields the first compatibility condition of the theory of characteristics:

$$(p_t + u p_x) - c^2 \, (\rho_t + u \rho_x) = 0 \tag{4.5.63}$$

where

$$c = \sqrt{\frac{\gamma p}{\rho}} \tag{4.5.64}$$

is the scaled speed of sound. Similarly, by adding and subtracting [$(M\,\rho c) \times$ Equation $(4.5.62)_2$] to / from Equation $(4.5.62)_3$ one obtains the compatibility conditions

$$\begin{array}{rcrcl} \left(p_t + (u + \frac{1}{M} c)\, p_x\right) & + & M\,\rho c\, \left(u_t + (u + \frac{1}{M} c)\, u_x\right) & = & 0 \\ \left(p_t + (u - \frac{1}{M} c)\, p_x\right) & - & M\,\rho c\, \left(u_t + (u - \frac{1}{M} c)\, u_x\right) & = & 0\,. \end{array} \tag{4.5.65}$$

The operators

$$\left(\frac{\partial}{\partial t}\right)_{\rm pp} = \frac{\partial}{\partial t} + u\,\frac{\partial}{\partial x} \qquad \text{and} \qquad \left(\frac{\partial}{\partial t}\right)^{\pm}_{\rm ac} = \frac{\partial}{\partial t} + (u \pm \tfrac{1}{M}c)\,\frac{\partial}{\partial x} \tag{4.5.66}$$

are "directional derivatives", describing time derivatives as seen by observers "pp" and "ac" moving with velocities u and $u \pm \frac{1}{M}c$, respectively. The observer motions $x_{\rm pp}(t)$ and $x^{\pm}_{\rm ac}(t)$ thus obey the evolution equations

$$\frac{dx_{\rm pp}}{dt} = u \qquad \text{and} \qquad \frac{dx^{\pm}_{\rm ac}}{dt} = u \pm \tfrac{1}{M}c\,. \tag{4.5.67}$$

In other words, $(\partial/\partial t)_{\rm pp}$ indicates temporal variations seen along a particle path, whereas $(\partial/\partial t)^{\pm}_{\rm ac}$ denotes time derivatives seen by an observer moving with an acoustic signal.

The three compatibility conditions from Equations (4.5.63) and (4.5.65) contain the same information as the original conservation laws (Equation (4.5.60)) or the primitive formulation (Equation (4.5.62)) as long as all required derivatives exist. The key advantage of this "characteristic formulation" is that it explicitly shows how information is transported in time. We will use this insight now to discuss the mathematical features of gas dynamic discontinuities. We consider Figure 4.5.4.1- 1 and ask, what information is

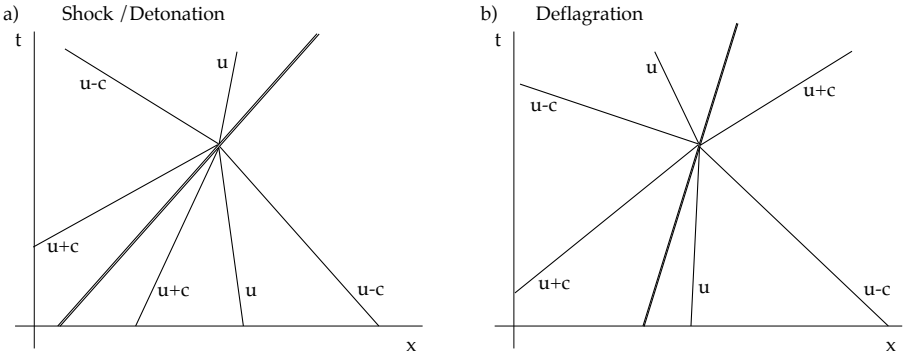

Figure 4.5.4.1- 1: Characteristic diagrams for shocks and detonations (a) and deflagrations (b)

available at any given time to determine the 2 states immediately in front of and behind a discontinuity together with its front propagation speed: For the species mass fractions we have $n_{\rm spec}$ equations from Equations (4.5.56) and (4.5.59), allowing us to determine the burnt gas composition, once the unburnt composition and the burnt gas pressure and temperature (or density) are known. (For a non-reactive front, such as a shock wave these reduce to the condition that the species mass fractions do not change across the front.)

Differentiating the fluxes $\rho Y_i u$ in the species transport equations (Equation (4.5.10)) and neglecting the right-hand-side expressions, one finds compatibility conditions for the species mass fractions in the unburnt gas,

$$\boldsymbol{Y}_t + u\,\boldsymbol{Y}_x = 0\,. \tag{4.5.68}$$

These equations state that the species mass fractions do not change along particle paths outside the reaction front. Based on this, one finds the unburnt gas composition in front of a discontinuity at any time t as follows: Track the particle path $dx_{pp}/dt = u$, which arrives at the front at time t, backwards in time until you reach the initial time $t = 0$. The composition found at that location is the same as the unburnt gas composition near the front at the later instance t (cf. Figure 4.5.4.1- 1).

Thus we only need to check whether there is a sufficient number of equations to determine pressures, densities, and velocities in the burnt and unburnt, (p_b, ρ_b, u_b) and (p_u, ρ_u, u_u), plus the front propagation speed D. These are altogether 7 unknowns.

Consider Figure 4.5.4.1- 1a, which shows the sketch of a propagating shock or detonation wave. The number of characteristic curves that *arrive* at the discontinuity from earlier times is 4. Adding the 3 jump conditions from Equation (4.5.55), we have 7 equations for the 7 unknowns. These turn out to be independent equations, and thus the burnt and unburnt states plus the propagation speed D are completely determined just through the equations of motion, the species transport equations outside the front, the Hugoniot jump conditions, and suitable initial or boundary data or both.

The situation is different for deflagrations as can be seen in Figure 4.5.4.1- 1b. The forward acoustic signal $dx^+_{ac}/dt = u + \frac{1}{M}c$ *emerges from* the discontinuity rather than *arriving at it*. Thus the associated compatibility conditions can only be used in determining the further evolution but not to connect the current states near the front to the given initial (and boundary) conditions. One determining equation for (p_b, ρ_b, u_b), (p_u, ρ_u, u_u) and D is missing! The missing relation is a burning velocity eigenvalue, providing an explicit functional relation between the pre- and post-front states and the propagation speed D. The burning rate law is typically given as

$$D = u_u + s(p_u, \rho_u, \boldsymbol{Y}_u) \tag{4.5.69}$$

with some explicit function $s(p, \rho, \boldsymbol{Y})$.

That a flame speed law must be provided in order to uniquely determine the propagation of a deflagration wave has a deeper physical reason than just the "number counting game" pursued above. Shock waves as well as detonations are governed by inviscid gas dynamics only. Chemical reactions in detonations are triggered by shock wave compression, and their exremely high, supersonic propagation speed renders the effects of molecular transport irrelevant. Once a shock has sufficiently compressed the gas, temperatures are high enough to lead to auto-ignition, and the reaction heat release sets in. The rate of fuel consumption is determined completely by this compression-ignition-reaction sequence that involves only inviscid gas dynamics.

This is in contrast to the physics of deflagrations. Here, the hot burnt gases preheat the unburnt gas right in front of the flame through heat conduction (or radiation or both) and chemical radicals diffuse out of the reaction zone into the unburnt gas region. Once this process of preheating and chemical preconditioning has lead to sufficient reactivity, combustion takes place and the front propagates. The whole process hinges on heat conduction and species diffusion, both of which are not represented in the characteristic analysis of the inviscid flow equations given above. We conclude that

The detailed processes within the flame structure crucially influence the flame propagation.

Consequences for numerical simulations of turbulent deflagrations. The importance of this simple statement for any attempt at numerical simulation of deflagration waves cannot be overestimated! Let us distinguish two very different alternative approaches:

1. detailed modelling of the inner flame structure, and
2. flame front tracking.

By the first approach one implements numerical representations of both the overall reaction and turbulent transport sub-mechanisms that are active within the flame region. As we have seen above, it is the detailed interplay between reaction rates and transport processes that is responsible for establishing the net unburnt gas mass consumption rate. As a consequence, equal emphasis must be given to either of these subprocesses. In other words, an excellent mean reaction rate model is useless unless combined with an equally sophisticated turbulent effective transport scheme because errors in the latter could completely falsify the overall combustion rates, regardless of the quality of the former. In addition, the "full-resolution approach" requires sufficient spatial and temporal numerical resolution of the flame region in order to achieve the desired accuracy in representing the reaction-transport interplay.

Flame front tracking approaches avoid the necessity of modelling the complex phenomena within a "flame brush". They represent a deflagration as a reactive discontinuity and obtain a closed equation system by supplying an explicit burning rate law as a function of the unburnt gas thermodynamic, composition, and turbulence state. The advantages of this approach over detailled modelling are (i) that it explicitly controls the net mass burning rate without relying on subtle interactions between submodels of net turbulent reaction rates and effective turbulent transport and (ii) that it allows much coarser spatial and temporal resolution. Its disadvantage is that one must supply effective turbulent flame speed functions, which can be derived from scratch only in particular regimes of turbulent combustion. Front tracking has one more advantage in the context of implementing experimental knowledge in a numerical simulation system: Measuring effective turbulent burning velocities experimentally is much easier than distinguishing detailed subprocesses within a flame brush by localized measurements.

We conclude that both approaches have their merits and preferred ranges of applications: In practical engineering applications, the front tracking approach is advantageous because (i) it has only a single modelled quantity, the turbulent burning velocity; and (ii) there is no need to resolve spatial scales on the order of the turbulent flame thickness. In contrast, detailled modelling of the turbulent suubprocesses within a flame brush is the more fundamental approach, by which one can, potentially, represent all the underlying physics leading to the establishment of the overall combustion rate. However, this approach is meaningful only if *all* the relevant subprocesses are properly modelled and resolved.

A flame front tracking scheme that allows the inclusion of a quasi-one-dimensional dynamic internal flame structure model is work in progress.

4.5.5 Numerical Representation of Deflagration Waves

4.5.5.1 Resolved turbulent flame structures

The advantages of an approach that relies on detailled numerical resolution of the internal structure of a deflagration are that

- All important physical sub-mechanisms within a turbulent flame zone as well as their interactions can be incorporated.
- The mathematical structure of the most popular turbulent combustion models is similar to a combination of standard non-reactive turbulent flow models and the laminar reactive Navier-Stokes equations. Thus available reactive flow solvers can be employed more or less "out of the box" for turbulent combustion simulations.

The disadvantages are that

- A detailed representation of the turbulent flame brush structure leads to minimum spatial resolution requirements that can become overwhelming for large-scale, industrial-size systems. This issue may enforce the use of dynamically adaptive grids, with all the added complexity.
- Advantage 2, above, holds only when the turbulent combustion model excludes certain non-standard effects, such as counter-gradient turbulent transport [4.49, 4.50]. If such effects are expected to be important, adequate numerical techniques must be implemented.

Unfortunately, a considerable number of physical effects that are expected to be important during the early stages of turbulent flame acceleration have been identified and are not properly represented by standard models. Bray lists the following, (see [4.1] and the extensive list of references therein):

- the modification of large-scale turbulent transport by heat release including the phenomenon of counter-gradient transport;
- the sensitivity of turbulent transport to pressure gradients.
- the generation of turbulence because of heat release;
- the modification of small-scale mixing, as characterized by viscous and scalar disspation, because of heat release;
- the modification of pressure-velocity fluctuation correlations in the second moment evolution equations as a result of heat release; and
- the introduction into the mean flow equations of additional characteristic length and time scales linked to laminar flame instabilities.

It is estimated that the importance of all these effects should decrease with increasing turbulence intensity and that it should become negligible as $u'/s_L \rightarrow \infty$. Thus successful simulations of high-speed turbulent combustion should be (and are) possible without inclusion of these effects. Yet, as stated earlier, accurate predictions of the transitional phase of flame acceleration require more sophisticated models and appropriate numerical techniques.

For example, implementations of the Bray-Moss-Libby model in the context of a consistent second-order closure are reported in Reference [4.141]. However, it is stated in Reference [4.1] that these authors did need to deviate from the original BML model in the closure of the second-order moment equations in order to overcome numerical difficulties arising from the non-standard structure of the BML model.

Given that there is no widespread agreement regarding the proper mathematical structure of a model that would incorporate all the effects mentioned above, little general advice can be given regarding the numerical techniques that should be employed or developed in order to cope with the arising complexities.

4.5.5.2 Flame front tracking

As mentioned above, flame front tracking requires the numerical representation of the flame geometry and its evolution *and* of the coupling between front and surrounding flow via the Rankine-Hugoniot conditions (Equation (4.5.55)).

*The level set or **G**-equation approach.* As discussed above, premixed flames propagate relative to the unburnt gas at the local burning velocity s. For a two-dimensional setting, the situation is sketched in Figure 4.5.5.2- 1. The propagation of points on a flame surface is determined by the superposition of convection by the unburnt gas flow and this self-propagation in the direction normal to the front

$$d\,\boldsymbol{x}_f/dt = \boldsymbol{v}_u + s\boldsymbol{n} = \boldsymbol{D}. \tag{4.5.70}$$

Here $\boldsymbol{n}$ is a unit normal vector on the front pointing towards the unburnt gas region. The level set or G-equation approach introduces a scalar field $G(\boldsymbol{x}, t)$ whose iso-surfaces

$$G(\boldsymbol{x}, t) = G_0 \tag{4.5.71}$$

are identified with flame fronts. Then

$$\boldsymbol{n} = -\left.\frac{\nabla G}{|\nabla G|}\right|_{G=G_0}. \tag{4.5.72}$$

The choice of G_0 is arbitrary but fixed for a single combustion event. The flame surface(s) $G = G_0$ naturally decompose the flow domain into unburnt gas ($G < G_0$) and burnt gas regions ($G > G_0$). Differentiating Equation (4.5.71) with respect to time and using Equation (4.5.70) one finds

$$\frac{\partial G}{\partial t} + \frac{d\boldsymbol{x}_f}{dt}\cdot\nabla G = \frac{\partial G}{\partial t} + \boldsymbol{D}\cdot\nabla G = 0\,, \tag{4.5.73}$$

the G-equation.

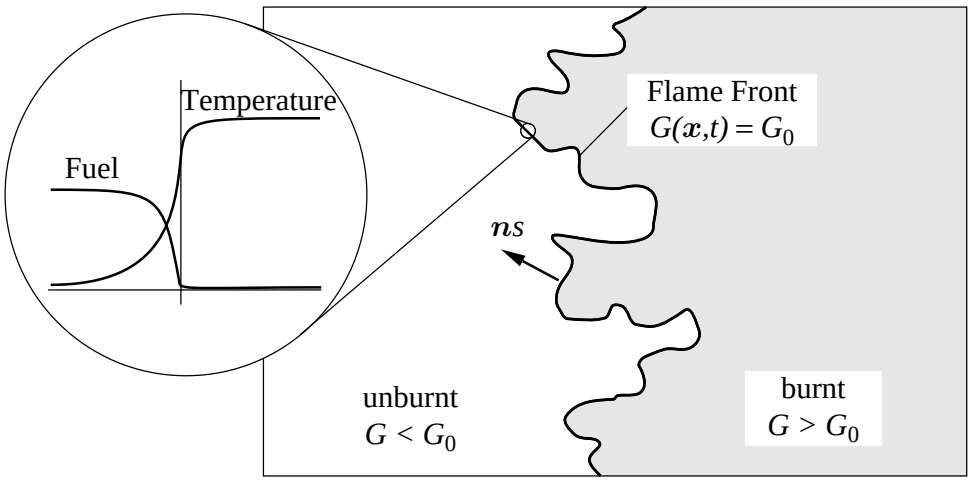

Figure 4.5.5.2- 1: Schematic representation of premixed flame front propagation

The key physical ingredients of the level set approach are the burning velocity law determining s as a function of thermo-chemical and flow conditions and some local features of the flame geometry. It is important to notice that s is defined as the relative velocity between points on the front and the unburnt

gas immediately *in front* of it. The relative velocity s_b between the burnt gas and the front differs from s because of the thermal gas expansion within the flame front and the associated jump of the normal velocity. Because of mass conservation the mass flux density normal to the front does not change across the discontinuity and the burnt gas relative speed is easily computed as

$$\rho s = (\rho s)_b = \rho_u s \quad \Rightarrow \quad s_b = \frac{\rho_u}{\rho_b} s \,. \tag{4.5.74}$$

Although both the flow velocity and the relative speed between flow field and front change across the flame, their sum, namely the vector $\boldsymbol{D}$ appearing in Equation (4.5.73), does not! This observation will be important in the subsequent construction of a numerical method.

Figure 4.5.5.2- 2 shows the temporal evolution of an initially sinusoidally distorted front according to Equation (4.5.73), with $s \equiv const.$ and with the unburnt gas at rest. The front motion then follows Huygens' principle, and one quickly observes the formation of sharp cusps on the front. Laminar flame theory, [4.96, 4.142], as well as modern theories of turbulent premixed combustion, [4.45, 4.77], yield modified, curvature dependent burning velocity laws of the type

$$s = s^0 - s^0 \mathcal{L} \kappa + \mathcal{L} \boldsymbol{n} \cdot \nabla \boldsymbol{v} \cdot \boldsymbol{n} \quad \text{where} \quad \kappa = \nabla \cdot \boldsymbol{n} \tag{4.5.75}$$

is the mean front curvature. The second and third terms describe the net effect of the (turbulent) diffusive processes (second term) and by outer straining of the flame by the surrounding flow field (third term). In detail, s^0 is the burning velocity of a plain, unstrained flame, $\mathcal{L}$ is an effective Markstein length, and κ is the local mean front curvature. As indicated in Figure 4.5.5.2- 2 the curvature is defined to be positive

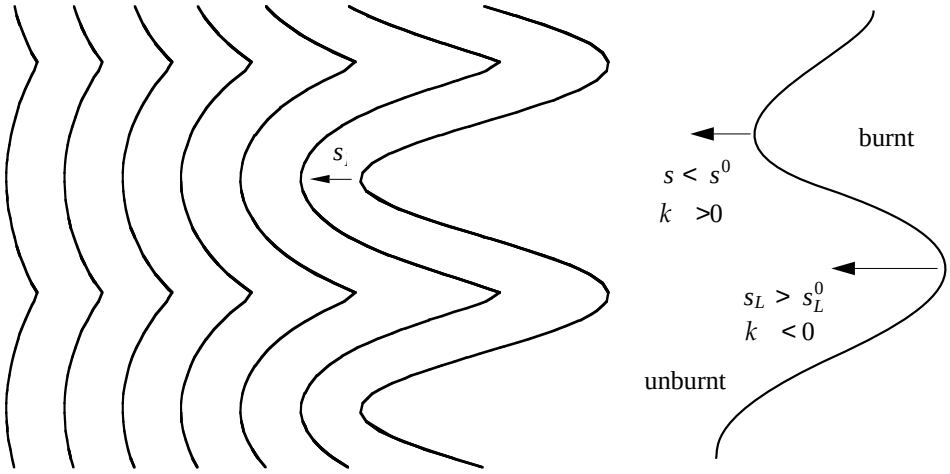

Figure 4.5.5.2- 2: Flame propagation according to Equation (4.5.73) for constant burning velocity s; schematic for the influence of curvature

when the front is convex with respect to the unburnt gas and vice versa. For positive Markstein numbers the curvature term thus prohibits the formation of sharp cusps on the flame front.

Determination of level sets away from the tracked front. There is one important issue that needs to be accounted for when dealing with "real" flames within which substantial chemical heat is released. The propagation Equation (4.5.73) is valid at the flame front only, since only at the front is the burning velocity s properly defined. Thus one needs to introduce additional constraints determining the time evolution of the scalar G away from the tracked interface. One option, proposed in Reference [4.62], is

to require the level set scalar to be a signed distance function away from the front. This is equivalent to requiring that

$$|\nabla G| = 1 \tag{4.5.76}$$

and the additional requirement that G be negative in the unburnt and positive in the burnt gas region. For a related numerical technique to enforce the distance function property, see Section 4.5.5.2.

Flame-flow coupling. Having adopted the level set approach to describe the evolution of the flame front geometry, one must next describe the mutual interactions between the tracked front and the surrounding flow. From Equation (4.5.70) and Equation (4.5.73) it is clear how the unburnt gas flow affects the flame motion: The flame propagation velocity consists of (i) passive advection by the unburnt gas velocity and (ii) of self-propagation induced by combustion. The unburnt gas conditions influence this latter part through explicit burning velocity laws as described in Section 4.5.4.

The front, in turn, influences the surrounding flow by enforcing the flame discontinuity jump conditions (Equation (4.5.55)) for the flow variables at the flame location $G(\boldsymbol{x}, t) = G_0$. Various methods have been developed in recent years to realize this coupling in the context of finite-volume methods, [4.53, 4.54, 4.99, 4.143 to 4.146]. These schemes mainly differ in their degree of complexity and detail and in their applicability to compressible and incompressible flows.

Chern and Colella [4.143], Bourlioux and Majda [4.144], and LeVeque and Shyue [4.145] consider compressible flows and treat the moving front surface as part of their time dependent numerical grid. For each of the subcells generated when a front intersects a grid-cell of the underlying computational mesh a complete conservative flux update is performed. The CFL-type time-step restrictions associated with updating small subcells are overcome by distributing excess accumulations of the conserved quantities among the neighbouring grid-cells. The schemes differ in how this is done in detail, but they all follow this common pattern.

The method described in Reference [4.53], which is also designed for compressible flows, compromises on the former schemes in that only *complete grid-cells* are updated by flux balances. The flame-generated subcells are used only in an "in-cell reconstruction step", which recovers burnt and unburnt gas conditions from the cell averages using a suitable set of recovery equations (see the appendix). The consequence is that, while the scheme *does* conserve mass, momentum, and energy between grid-cells and globally, it is *not* conservative with respect to these subcells. The method therefore does not automatically conserve mass, momentum, and energy between the pre- and post-front regions. For flame fronts, this just amounts to numerical truncation errors affecting the net burning rate and is not critical. However, in tracking a passive non-reactive fluid interface, such as the surface of a water droplet in air, this scheme would not conserve the droplet mass. An associated improvement is work in progress [4.98].

Terhoeven [4.146] and Klein [4.99], to our knowledge, are the first to propose a flame front tracking scheme for zero Mach number flows in the finite-volume context (see, however, also [4.147]). The key ideas are the same as those in Reference [4.53], but there are important modifications that become indispensable in the limit of small and zero Mach numbers. The key difficulty has been discussed earlier in Section 4.5.2. The second-order pressure p_2 in a low Mach number pressure expansion is responsible for flow accelerations. Within the flame discontinuity there is an order $O(1)$ density change and an associated flow acceleration. This can be accomplished only through a pressure discontinuity. The consequence is that the second-order pressure must satisfy a Poisson equation with a singular source term that ensures the appropriate pressure jump across the flame surface. For more detail the reader may wish

to consult the original references.

Fedkiw et al. [4.54] again consider compressibe flows, but go one step further in simplifying the approach. By compromising on conservation also for the complete "mixed cells", they are able to design a numerical method that is very attractive because of its simplicity and nearly dimension-independent formulation.

A sample result obtained using the capturing/tracking hybrid scheme from Reference [4.53] is described in Figs. 4.5.5.2- 3 and 4.5.5.2- 4. The RUT test h11 has been reproduced using a two-dimensional approximation, a standard $k-\epsilon$ turbulence model, and Damköhler's law to represent the effective turbulent burning velocity as

$$s_T = s_L + u' \qquad \text{where} \qquad u' = \sqrt{2k} \tag{4.5.77}$$

with k from the $k-\epsilon$ model data in the unburnt gas immediately in front of the flame. The coloured density contours show the propagation of the sharp flame surface in time, and the second figure shows a comparison of space-time diagrams of the flame tip location as taken from experiment and computation. It turns out that the initial phase is slightly misrepresented, in that the computed flame acceleration is too slow. Yet as soon as the first obstacle is reached, the experimental and computed flame locations agree convincingly well.

4.5.6 Numerical Issues of Stiff and Fast Chemistry

A typical chemical species balance equation reads

$$\frac{\partial \rho Y_i}{\partial t} + \nabla\cdot(\rho Y_i \boldsymbol{v}) + \nabla\cdot(\boldsymbol{j}_i) = -\rho \sum_{k=1}^{n_{\text{reac}}} a_i^k \omega_k(\boldsymbol{Y}, p, T)\,. \tag{4.5.78}$$

Here $\omega_k(\boldsymbol{Y}, p, T)$ is the reaction rate of the kth chemical reaction, and a_i^k is the stoichiometric coefficient of species i in the kth reaction. The standard form of the kth elementary reaction may read

$$\sum_{j=1}^{n_{\text{spec}}} a_j^{k,-} X^j \leftrightarrow \sum_{j=1}^{n_{\text{spec}}} a_j^{k,+} X^j \tag{4.5.79}$$

and then

$$a_j^k = a_j^{k,+} - a_j^{k,-}\,. \tag{4.5.80}$$

The classical Arrhenius law of mass action expressions for the reaction rate ω_k reads

$$\omega_k(\boldsymbol{Y}, p, T) = K_k^+ \, e^{-T_k^+/T} \prod_{j=1}^{n_{\text{spec}}} Y_j^{a_j^{k,+}} - K_k^- \, e^{-T_k^-/T} \prod_{j=1}^{n_{\text{spec}}} Y_j^{a_j^{k,-}} \tag{4.5.81}$$

The problems of "stiff, fast and complex" chemistry arise, because typically one has

$$K_k^+,\; K_k^-,\; n_{\text{spec}},\; n_{\text{reac}},\; \frac{T_k^+}{T_\infty},\; \frac{T_k^-}{T_\infty} \;\gg 1 \tag{4.5.82}$$

where T_∞ is a characteristic temperature in the system.

Although the requirements resulting from large numbers of species and reactions are more or less obvious (heavy computer time and memory demands), the issues of stiffness and rapidity of chemical reactions deserve an explanation.

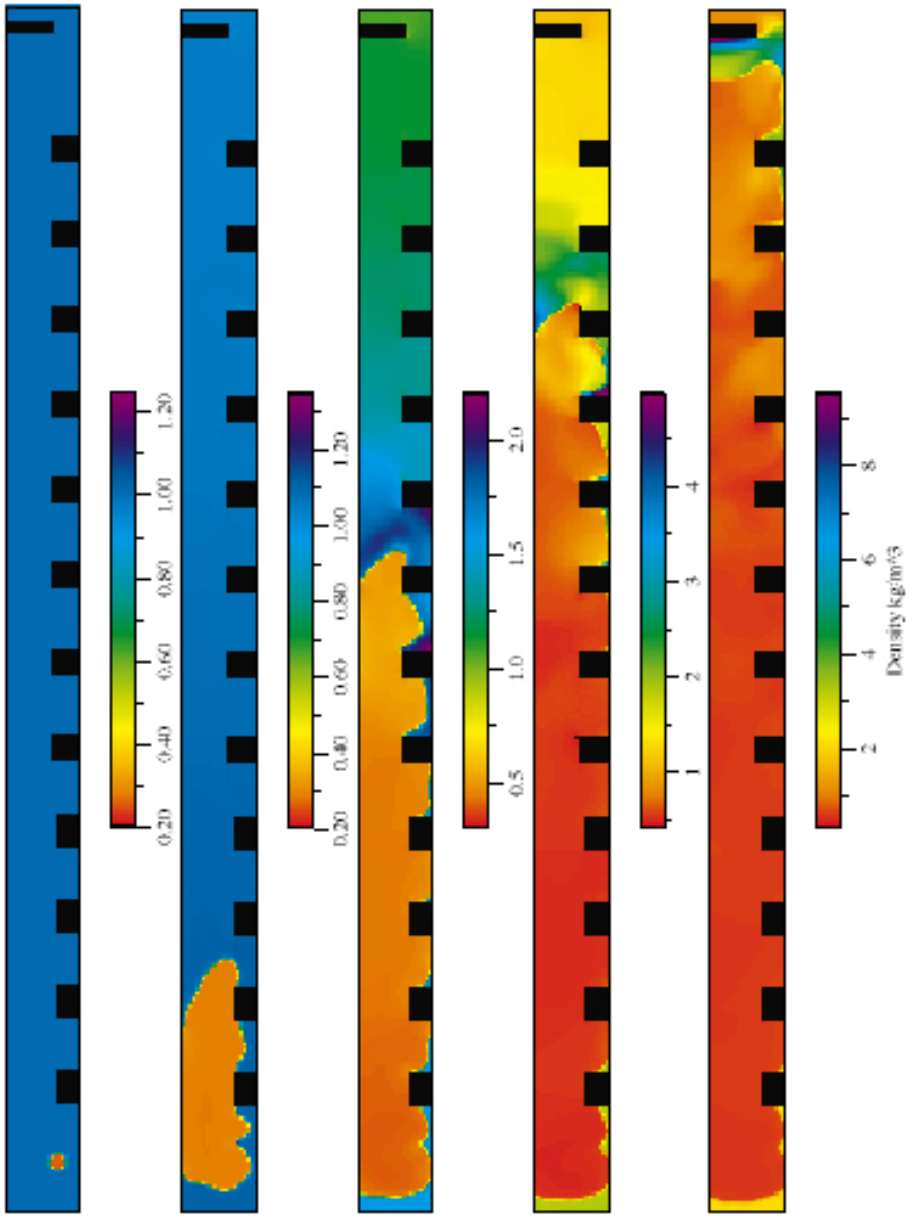

Figure 4.5.5.2- 3: Sequence of density contours as computed in a two-dimensional model for RUT test h11 using the flame front capturing/tracking hybrid scheme from Reference [4.53]

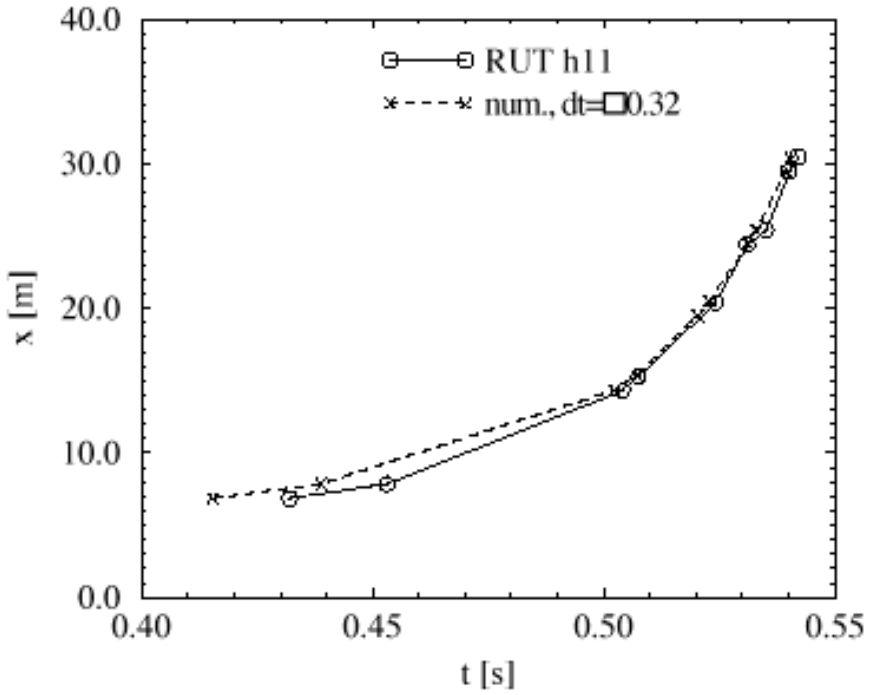

Figure 4.5.5.2- 4: Comparison of the time history of flame propagation in the test case from Figure 4.5.5.2- 3

4.5.6.1 Stiffness

For stiff reations, one or both of the reaction rate coefficients $K_k^{\pm} \exp(-T_k^{\pm}/T)$ is very large, much larger—in fact—than the inverse of a typical characteristic time of flow field evolution and of the actual time scale of reaction progress. As a consequence, the kth reaction must be in an approximate balance, with $|\omega_k| \ll K_k^{\pm} \exp(-T_k^{\pm}/T)$. Suppose now, that numerical approximation errors induce a perturbation of one of the species mass fractions $\delta Y_i \ll Y_i$. The resulting perturbation of the reaction rate is

$$\delta\omega_k = \left(K_k^+ \, e^{-T_k^+/T} \prod_{j \neq i} Y_j^{a_j^{k,+}} - K_k^- \, e^{-T_k^-/T} \prod_{j \neq i} Y_j^{a_j^{k,-}} \right) \delta Y_i \, . \tag{4.5.83}$$

One immediately finds that

$$\frac{\delta\omega_k}{\omega_k} \gg \frac{\delta Y_i}{Y_i} \tag{4.5.84}$$

indicating that minute errors in the species mass fractions induce large fluctuations of the reaction rates. Obviously, when the rate coefficients are sufficiently large, such perturbations lead to chemical kinetic responses with time scales that are orders of magnitude shorter than the actual characteristic chemical time scale of the exact solution. Extremely robust numerical integration schemes must be employed to handle this kind of situation without undue unstable numerical response.

However, even a robust, non-oscillatory numerical treatment is insufficient when the chemical species involved play a crucial role for the overall reaction progress. This is the case, for example, for chemical radicals such as the Hydrogen atom. These species are responsible for opening the reaction paths that

produce the major heat release in typical combustion systems. At the same time, they are extremely reactive, so that their consumption kinetics is extremely fast—in contrast to their production, which is typically much slower. The result is that radicals are consumed immediately whenever they are produced and that their mass fractions always remain very small. Since, on the other hand, they induce the primary breakup of the fuel species, it is adamant that their minute concentrations be computed very accurately. Hence robustness and accuracy are of equal importance and dynamically adaptive numerical techniques and error control must be invoked. The subtle numerical problems associated with stiff relaxation processes are discussed extensively in textbooks on the matter, such as Reference [4.148]. Most of these texts address systems of ordinary differential equations.

Obviously, the problem is aggravated when reaction processes in multi-dimensional flows are to be computed. We emphasize that the simple coupling of highly accurate stiff ODE solvers with standard multi-dimensional flow solvers through the popular operator splitting technique from Reference [4.149], will not automatically lead to a satisfactory solution. The sophisticated error control in the stiff ODE solvers will not indicate the additional errors induced by operator splitting between fluid mechanics and chemistry. Hence even though that approach will allow the construction of robust numerical methods, accuracy can be utterly corrupted.

We also emphasize that temporal and spatial adaptivity alone is insufficient when it is not combined with sophisticated refinement indicators that are based on fully multi-dimensional error control. Unfortunately, rigorously supported error estimators for large Reynolds number compressible and zero Mach number flows are work in progress at this time even for non-reactive flows [4.107, 4.108]!

4.5.6.2 Fast Chemistry

The physics associated with rapid heat release is distinguished here from the issues of stiff chemistry, even though they are closely related in that both are associated with short, chemistry-induced time scales. By the label "fast chemistry" we denote a situation where the actual time scale of chemical heat release whenever it occurs is much shorter than the characteristic time scales of the surrounding flow. Because of the tight coupling of chemical reaction progress and fluid mechanics through total energy conservation, fast chemical reactions are in all practical situations associated with the establishment of thin combustion zones. This statement holds for benign low Mach number diffusion flames (as on candles) as well as for the most violent combustion events, detonation waves. The combustion zones can be either thin laminar or quasi-laminar flames on the smallest scales or complete turbulent flame brushes when the overall length scale of the considered flow is sufficiently large. The latter is true, for example, for large-scale industrial devices.

In numerical simulations one is faced with the options of either developing sophisticated adaptive numerical techniques that allow one to resolve in detail the thin reaction fronts or to develop combined models and numerical schemes that handle these fronts as infinitily thin reactive surfaces. The former approach requires accurate modelling and numerical representation of all aero-thermodynamic processes that interact within the combustion zone. The advantage of that approach is, obviously, that each of these submechanisms can be accounted for and its effect assessed. The disadvavage is that in fact all the subprocesses *must* be represented properly to obtain acceptably accurate answers, (see also Section 4.5.4). The latter approach requires an accurate representation of the coupling between the reaction front and the surrounding flow and an equally accurate representation of the response of the reaction zone to fluid mechanical perturbations in the vicinity. The advantage of this approach is that it allows much coarser numerical resolution than the former and that it has fewer mechanisms to be modelled and computed,

such as flame speeds and effective jump conditions. The disadvantage is that effects on the length and time scale of the internal combustion zone structure are lost. (Compromises between both approaches are work that is in progress.)

Unless in a direct numerical simulation (DNS) of the compressible reactive Navier-Stokes equations all length and time scales are resolved, the effects of chemical kinetics enter in both approaches through suitable subgrid-scale turbulent combustion models. Notice that with the expected computational capacities for the next decade one cannot expect to resolve by DNS realistic scale turbulence combustion processes relevant to industrial safety problems. Hence the issue of an accurate integration of chemical species transport equations with detailed chemistry, as discussed in the previous subsection, becomes irrelevant. In fact, the turbulent combustion submodels most often have little in common with detailed chemical kinetics (see Section 4.3), so that the numerical algorithmic requirements are very different.

4.5.7 Computational Chemistry Reduction

The issues of stiffness and the overwhelming complexity of detailed chemical kinetics has fostered widespread interest in "reduced chemical kinetics" for decades [4.6, 4.90, 4.91]. Explicit analytical approaches that are based on asymptotic limit considerations have been discussed in Section 4.4.2 above. Here, we summarize a number of alternative techniques that are enjoying increasing popularity because of the fact that they are largely algorithmic and reduce the demand for chemical kinetics expertise that comes with the more traditional explicit reduction strategies.

4.5.7.1 Crucial observations

Consider a system of ordinary differential equations that might describe chemical reactions in a homogenous gaseous system,

$$\frac{d\boldsymbol{Y}}{dt} = \boldsymbol{R}(\boldsymbol{Y})\,. \tag{4.5.85}$$

The shortest time scales inherent in such a system can be assessed, on the one hand, by the inverse of the largest component of the rate vector $\boldsymbol{R} = \{R_i\}_{i=1}^n$, that is,

$$\tau_0 = \min_i \left(|R_i(\boldsymbol{Y})|\right)\,. \tag{4.5.86}$$

The crucial characteristic of stiff reaction systems, however, lies in the fact explained above, that there are hidden time scales much shorter than those visible in the actual evolution of the system and characterized by Equation (4.5.86). These inherent time scales can be assessed by considering the following transformations: The rate of change of the reaction rate vector $\boldsymbol{R}$ itself is governed by

$$\frac{d\boldsymbol{R}}{dt} = \left(\frac{\partial \boldsymbol{R}}{\partial \boldsymbol{Y}}\right)^T \cdot \frac{d\boldsymbol{Y}}{dt} = \boldsymbol{J}^T \cdot \boldsymbol{R}\,, \tag{4.5.87}$$

where $\boldsymbol{J} = \{J_{i,j}\}_{i,j=1}^n = \{\partial R_i/\partial Y_j\}_{i,j=1}^n$ is the Jacobian of the rate vector. A straightforward perturbation analysis shows that the same equation is also satisfied by perturbations $\delta\boldsymbol{Y}$ of the solution $\boldsymbol{Y}(t)$, that is,

$$\frac{d\delta\boldsymbol{Y}}{dt} = \left(\frac{\partial \boldsymbol{R}}{\partial \boldsymbol{Y}}\right)^T \cdot \delta\boldsymbol{Y} = \boldsymbol{J}^T \cdot \delta\boldsymbol{Y}\,. \tag{4.5.88}$$

Consider next an eigenvalue decomposition of the Jacobian $\boldsymbol{J}$ of the form

$$\boldsymbol{J} = \sum_{j=1}^{n} \lambda_j \boldsymbol{r}_j \circ \boldsymbol{\ell}^j \,, \tag{4.5.89}$$

where λ_j is the jth eigenvalue of the Jacobian, and $\boldsymbol{r}_j, \boldsymbol{\ell}^j$ are the associated right and left eigenvectors, respectively. (To streamline the discussion we do not address complications that may arise for incomplete sets of eigenvectors, multiple eigenvalues etc.)

Let the eigenvalues be ordered in an increasing sequence, so that

$$\lambda_1 < \lambda_2 < \ldots < \lambda_{j_0} < 0 < \lambda_{j_0+1} < \ldots < \lambda_n \tag{4.5.90}$$

Typical stiff behaviour arises when the first few eigenvalues are very large by modulus, that is, when

$$|\lambda_1|, |\lambda_2| < \ldots \gg 1 \,. \tag{4.5.91}$$

A decomposition of $\delta\boldsymbol{Y}$ with respect to the eigenvectors $\boldsymbol{r}_j$ according to

$$\delta\boldsymbol{Y} = \sum_{j=1}^{n} \phi^j(t) \boldsymbol{r}_j \tag{4.5.92}$$

with the $\boldsymbol{r}_j$ essentially frozen on the short relaxation time scales associated with λ_j yields

$$\frac{d\phi_j}{dt} = -\lambda_j \phi_j(t) \,. \tag{4.5.93}$$

This equation indicates, in an asymptotic sense for large $|\lambda_j|$, a rapid exponential decay of the solution component in the direction of the jth right eigenvector.

These relaxing degrees of freedom are unimportant because they will always merely drive the solution back onto submanifolds in state space where the related degree of freedom is relaxed out. This will be the case when ever the reaction vector $\boldsymbol{R}$ does not excite these fast relaxing modes; that is, when $\boldsymbol{R}$ has no component in the direction of the "fast" $\boldsymbol{r}_j$. This requirement can be cast into an algebraic constraint for the "slow" submanifolds in the space of $\boldsymbol{Y}$:

$$\boldsymbol{\ell}^j(\boldsymbol{Y}) \cdot \boldsymbol{R}(\boldsymbol{Y}) = 0 \qquad \text{for all } j \text{ satisfying } \lambda_j < 0 \text{ and } |\lambda_j| \gg 1 \,. \tag{4.5.94}$$

4.5.7.2 ILDMs – Intrinsic lower-dimensional manifolds

The idea in Reference [4.150] is to a priori constrain the state vector $\boldsymbol{Y}$ to submanifolds defined by Equation (4.5.94) or similar modified algebraic constraints. Since these algebraic relations depend only on the chemical rate funtion, they can be determined *before* an actual computation is started to solve the dynamical system (Equation (4.5.85)). The manifolds are actually tabulated and the chemistry is then treated in a computation by means of lookup tables rather than by actually solving the full ODE system. The approach has been validated extensively in References [4.150 to 4.152] and was shown to yield results that cover those from standard reduced chemical kinetics as discussed in Section 4.4.2. On the other hand, it can generate automatically different relevant subsystems that may emerge in different regimes of state space and that would require separately derived standard reduced schemes if one were to follow the explicit asymptotics-based approach.

A prominent example relevant to the present applications is the transition from auto-ignition to flame propagation chemistry. Auto-ignition mechanisms must include the details of radical production and thermal buildup, whereas the radicals in a propagating flame are supplied via molecular transport from the reaction zone. This elucidates that there can be crucial differences in the details of the effective reaction paths, depending on how the reaction system is coupled into a flow field.

A caveat is associated with the embedding of chemical reactions in a flow field. In this case, the governing equations for the species mass concentrations are not ordinary differential equations as in Equation (4.5.85), but full multi-dimensional transport equations

$$\frac{\partial \rho \boldsymbol{Y}}{\partial t} + \nabla\cdot(\rho \boldsymbol{Y} \boldsymbol{v}) + \nabla\cdot(\boldsymbol{j}) = \rho \boldsymbol{R}(\boldsymbol{Y}, p, T)\,. \tag{4.5.95}$$

Not only is this equation equipped with the transport terms resulting from convection and diffusion, but one also must include in $\boldsymbol{R}$ the dependence on two thermodynamic background variables, such as pressure and temperature. Although the key idea behind the ILDM approach is still valid, namely that one may expect the mass fraction vector to evolve in the immediate vicinity of the ILDMs, deviations occur because of these additional terms and they must be accounted for.

The conceptual problems to be overcome are that (i) the manifolds now depend on the thermodynamic backgound state and can thus vary with time and that (ii) the transport terms $\nabla\cdot(\rho \boldsymbol{Y} \boldsymbol{v}) + \nabla\cdot(\boldsymbol{j})$ will generally have components in the direction of the fast eigenvectors of $\boldsymbol{J}$. Even though strong efforts at overcoming these issues are on their way, application of the ILDM approach in dynamic reactive flow computations based on the standard conservation equations is by far not standard today. The approach has found considerably more resonance in the context of Monte Carlo PDF methods for turbulent combustion. As discussed in Section 4.3.7, the PDF is represented in a Monte Carlo simulation approximately by an ensemble of particles that undergo their individual histories. Part of that particle history, which is typically represented numerically by operator splitting, is the reaction progress according to an ODE as in Equation (4.5.85). In this case, one can take full advantage of the ILDM approach.

It should be mentioned that much of the development efforts for ILDM methods have gone into a quite technical issue that has little to do with the underlying fundamental and quite intriguing ideas: Organizing computationally efficient tabulation and lookup table procedures has proven to be more of an obstacle in the implementations that was probably expected originally. It turns out that quite sophisticated numerical techniques need to be invoked to really benefit from the advantages that the ILDM approach formally promises to offer.

4.5.7.3 CSP – Computational singular perturbations

The CSP approach [4.153, 4.154] aims at an algorithmic realization of concepts of asymptotic analysis. The key issues in simplifying complex chemical kinetics are

- to appropriately select relevant fast and slow time scales,
- to identify the characteristic dynamics associated with the fast scales, and
- to then pass to a limit where all the fast modes are relaxed and the overall evolution is governed by the slower time scales of interest only.

Consider again the evolution equation for the n-dimensional reaction rate vector $\boldsymbol{R}$ from Equation (4.5.87). Generally, one may turn this vector equation into a set of coupled scalar amplitude equations by decomposing $\boldsymbol{R}$ w.r.t. some basis $\{\boldsymbol{a}_i\}_{i=1}^n$:

$$\boldsymbol{R}(t) = \sum_{i=1}^{n} f^i(t)\, \boldsymbol{a}_i(t)\,. \tag{4.5.96}$$

For future reference, we introduce the dual basis $\{\boldsymbol{b}^i\}_{i=1}^n$ by

$$\boldsymbol{b}^i \cdot \boldsymbol{a}_j = \delta^i_j\,. \tag{4.5.97}$$

We left-multiply Equation (4.5.87) by $\boldsymbol{b}^i$ to obtain

$$\frac{df^i}{dt} + \sum_{j=1}^{n} f^j \left(\boldsymbol{b}^i \cdot \frac{d\boldsymbol{a}_j}{dt}\right) = \sum_{j=1}^{n} f^j \left(\boldsymbol{b}^i \cdot \boldsymbol{J} \cdot \boldsymbol{a}_j\right)\,. \tag{4.5.98}$$

In a more compact notation we have

$$\frac{df^i}{dt} = \sum_{j=1}^{n} f^j\, \Lambda^i_j\,, \tag{4.5.99}$$

where

$$\Lambda^i_j(t) = \boldsymbol{b}^i(t) \cdot \left(-\frac{d\boldsymbol{a}_j}{dt} + \boldsymbol{J}(t) \cdot \boldsymbol{a}_j(t)\right)\,. \tag{4.5.100}$$

If the considered system was linear, one could diagonalize the matrix $\{\Lambda^i_j\}$ and then solve n decoupled linear first-order equations exactly. The largest eigenvalues of the matrix (by modulus) would indicate the "fast modes", and the associated solution components would decay most rapidly if these eigenvalues were negative.

Chemical kinetics equations are generally highly non-linear and such an exact decoupling will not occur. However, one may seek to achieve at least an approximate decoupling of fast and slow motions in state space by choosing basis vectors $\{\boldsymbol{a}_i\}_{i=1}^n$ that lead to an approximately block-diagonal structure of $\{\Lambda^i_j\}$. An algorithmic procedure is proposed in References [4.153, 4.154] that allows an iterative improvement of the underlying basis in state space in that the coupling between fast and slow subspaces decreases as ϵ^j, where ϵ is the time scale separation between the "current active time scale" (the fastest of the slow modes) and the slowest of the fast modes and j is the iteration index.

The CSP approach is intriguing in that it allows one, but does not require, to construct a simplified limit system with fewer degrees of freedom similar to the ILDM system. One can as well use the subdivision in state space into fast and slow modes in order to resolve numerically all the scales, but to apply specialized numerical techniques to the fast and slow subdynamics.

4.6 Summary

This chapter has compiled the state of the art in both the modelling and numerical simulation of FA and the transition to detonation. Summaries have been provided of main-stream and advanced models for flow turbulence, turbulent combustion, and for the efficient representation of chemical kinetics. Numerical methods for flow field simulations have been discussed with an emphasis on the present topic of FA and DDT.

4.6.1 Industry-level Modelling versus Current State of Research

In discussing computational modelling, one must distinguish between the needs of everyday engineering and scientific efforts at exploring the fundamental processes of a given phenomenon. Typically, engineering assessments require mainly an upper limit of potential loads, which then serve as the basis for the design of safety measures. Unfortunately, when dealing with combustion in large-scale systems and with a wide range of possible scenarios regarding gas composition and distribution, the potential upper load limits are subject to considerable statistical variation. As a consequence, simplified assessment tools can lead to either unacceptable conservatism or unacceptable uncertainties. Hence the demand for improved insight into the fundamental mechanisms of FA and DDT and the efforts at developing detailed numerical prediction tools as described in this chapter. (Simplified models of reduced complexity that can be used in routine engineering applications will be discussed in the next chapter.)

4.6.2 Adequate Levels of Modelling Detail and Numerical Resolution

Because of the complexity of the phenomena involved in FA and DDT, such as flow turbulence, chemical kinetic effects, multiple length scales, flame-acoustic interactions etc., various levels of modelling detail must be distinguished.

At the coarsest level, there are the lumped-parameter models, to be discussed shortly, which decompose a system into a finite, relatively small number of compartments. Conservation of mass and energy is formulated for these systems of interconnected subvolumes, and overall estimates of global pressures and average temperatures are obtained. Naturally, these models do not resolve the underlying reacting flow fields. In other words, the balance of momentum is not considered in detail. Also, it is not possible—except through qualitative parametrizations—to incorporate the effects of local events that may lead to sizeable global effects.

The interaction between energy and momentum becomes important for high-speed combustion, such as high-speed turbulent deflagrations and detonations. Here, a large percentage of the combustion energy release is converted to kinetic energy. It has been shown, for example, in Reference [4.155] that the resulting pressure pulses may lead to effective pressure loads that by far excede those expected from quasi-static (lumped-parameter) estimates. The next level of computational and modelling complexity thus involves simulation tools that allow the representation of global unsteady but statistically averaged flow fields and large-scale pressure waves. These simulation tools typically rely on coarse-grained computational meshes with grid sizes comparable to the integral scales of turbulence. Such codes are able to provide estimates for the influence of momentum exchanges and, in particular, allow a much improved assessment of potential structural loads that are due to high-speed combustion events.

These statistically averaged models include mean combustion rate models that are suitable to describe a well-established and relatively stable reaction progress. They also do allow the modelling of bulk effects of chemical kinetics, such as transitions between different regimes of turbulent combustion depending on whether chemical time scales are much shorter, comparable to, or longer than the characteristic time scales of turbulence. However, this kind of approach still misses out on those events that are triggered by localized processes but then develop into global combustion events. Unfortunately, some of the most dangerous mechanisms of deflagration-to-detonation transition are of that type: Local sequential or hot spot ignition may trigger the onset of detonation through gas-dynamic-reactive resonances, but the triggering event itself is a highly stochastic, localized, and rare event. Reliable modelling of this kind of process is not possible on the basis of standard statistical models of turbulence and turbulent combustion.

One rather needs sophisticated dynamic mesh refinement and models suitable to represent the smallest flow scales. A promising compromise between fully resolved DNS based on the reactive Navier-Stokes equations and statistical turbulence models is large eddy simulation.

Table 4.6.2-1 summarizes the orders of magnitude of the smallest length scales to be resolved in a typical nuclear reactor safety application under these different modelling paradigms.

Table 4.6.2-1: Rough estimate of resolution requirements as a function of modelling detail

Model Class	Smallest Scale	Resolved Processes
Lumped-Parameter Models	> 1 m	Large-scale-averaged (quasi-) thermodynamic balances
Statistical Turbulence Models	$0.1 \ldots 1$ m	Averaged flow quantities, *including* momentum balances *excluding* localized, rare events
Large Eddy Simulation (LES)	$0.01 \ldots 0.1$ m	Non-linear unsteady motions, *including* large-scale turbulence *excluding* disspation scales combustion scales localized, rare events
Direct Numerical Simulation (DNS)	$10^{-5} \ldots 10^{-2}$ m	All processes and full range of scales of underlying continuum model

4.6.2.1 Under-resolved computations

The estimates in Table 4.6.2-1 demonstrate that the interplay of various physical mechanisms typically occurs over a range of characteristic length (and time) scales. The non-linearity of the underlying governing equations dictates that processes occuring on different scales interact in a non-negligible fashion. As a consequence, any numerical computation that does not resolve all the length scales described by its model equations is generally bound to produce uncontrolled errors because it neglects the interactions on and with the small, unresolved scales. In particular, a DNS based on the reactive Navier-Stokes equations cannot be expected to correctly represent the evolution of a combustion process if the smallest flow and chemical reaction scales are not properly resolved. (As a rule of thumb, the grid Reynolds number, $\mathrm{Re}_{\mathrm{gr}} = u_{\mathrm{ref}}\Delta/\nu$, with Δ the computational grid size, should be or order unity or less.

Computations that do not satisfy this kind of criterion might, under special circumstances regarding initial and boundary data, yield valuable insight. But they should be interpreted with extreme care and should not be accepted as DNS in the original sense of the term.

4.6.3 Reproducibility and Predictability

The interpretation of the results of computational modelling must take into account the statistical nature of the processes modelled. It may be found found, for example, from the experiments to be reported in Chapter 5 that some experimental set-ups and combustible mixtures lead to very reproducible high-speed combustion events, whereas more marginal mixtures and only slightly obstacle-loaded configurations tend to produce large fluctuations in terms of the resulting overall flow fields. Importantly, there is, at

best, a weak correlation between the violence of an event and its marginality.

As one tries to narrow down the boundaries of existence of detonation and high-speed deflagration one must deal with increasingly marginal mixtures. Predictive modelling then requires a drastically increased amount of detail as well as the recognition of the very different statistical nature of turbulent combustion in these regimes. Among, say, 100 benign cases of combustion there may still be a few cases where transition to detonation occurs and effective structural loads are an order of magnitude larger than the average ones. We are not aware of a reliable modelling approach that would allow incorporation of such rare but important events and would still be comparable in complexity with standard statistical models of turbulence and turbulent combustion. Hence there is a demand for sophisticated DNS and LES tools.

4.6.4 Complex Geometries and Scaling

There is currently a principal difficulty in the context of model validation that is related to the scaling issues discussed in Section 4.5.1.1. None of the existing subgrid-scale turbulence closures is rigorously derived from first principles, i.e., from the original governing equations. One may thus expect that the similarity laws associated with the non-dimensional characteristic quantities, such as the Reynolds, Peclet, Mach, Froude, and Damköhler numbers will generally not be perfectly satisfied by the resulting effective models. As a consequence, one finds that application of one and the same model to geometrically similar but differently sized systems requires adjustment of a number of free modelling parameters. This is a highly non-negligible issue in nuclear reactor safety, because there are only very experimental set-ups of a geometrical size comparable to a real reactor containment.

The upscaling or downscaling of computational results therefore must be considered an unresolved question to this date. The availability of experimental results for geometrically exactly similar, but resized set-ups would be of outmost value for model validation.

There is another more subtle issue related to this same problem area: One typical and important way of validating a numerical flow solver is to perform convergence studies with respect to grid refinement. One considers one and the same physical situation and increases the numerical resolution (= decreases the mesh size) in a sequence of computations. Ideally, the results obtained should converge to the same limiting fields at a rate that depends on the order of accuracy of the numerical discretizations employed. Consider now a full-fledged simulation of a nuclear reactor containment. Such a simulation will typically include subgrid-scale models for small-scale obstacles and solid structures, as described in Section 4.2.5. Now, upon grid refinement the size of the smallest resolvable obstacle decreases in proportion with the mesh size. As a consequence, the underlying continuum problem that one is trying to solve changes, and the notion of "convergence" must be reconsidered.

In fact, there are at least two principally different interpretations of convergence:

- Convergence in a practical sense would postulate that the subgrid-scale models be applied only to the unresolved scales on any given grid. A convergence criterion would then require that the results of a fine-mesh computation, when restricted to the former coarse-grid, yield the same grid cell averages as did the coarse grid computations. Notice, however, that under this strategy more and more of the small-scale geometrical features of obstacles becomes resolved on the grid—the smallest resolved features corresponding to a fixed number of grid cells. Numerical truncation errors on the small-scale level will then not decrease with grid refinement and convergence in the

sense of numerical analysis is not achieved.

- A sound convergence study in the sense of numerical analysis would, in contrast, fix the continuum problem to be solved and then study the solution behaviour as the grid is refined. In particular, it would be decided once and for all of the compared computations which obstacles would be resolved and which ones be represented only by subgrid-scale models. This classification would not change with grid refinement. This latter approach is somewhat counter-intuititive and not widely used, but it is the only approach allowing one to verify that numerical truncation errors diminish with grid refinement.

4.7 References

[4.1] K. N. C. Bray, Challenges in Turbulent Combustion. In *Introduction to Turbulent Combustion*. (L. Vervisch, D. Veynante and D. Olivari, (editors)). The von Karman Institute, Rhode St. Genése, Belgium, 1999.

[4.2] A.N. Kolmogorov, Local Structure of Turbulence in Incompressible Viscous Fluids for Very Large Reynolds Number. Dol. Akad. Nauk SSSR, Vol. 30, 1941, 299–303.

[4.3] A.N. Kolmogorov, Equations of Turbulent Motion of an Incompressible Fluid. Izvestia Academy of Sciences, USSR; Physics, Vol. 6, 1942, 56–58.

[4.4] O. Reynolds, On the Dynamical Theory of Incompressible Viscous Fluids and the Determination of the Criterion. Philosophical Transactions of the Royal Society of London, Vol. A186, 1895, 123 ff.

[4.5] D. C. Wilcox, *Turbulence Modelling for CFD.* DCW Industries, Inc., La Canada, CA, second edition, 1998.

[4.6] F. A. Williams, *Combustion Theory.* Addison-Wesley Publishing Company, Menlo Park, CA, USA, second edition, 1985.

[4.7] B. S. Baldwin and H. Lomax, Thin-Layer Approximation and Algebraic Model for Separated Turbulent Flows. AIAA paper, 78-257, 1978.

[4.8] P. G. Saffman, A Model for Inhomogeneous Turbulent Flow. Proceedings of the Royal Society of London, Vol. A317, 1970, 417–433.

[4.9] B. E. Launder and D. B. Spalding, *Mathematical Models of Turbulence.* Academic Press, New York, NY, USA, 1972.

[4.10] C. G. Speziale, R. Abid and Anderson E. C., A Critical Evaluation of Turbulence Models for Near-Wall Turbulence. AIAA paper, 90-1481, 1990.

[4.11] B. R. Smith, The k-$k\ell$ Turbulence and Wall Layer Model for Compressible Flows. AIAA paper, 90-1483, 1990.

[4.12] B. R. Smith, A Near Wall Model for the k-ℓ Two Equation Turbulence Model. AIAA paper, 94-2386, 1994.

[4.13] W. P. Jones and B. E. Launder, The Prediction of Laminarization with a Two-Equation Model of Turbulence. International Journal for Heat and Mass Transfer, Vol. 15, 1972, 301–314.

[4.14] O. Zeman, Dilatational Dissipation: The Concept and Application in Modelling Compressible Mixing Layers. Physics of Fluids, Vol. A 2, 1990, 178–188.

[4.15] S. Sarkar, The Pressure-Dilatation Correlation in Compressible Flows. Physics of Fluids, Vol. A 4, 1992, 2674–2682.

[4.16] D. C. Wilcox, Dilatational Dissipation Corrections for Advanced Turbulence Models. AIAA Journal, Vol. 30, 1992, 2639–2646.

[4.17] B. E. Launder, G. J. Reece and W. Rodi, Progress in the Development of a Reynolds Stress Closure. Journal of Fluid Mechanics, Vol. 68, 1975, 537–566.

[4.18] B. E. Launder, (editor), *5th Biennial Colloquium on Computational Fluid Dynamics*. Manchester Insitute of Science and Technology, Manchester, UK, 1992.

[4.19] D. C. Wilcox and M. W. Rubesin, Progress in Turbulence Modelling for Complex Flow Fields Including Effects of Compressibility. NASA Tech. Rep., Vol. TP-1517, 1980.

[4.20] D. C. Wilcox, Multiscale Model for Turbulent Flows. AIAA Journal, Vol. 26, 1988, 1311–1320.

[4.21] M. Oberlack, Closure of the Dissipation Tensor and the Pressure–Strain Tensor Based on the Two-Point Correlation Equation. In *Turbulent Shear Flows 9*. (F. Durst, N. Kasagi, B. E. Launder, F. W. Schmidt, K. Suzuki and J. H. Whitelaw, (editors)). Springer, 1993.

[4.22] M. Oberlack and N. Peters, Closure of the Two-Point Correlation Equation in Physical Space as a Basis for Reynolds Stress Models. In *Near-Wall Turbulent Flows*. (R. M. C. So, C. G. Speziale and B. E. Launder, (editors)). Elsevier, 1993.

[4.23] M. Oberlack, Non-Isotropic Dissipation in Non-Homogeneous Turbulence. Journal of Fluid Mechanics, Vol. 350, 1997, 351–374.

[4.24] J. C. Rotta, *Turbulente Strömungen [Turbulent Flows]*. Teubner, Stuttgart, 1972.

[4.25] J. H. Ferziger, Large Eddy Simulations of Turbulent Flows. AIAA paper, 78-347, 1978.

[4.26] J. Smagorinsky, General Circulation Experiments with the Primitive Equations I: The Basic Experiment. Monthly Weather Review, Vol. 91, 1963, 99–164.

[4.27] M. Germano, U. Piomelli, P. Moin and W. Cabot, A Dynamic Subgrid Scale Large Eddy Viscosity Model. Physics of Fluids, Vol. A3, 1991, 1760 ff.

[4.28] J. H. Ferziger, Recent Advances in Large Eddy Simulation. In *Engineering Turbulence Modelling and Experiments 3*. (W. Rodi and G. Begeles, (editors)). Elsevier, New York, 1996, 163 ff.

[4.29] M. Lesieur and O. Metais, New Trends in Large Eddy Simulations of Turbulence. Annual Review of Fluid Mechanics, Vol. 28, 1996, 45 ff.

[4.30] W. Rodi, Comparison of LES and RANS Calculations of the Flow Around Bluff Bodies. Journal of Wind Engineering and Industrial Aerodynamics, Vol. 69-71, 1997, 55–75.

[4.31] W. Rodi, Large Eddy Simulation of the Flow Around Bluff Bodies – State of the Art. International Journal of the Japan Society of Mechanical Engineering, Vol. B41(2), 1998, 432–454.

[4.32] D. K. Lilly, On the Application of Eddy Viscosity Concept in the Intertial Subrange of Turbulence. National Center for Atmospheric Research, Boulder, CO, USA, Manuscript 123, 1966.

[4.33] J. W. Deardorff, The Use of Subgrid Turbulent Transport in a Three-Dimensional Model of Atmospheric Turbulence. ASME Journal of Fluids Engineering, Vol. 95, 1973, 429–438.

[4.34] J. Bardina, J. H. Ferziger and W. C. Reynolds, Improved Turbulence Models Based on Large Eddy Simulation of Homogeneous Incompressible Turbulent Flows. Stanford University, Department of Engineering Report TF-19, 1983.

[4.35] C. Meneveau, T. S. Lund and W. Cabot, A Lagrangian Dynamic Subgrid Scale Model of Turbulence. Journal of Fluid Mechanics, Vol. 319, 1996, 353–385.

[4.36] D. C. Haworth and K. Jansen, Large Eddy Simulation on Unstructured Deforming Meshes: Towards Reciprocating IC Engines. Computers and Fluids, Vol. to appear, 1999.

[4.37] D. C. Haworth, Turbulent Combustion Modelling and Applicatoins. In *Introduction to Turbulent Combustion*. (L. Vervisch, D. Veynante and D. Olivari, (editors)). The von Karman Institute, Rhode St. Genése, Belgium, 1999.

[4.38] J. Jimenez, On Why Dynamics Subgrid Scale Models Work. CTR Annual Research Briefs, Stanford University, Center for Turbulence Research, 1995.

[4.39] N. R. Popat, C. A. Catlin, B. J. Arntzen, R. P. Lindstedt, B. H. Hjertager, T. Solberg, O. Saeter and H. Van den Berg, Investigations to Improve and Assess the Accuracy of Computational Fluid Dynamic Based Explosion Models. Journal of Hazardous Materials, Vol. 45, 1996, 1–25.

[4.40] W. T. Sha, C. I. Yang, T. T. Kao and S. M. Cho, Multidimensional Numerical Modeling of Heat Exchangers. Journal of Heat Transfer, Vol. 104, 1982, 417–425.

[4.41] S. V. Patankar and D. B. Spalding, A Calculation Procedure for the Transient and Steady Behaviour of Shell-and-Tube Heat Exchangers. In *Heat Exchangers: Design and Theory Source Book*. (N.H Afgan and E.V. Schlunder, (editors)). McGraw-Hill, 1974, 155–176.

[4.42] N. Peters, Laminar Flamelet Concepts in Turbulent Combustion. In *21st Symposium (International) on Combustion*. The Combustion Institute, Pittsburgh, PA, USA, 1986, 1231–1250.

[4.43] N. Peters, The Turbulent Burning Velocity for Large Scale and Small Scale Turbulence. Journal of Fluid Mechanics, Vol. 384, 1999, 107–132.

[4.44] A. Majda and J. Sethian, The Derivation and Numerical Solution of the Equations for Zero Mach Number Combustion. Combustion Science and Technology, Vol. 42, 1985, 185–205.

[4.45] N. Peters, A Spectral Closure for Premixed Turbulent Combustion in the Flamelet Regime. Journal of Fluid Mechanics, Vol. 242, 1992, 611–629.

[4.46] L. Vervisch and D. Veynante, Turbulent Combustion Modelling. In *Introduction to Turbulent Combustion*. (L. Vervisch, D. Veynante and D. Olivari, (editors)). The von Karman Institute, Rhode St. Genése, Belgium, 1999.

[4.47] K. N. C. Bray and N. Peters, Laminar Flamelets in Turbulent Flames. In *Turbulent Reacting Flows*. (F. A. Williams and P. A. Libby, (editors)). Academic Press, London, 1994, 63–113.

[4.48] B. H. Hjertager, Simulation of Transient Compressible Turbulent Reactive Flows. Combustion Science and Technology, Vol. 27, 1982, 159 ff.

[4.49] K. N. C. Bray, J. Moss and P. A. Libby, Turbulent Transport in Premixed Turbulent Flames. In *Convective Transport and Instability Phenomena*. (J. Zierep and H. Oertel, (editors)). University of Karlsruhe, Karlsruhe, Germany, 1982.

[4.50] K. N. C. Bray, M. Champion and P. A. Libby, The Interaction between Turbulence and Chemistry in Premixed Turbulent Flames. In *Turbulent Reacting Flows*. (R. Borghi and S. Murphy, (editors)), Lecture Notes in Engineering, Vol. 40. Springer, Heidelberg, 1989.

[4.51] A. Kotchourko, W. Breitung, A. Veser and S. Dorofeev, Tube Experiments and Numerical Simulation on Tuburlent Hydrogen-Air Combuston. In *21st International Symposium on Shockwaves*, Australia, July 1997.

[4.52] W. Breitung, A. Kotchourko, A. Veser and W. Scholtyssek, Reactive Flow Simulation in Complex 3D Geometries using the COM3D Code. In *Severe Accident Research*, Japan. Nov., 1998.

[4.53] V. Smiljanovski, V. Moser and R. Klein, A Capturing-Tracking Hybrid Scheme for Deflagration Discontinuities. Journal of Combustion Theory and Modelling, Vol. 2(1), 1997, 183–215.

[4.54] R. P. Fedkiw, T. Aslam and S. Xu, The Ghost Fluid Method for Deflagration and Detonation Discontinuities. Journal of Computational Physics, Vol. xx, 1999, to appear.

[4.55] A. J. Chorin, Flame Advection and Propagation Algorithms. Journal of Computational Physics, Vol. 35, 1980, 1–11.

[4.56] Z. H. Teng, A. J. Chorin and T. P. Liu, Riemann Problems for Reacting Gas, with Application to Transition. SIAM Journal of Applied Mathematics, Vol. 42(5), 1982.

[4.57] G. Damköhler, Der Einfluss der Turbulenz auf die Flammengeschwindigkeit in Gasgemischen [The Influence of Turbulence on Flame Velocities in Gas Mixtures]. Zeitschrift für Elektochemie und angewandte Physikalische Chemie, Vol. 46, 1940, 601–626.
See also NACA Technical Memorandum 1112, 1947.

[4.58] V. Moser, *Simulation der Explosion magerer Wasserstoff-Luft-Gemische in großskaligen Geometrien [Explosion Simulation for Lean Hydrogen-Air Mixtures in Large Scale Geometries]*. PhD thesis, RWTH Aachen, 1997.

[4.59] D. Spalding, Mixing and Chemical Reaction in Steady Confined Turbulent Flames. In *13th Symposium (International) on Combustion*. The Combustion Institute, Pittsburgh, PA, USA, 1971, 649–657.

[4.60] B. F. Magnussen and B. H. Hjertager, On Mathematical Modelling of Turbulent Combustion with Special Emphasis on Soot Formation and Combustion. In *16th Symposium (International) on Combustion*. The Combustion Institute, Pittsburgh, PA, USA, 1976, 719–729.

[4.61] V. Yakhot, Propagation Velocity of Premixed Turbulent Flames. Combustion Science and Technology, Vol. 60, 1988, 191–214.

[4.62] M. Sussman, P. Smereka and S. Osher, A Level Set Approach for Computing Solutions to Incompressible Two-Phase Flow. Journal of Computational Physics, Vol. 114, 1994, 146–159.

[4.63] F. Gouldin, An Application of Fractals to Modelling Premixed Turbulent Flames. Combustion and Flame, Vol. 68, 1987, 249 ff.

[4.64] L. Vervisch, E. Bidaux, K. N. C. Bray and W. Kollmann, Surface Density Functions in Premixed Turbulent Combustion Modeling; Similarities Between the Probability Density Function and Flame Surface Density Approaches. Physics of Fluids, Vol. A 7, 1995, 2496–2503.

[4.65] L. Vervisch W. Kollmann and K. N. C. Bray, Dynamics of Iso-Concentration Surfaces in Premixed Turbulent Flames. 10th Symposium on Turbulent Shear Flows, Vol. 10, 1995.

[4.66] R. S. Cant, S. Pope and K. N. C. Bray, Modelling of Flamelet Surface to Volume Ratio in Turbulent Premixed Combustion. In *23th Symposium (International) on Combustion.* The Combustion Institute, Pittsburgh, PA, USA, 1990, 809–815.

[4.67] S. Candel and T. Poinsot, Flame Stretch and the Balance Equation for the Flame Area. Combustion Science and Technology, Vol. 70, 1990, 1–15.

[4.68] C. Meneveau and T. Poinsot, Stretching and Quenching of Flamelets in Premixed Turbulent Combustion. Combustion and Flame, Vol. 86, 1991, 311–332.

[4.69] W. Cheng and J. Diringer, Numerical Modelling of SI-Engine Combustion with a Flame Sheet Model. SAE paper 910268, 1991.

[4.70] T. Mantel and R. Borghi, A New Model of Premixed Wrinkled Flame Propagation Based on a Scalar Dissipation Equation. Combustion and Flame, Vol. 96, 1994, 443 ff.

[4.71] A. Trouvé and T. Poinsot, The Evolution Equation for the Flame Surface Density. Journal of Fluid Mechanics, Vol. 278, 1994, 1–31.

[4.72] D. Veynante, J. Piana, J. Duclos and C. Martel, Experimental Analysis of a Flame Surface Density Model for Premixed Turbulent Combustion. In *26th Symposium (International) on Combustion.* The Combustion Institute, Pittsburgh, PA, USA, 1996, 413–420.

[4.73] K. N. C. Bray, The Challenge of Turbulent Combustion. In *26th Symposium (International) on Combustion.* The Combustion Institute, Pittsburgh, PA, USA, 1996, 413–420.

[4.74] D. Veynante, A. Trouvé, K. N. C. Bray and T. Mantel, Gradient and Countergradient Scalar Transport in Turbulent Premixed Flames. Journal of Fluid Mechanics, Vol. 332, 1997, 263–293.

[4.75] C. J. Rutland and A. Trouvé, Direct Simulations of Premixed Turbulent Flames with Non-unity Lewis Numbers. Combustion and Flame, Vol. 94, 1993, 41–57.

[4.76] A. Trouvé, D. Veynante, K. N. C. Bray and T. Mantel, The Coupling Between Flame Surface Dynamics and Species Mass Conservation in Premixed Turbulent Combustion. In *Summer Program of the Center of Turbulence Research.* (P. Moin, J. H. Ferziger and W. C. Reynolds, (editors)). Center for Turbulence Research, Stanford University, Stanford, CA, USA, 1994.

[4.77] P. A. Libby and F.A. Williams, *Turbulent Reacting Flows.* Academic Press, London, UK, 1994.

[4.78] T. Poinsot, T. Echekki and M. Mungal, A Study of the Laminar Flame Tip and Implications for Premixed Turbulent Combustion. Combustion Science and Technology, Vol. 81, 1994, 45 ff.

[4.79] R. W. Bilger, The Structure of Turbulent Non-Premixed Flames. In *22nd Symposium (International) on Combustion.* The Combustion Institute, Pittsburgh, PA, USA, 1988.

[4.80] R. W. Bilger, Turbulent Diffusion Flames. Annual Review of Fluid Mechanics, Vol. 21, 1989, 101–135.

[4.81] R. W. Bilger, Conditional Moment Closure for Turbulent Reacting Flows. Physics of Fluids, Vol. 5, 1993, 327–334.

[4.82] R. W. Bilger and N. Peters, Comment and Reply on the "Assessment of Combustion and Submodels for Turbulent Nonpremixed Hydrocarbon Flames" by N. Swaminathan and R. W. Bilger. Combustion and Flame, Vol. 116, 1999, 677 ff.

[4.83] S. B. Pope, PDF Method for Turblent Reacting Flows. Progress in Energy and Combustion Science, Vol. 11, 1985, 119–195.

[4.84] C. Dopazo, Recent Developments in pdf Methods. In *Turbulent Reacting Flows*. (P. A. Libby and F. A. Williams, (editors)). Academic Press, London, 1994, 375–474.

[4.85] M. S. Anand and S. B. Pope, Calculations of Premixed Turbulent Flames by pdf Methods. Combustion and Flame, Vol. 67, 1987, 127ff.

[4.86] T. Butler and P. O'Rourke, A Numerical Method for Two-Dimensional Unsteady Reacting Flows. In *16th Symposium (International) on Combustion*. The Combustion Institute, Pittsburgh, PA, USA, 1977, 103–1515.

[4.87] A. Bourlioux, V. Moser and R. Klein, Large Eddy Simulation of Turbulent Premixed Flames Using a Capturing/Tracking Hybrid Approach. presented at 6th Intl. Conf. on Numerical Combustion, New Orleans, Louisiana, USA, 1996.

[4.88] S. Menon, Large Eddy Simulation of Combustion Instabilities. presented at 6th Intl. Conf. on Numerical Combustion, New Orleans, Louisiana, USA, 1996.

[4.89] M. Boger, D. Veynante and A. Trouvé, Direct Numerical Simulation Analysis of Flame Surface Density Concept for Large Eddy Simulation of Turbulent Premixed Combustion. In *27th Symposium (International) on Combustion*. The Combustion Institute, Pittsburgh, PA, USA, 1998.

[4.90] N. Peters, Systematic Reduction of Flame Kinetics: Principles and Details. In *Progress in Aeronautics and Astronautics*. (J. R. Bowen, N. Manson, A. K. Oppenheim and R. I. Soloukhin, (editors)). AIAA, 1988, 67–86.

[4.91] N. Peters and B. Rogg, *Reduced Kinetic Mechanisms for Applications in Combustion Systems*. Lecture Notes in Physics, Vol. 15. Springer Verlag, Heidelberg, 1993.

[4.92] H. Pitsch, N. Peters and K. Seshadri, Numerical and Asymptotic Studies of the Structure of Premixed Iso-Octane Flames. In *26th Symposium (International) on Combustion*. The Combustion Institute, Pittsburgh, PA, USA, 1996, 763–771.

[4.93] N. Peters and F. A. Williams, Asymptotic Structure of Stoichiometric Methane-Air Flames. Combustion and Flame, Vol. 68, 1987, 185–207.

[4.94] L. R. Petzold, A Description of DASSL: A Differential-Algebraic System Solver. In *Scientific Computing*. (R. S. Stepleman, (editor)). North-Holland, Amsterdam, New York, 1982, 65–68.

[4.95] K. E. Brenan, S. L. Campbell and L. R. Petzold, *Numerical Solution of Initial-Value Problems in Differential-Algebraic Equations*. North-Holland, Amsterdam, New York, 1989.

[4.96] M. Matalon and B. J. Matkowsky, Flames as Gasdynamic Discontinuities. Journal of Fluid Mechanics, Vol. 124, 1982, 239–259.

[4.97] R. Klein, Semi-Implicit Extension of a Godunov-Type Scheme Based on Low Mach Number Asymptotics I: One-Dimensional Flow. Journal of Computational Physics, Vol. 121, 1995, 213–237.

[4.98] Th. Schneider, N. Botta, R. Klein and K. J. Geratz, Extension of Finite Volume Compressible Flow Solvers to Multi-Dimensional, Variable Density Zero Mach Number Flows. Journal of Computational Physics, Vol. 155, 1999, 248–286.

[4.99] R. Klein, Numerics in Combustion. In *Introduction to Turbulent Combustion*. (L. Vervisch, D. Veynante and D. Olivari, (editors)). The von Karman Institute, Rhode St. Genése, Belgium, 1999.

[4.100] C. A. J. Fletcher, *Computational Techniques for Fluid-Dynamics—Fundamental and General Techniques*, Vol. 2. Springer Verlag, New York, 1988.

[4.101] R. I. Issa, Solution of the Implicitly Discretised Fluid Flow Equations by Operator-Splitting. Journal of Computational Physics, Vol. 62, 1986, 40–65.

[4.102] J. Kim and P. Moin, Application of a Fractional Step Method to Incompressible Navier-Stokes Equations. Journal of Computational Physics, Vol. 59, 1985, 308–323.

[4.103] S. V. Patankar, *Numerical Heat Transfer and Fluid Flow.* Hemisphere Publishing Corporation, 1980.

[4.104] R. Klein and N. Peters, Cumulative Effects of Weak Pressure Waves During the Induction Period of a Thermal Explosion in a Closed Cylinder. Journal of Fluid Mechanics, Vol. 187, 1988, 197–230.

[4.105] J. Sesterhenn, B. Müller and H. Thomann, Computation of Compressible Low Mach Number Flow. Computational Fluid Dynamics, Vol. 2, 1992, 829–833.

[4.106] R. J. LeVeque, *Numerical Methods for Conservation Laws.* Birkhäuser Verlag, Zürich, Schweiz, 1992. IBSN 0-521-43009-7.

[4.107] D. Kröner, (editor), *Numerical Schemes for Conservation Laws.* Wiley and Teubner, Stuttgart, Leipzig, 1996.

[4.108] D. Kröner, M. Ohlberger and C. Rhode, (editors), *An Introduction to Recent Developments in Theory and Numerics for Conservation Laws.* Lecture Notes in Computional Science and Engineering, Vol. 5. Springer, Berlin, Heidelberg, New York, 1998.

[4.109] T. J. R. Hughes, Multiscale Phenomena: Green's Functions, the Dirichlet-to-Neumann Formulation, Subgrid Scale Models, Bubbles and the Origins of Stabilized Methods. Computer Methods in Applied Mechanics and Engineering, Vol. l27, 1995, 387–401.

[4.110] R. Löhner, K. Morgan, J. Peraire and M. Vahdati, Finite Element Flux Corrected Transport (FEM-FCT) for the Euler and Navier-Stokes Equations. International Journal for Numerical Methods in Fluids, Vol. 7, 1997, 1093–1109.

[4.111] E.S. Oran and J.P. Boris, *Numerical Simulation of Reactive Flow.* Elsevier Science Publ., New York, 1987.

[4.112] P. D. Lax and B. Wendroff, Systems of Conservation Laws. Communications in Pure and Applied Mathematics, Vol. 13, 1960, 568–582.

[4.113] H. Bijl and P. A. Wesseling, Unified Method for Computing Incompressible and Compressible Flows in Boundary-Fitted Coordinates. Journal of Computational Physics, Vol. 141, 1998, 153–173.

[4.114] K.J. Geratz, R. Klein, C.-D. Munz and S. Roller, Multiple Pressure Variable (MPV) Approach for Low Mach Number Flows Based on Asymptotic Analysis. In *Flow Simulation with High-Performance Computers II. DFG Priority Research Programme Results*. (E. H. Hirschel, (editor)), Notes on Numerical Fluid Mechanics, Vol. 53. Vieweg Verlag, Braunschweig, 1996.

[4.115] S. Roller, C.-D. Munz, K.J. Geratz and R. Klein, The Extension of Incompressible Flow Solvers to the Weakly Compressible Regime. Theoretical and Numerical Fluid Dynamics, 1999, submitted for publication.

[4.116] D. N. Williams, L. Bauwens and Elaine S. Oran, Detailed Structure and Propagation of Three-Dimensional Detonations. In *26th Symposium (International) on Combustion*. The Combustion Institute, Pittsburgh, PA, USA, 1996, 649–657.

[4.117] B. Einfeldt, On Godunov-Type Methods for Gas Dynamics. SIAM Journal of Numerical Analysis, Vol. 25, 1988, 294–318.

[4.118] P. Colella, A. Majda and V. Roytburd, Theoretical and Numerical Structure for Reacting Shock Waves. SIAM Journal of Scientific and Statistical Computing, Vol. 7, 1986, 1059–1080.

[4.119] R. B. Pember, Numerical Methods for Hyperbolic Conservation Laws with Stiff Relaxation I. Spurious Solutions. SIAM Journal of Applied Mathematics, Vol. 53, 1993, 1293–1330.

[4.120] R.J. LeVeque and H.C. Yee, A Study of Numerical Methods for Hyperbolic Conservation Laws with Stiff Source Terms. Journal of Computational Physics, Vol. 86, 1990, 187–210.

[4.121] A. C. Berkenbosch, R. Kaaschieter and R. Klein, Detonation Capturing for Stiff Combustion Chemistry. Combustion Theory and Modelling, Vol. 2, 1998.

[4.122] A. J. Chorin, A Numerical Method for Solving Incompressible Viscous Flow Problems. Journal of Computational Physics, Vol. 2, 1967, 12–26.

[4.123] A. J. Chorin, Numerical Solution of the Navier-Stokes Equations. Mathematics of Computation, Vol. 22, 1968, 745–762.

[4.124] A. J. Chorin, On the Convergence of Discrete Approximations to the Navier-Stokes Equations. Mathematics of Computation, Vol. 23, 1969, 341–353.

[4.125] J. Lang, Adaptive Incompressible Flow Computations with Linearly Implicit Time Discretization and Stabilized Finite Elements. In *Computational Fluid Dynamics '98*. (K.D. Papailiou, D. Tsahalis, J. Periaux, C. Hirsch and M. Pandolfi, (editors)), John Wiley & Sons, New York. 1998.

[4.126] R. Rannacher, On Chorin's Projection Method for the Incompressible Navier-Stokes Equations. In *The Navier-Stokes Equations II—Theory and Numerical Methods*. (J. G. Heywood, (editor)), Vol. number 1530 in *Lecture Notes in Mathematics*. Springer Verlag, Berlin, 1992, 167–183.

[4.127] K. C. Karki and S. V. Patankar, Pressure Based Calculation Procedure for Viscous Flows at all Speeds in Arbitrary Configurations. AIAA Journal, Vol. 27, 1989, 1167–1174.

[4.128] C. M. Rhie, Pressure-Based Navier-Stokes Solver Using the Multigrid Method. AIAA Journal, Vol. 27, 1989, 1017–1018.

[4.129] W. Shyy, Elements of Pressure-Based Computational Algorithms for Complex Fluid Flow and Heat Transfer. Advances in Heat Transfer, Vol. 24, 1994, 191–275.

[4.130] P. Haldenwang, J. Daou, B. Denet and C. Nicoli, Low Mach Number Combustion Modelling for Droplet and Spray. presented at 5th Intl. Conference on Numerical Combustion, SIAM, York, UK, March 30 - April 1, 1998, 1998.

[4.131] R. I. Issa, A. D. Gosman and A. D. Watkins, The Computation of Compressible and Incompressible Recirculating Rlows by a Non-Iterative Implicit Scheme. Journal of Computational Physics, Vol. 62, 1986, 66–82.

[4.132] R. S. Cant and K. N. C. Bray, A Theoretical Model of Premixed Turbulent Combustion in Closed Vessels. Combustion and Flame, Vol. 76, 1989, 243–263.

[4.133] R. S. Cant and K. N. C. Bray, Strained Laminar Flamelet Calculation of Premixed Turbulent Combustion in a Closed Vessel. In *22nd Symposium (International) on Combustion*. The Combustion Institute, Pittsburgh, PA, USA, 1988, 791–799.

[4.134] J. B. Bell and D. L. Marcus, A Second-Order Projection Method for Variable-Density Flows. Journal of Computational Physics, Vol. 101, 1992, 334–348.

[4.135] M. Lai, J. B. Bell and P. Colella, A Projection Method for Combustion in the Zero Mach Number Limit. AIAA paper, 93-3369, 1993.

[4.136] J. van Kan, A Second-Order Accurate Pressure-Correction Scheme for Viscous incompressible flow. SIAM Journal of Scientific and Statistical Computing, Vol. 7, 1986, 870–891.

[4.137] P. M. Gresho, R. L. Sani and M. Engelman, *Incompressible Flow and the Finite Element Method*. John Wiley & Sons, New York, 1991.

[4.138] A.S. Almgren, J.B. Bell, P. Colella, L.H. Howell and M.L. Welcome, A Conservative Adaptive Projection Method for the Variable Density Incompressible Navier-Stokes Equations. LBNL Preprint, Vol. 39075 UC-405, 1996.

[4.139] M. J. Berger and P. Colella, Local Adaptive Mesh Refinement for Shock Hydrodynamics. Journal of Computational Physics, Vol. 82, 1989, 67–84.

[4.140] R. B. Pember, P. Colella, L. H. Howell, A. S. Almgren, J. B. Bell, K. C. Kaufman, W. A. Fiveland and J. P. Jessee, The Modeling of a Laboratory Natural Gas-Fired Furnace with a Higher-Order Projection Method for Unsteady Combustion. LBNL Preprint, Vol. LBNL-38800, 1996.

[4.141] P. Bailly and M. Champion, Counter-Gradient Diffusion in a Confined Turbulent Premixed Flame. Physics of Fluids, Vol. 9, 1997, 766–775.

[4.142] P. Clavin, Dynamic Behavior of Premixed Flame Fronts in Laminar and Turbulent Flows. Progress in Energy and Combustion Science, Vol. 11, 1985, 1–59.

[4.143] I. Chern and P. Colella, A Conservative Front Tracking Method for Hyperbolic Conservation Laws. UCRL-97200, Lawrence Livermore National Laboratory, 1987.

[4.144] A. Bourlioux and A. J. Majda, Theoretical and Numerical Structure for Two-Dimensional Unstable Detonations. Combustion and Flame, Vol. 90, 1992, 211–229.

[4.145] R. J. LeVeque and K.-M. Shyue, Two-Dimensional Front Tracking Based on High Resolution Wave Propagation Methods. Journal of Computational Physics, Vol. 123, 1996, 35–368.

[4.146] P. Terhoeven, *Ein numerisches Verfahren zur Berechnung von Flammenfronten bei kleiner Mach-Zahl [A Numerical Method for Flame Front Tracking at Low Mach Numbers]*. PhD thesis, RWTH Aachen, 1998.

[4.147] B. T. Helenbrook, L. Martinelli and C. K. Law, A Numerical Method for Solving Incompressible Flow Problems with a Surface of Discontinuity. Journal of Computational Physics, Vol. 148, 1999, 366–396.

[4.148] P. Deuflhard and A. Hohmann, *Numerical Analysis. A First Course in Scientific Computation.* W. de Gruyter, Berlin, New York, 1995.

[4.149] G. Strang, On the Construction and Comparison of Difference Schemes. SIAM Journal of Numerical Analysis, 1968, 506–517.

[4.150] U. Maas and S. B. Pope, Simplifying Chemical Kinetics: Intrinsic Lower Dimensional Manifolds in Composition Space. Combustion and Flame, Vol. 88, 1992, 239–264.

[4.151] U. Maas and S. B. Pope, Implementation of Simplified Chemical Kinetics Based on Intrinsic Low-Dimensional Manifolds. In *24th Symposium (International) on Combustion.* The Combustion Institute, Pittsburgh, PA, USA, 1992, 103–112.

[4.152] U. Maas and S. B. Pope, Laminar Flame Calculations Using Simplified Chemical Kinetics Based on Intrinsic Low-Dimensional Manifolds. In *25th Symposium (International) on Combustion.* The Combustion Institute, Pittsburgh, PA, USA, 1994, 1349–1359.

[4.153] S. H. Lam and D. A. Goussis, The CSP Method for Simplifying Kinetics. International Journal of Chemical Kinetics, Vol. 26, 1994, 461–486.

[4.154] H. S. Lam, Reduced Chemistry Modeling and Sensitivity Analysis. In *Aerothermochemistry for Hypersonic Technology 1994-1995*. (D. Olivari, (editor)). The von Karman Institute, Rhode St. Genése, Belgium, 1995.

[4.155] W. Breitung and R. Redlinger, Containment Pressure Loads from Hydrogen Combustion in Unmitigated Severe Accidents. Nuclear Technology, Vol. 111(3), 1995, 395–419.